EXPERIMENTAL ANALYSIS AND MODELLING OF WEAR IN ROCKET RAIL LAUNCHERS

A THESIS SUBMITTED TO
THE GRADUATE SCHOOL OF NATURAL AND APPLIED SCIENCES
OF
MIDDLE EAST TECHNICAL UNIVERSITY

BY

EMRE AÇMAZ

IN PARTIAL FULFILLMENT OF THE REQUIREMENTS
FOR
THE DEGREE OF MASTER OF SCIENCE
IN
MECHANICAL ENGINEERING

DECEMBER 2011

Approval of the Thesis:

EXPERIMENTAL ANALYSIS AND MODELLING OF WEAR IN ROCKET RAIL LAUNCHERS

submitted by **EMRE AÇMAZ** in partial fulfillment of the requirements for the degree of **Master of Science in Mechanical Engineering Department, Middle East Technical University** by,

Prof. Dr. Canan ÖZGEN _____
Dean, Graduate School of **Natural and Applied Sciences**

Prof. Dr. Süha ORAL _____
Head of Department, **Mechanical Engineering**

Prof. Dr. Metin AKKÖK _____
Supervisor, **Mechanical Engineering Dept., METU**

Examining Committee Members:

Prof. Dr. Eres SÖYLEMEZ _____
Mechanical Engineering Dept., METU

Prof. Dr. Metin AKKÖK _____
Mechanical Engineering Dept., METU

Prof. Dr. Suat KADIOĞLU _____
Mechanical Engineering Dept., METU

Assist. Prof. Gökhan ÖZGEN _____
Mechanical Engineering Dept., METU

M.Sc. Eng. Bülent ACAR _____
Unit Head, ROKETSAN

Date: 16.12.2011

I hereby declare that all information in this document has been obtained and presented in accordance with academic rules and ethical conduct. I also declare that, as required by these rules and conduct, I have fully cited and referenced all material and results that are not original to this work.

Name, Last name: Emre AÇMAZ

Signature:

ABSTRACT

EXPERIMENTAL ANALYSIS AND MODELLING OF WEAR IN ROCKET RAIL LAUNCHERS

Açmaz, Emre

M.Sc., Department of Mechanical Engineering

Supervisor : Prof. Dr. Metin Akkök

December 2011, 129 Pages

Launchers are military systems that are responsible for communication with munitions, safe separation and aiming of rockets and missiles to the target. Since they are military equipments, they are used in harsh environments. One of the most important design considerations for military equipment is its maintainability and one of the most important parameter which affects the maintainability is wear in launchers. Therefore, for predicting the life-time of a launcher, wear should be investigated beside other parameters such as fatigue etc.

This thesis study includes experimental and modeling study about dry sliding wear in some mechanical parts of a typical rail launcher that is used in helicopters. Firstly, measurements about the material loss, which is generated during firing of missiles, were made on launcher components which have interfaces with missile. Then, these results were used to simulate the wear phenomenon by using a commercial finite element program, ANSYS. By the help of finite element model, crack initiation period depending on wear is tried to be evaluated without making additional firing tests.

Keywords: Wear, Dry Sliding Wear, Rail launcher, Finite Element Analysis, ANSYS

ÖZ

RAYLI LANÇERLERDE OLUŞAN AŞINMANIN DENEYSEL ANALİZİ VE MODELLENMESİ

Açmaz, Emre

Yüksek Lisans, Makina Mühendisliği Bölümü

Tez Yöneticisi : Prof. Dr. Metin Akkök

Aralık 2011, 129 Sayfa

Lançerler, mühimmatla haberleşmeyi sağlayan, roketleri ve füzeleri hedefe doğru hizalamakta ve onların güvenli ayrılmasını sağlamakta kullanılan askeri sistemlerdir. Lançerler askeri teçhizatlar oldukları için çok zorlu koşullarda görev yapmaları istenir. Lançer tasarımında ihtiyaç duyulan tasarım kriterlerinin en önemlilerinden biri sürdürülebilirliktir ve sürdürülebilirliği etkileyen en önemli parametrelerden biri de aşınmadır. Bu nedenle, herhangi bir lançer için kullanım ömrü hesaplanmak istendiğinde, yorulma gibi aşınma da bir parametre olarak incelenmelidir.

Bu tez çalışması, helikopterlerde kullanılan tipik bir raylı lançerlerin mekanik parçalarında oluşan kuru aşınmanın deneysel analizini ve modellenmesini içermektedir. Öncelikle, füze ateşlenmesi sırasında füze ile teması olan lançer parçaları üzerinde oluşan aşınma miktarı ölçülmüştür. Daha sonra, bu ölçüm sonuçları parçalar üzerinde oluşan aşınmanın ticari bir sonlu elemanlar yazılımı olan ANSYS ile modellenmesi amacıyla kulanılmıştır. Sonlu elemanlar yazlımının yardımıyla, daha fazla atışlı teste ihtiyaç duymadan lançer parçalarında aşınma kaynaklı çatlak oluşma süresi belirlenmeye çalışılmıştır.

Anahtar kelimeler: Aşınma, Kuru Aşınma, Raylı Lançerler, Sonlu Elemenlar Analizi, ANSYS

To my dear family

ACKNOWLEDGEMENTS

Firstly, I would like to express deepest thanks and gratitude to my supervisor Prof. Dr. Metin Akkök for his guidance and support throughout this work.

I would like to express my sincere appreciation to Mr. Bülent Acar for his guidance through out thesis study like a co-supervisor.

I would like to thank to Roketsan Missiles Industries for partially supporting this study. I am grateful to all my friends, my superiors and colleagues, especially Mr. Tuncay Tunç for his support in test activities, in Roketsan for their patience and valuable comments.

I would also thank to Assist. Prof. Dr. Uğur Malayoğlu and Research Assistant Kadir Çelik Tekin from Department of Metallurgical and Materials engineering in Dokuz Eylül University for their effort in making measurements of test parts, without their effort thesis would be meaningless.

Last but never least, my special appreciation goes to my family, Hacer (mother), Selim (father) and Duygu (wife) AÇMAZ; Melda (sister) and Tolga (sister's husband) ÖZDEN. Their dedication, love and persistent confidence on me, has taken the load off my shoulder. Without their presence, this thesis would not have been possible.

TABLE OF CONTENTS

LIST OF TABLES

TABLES

LIST OF FIGURES

FIGURES

CHAPTER 1

INTRODUCTION

Since mechanical systems are affected severely by wear, maintenance procedures are applied to them. However, persistence is very important for military equipment and in a war period, maintenance procedures are in second importance. Therefore, while designing military equipments, problems that may decrease the life-time, like wear, must be carefully handled.

In this thesis study, a typical helicopter launcher system was inspected in order to find out its wear performance. Firing tests were made with a missile of approximately 35 kg and 40 m/s launcher exit velocity. Wear measurements were made on launcher components. A numerical simulation of wear was constructed in order to prevent dependency on firing tests for evaluating wear performance.

1.1 CONSTRUCTION OF HELICOPTER LAUNCHER

Rockets are launched from variety of launcher systems. These launchers vary with the properties of the launched rockets. Some can be in huge dimensions and needs a group of people to control, some can be in a little and compact design to be portable. But no matter how they change, all of the rocket launchers are used to aim rockets and missiles and give them an initial velocity which is essential to minimize tip-off at the beginning of the flight. As aiming equipment, launchers are affected severely by firing effects of rockets. They are encountered with mechanical and thermal wear problems as a result of high speed and load of rockets.

Launchers, used on helicopters, carry missiles or rockets which are fired from air to land or air to air targets. In Figure 1-1, a typical launcher (Hellfire M299) can be seen to give an idea about launcher which is used in thesis work.

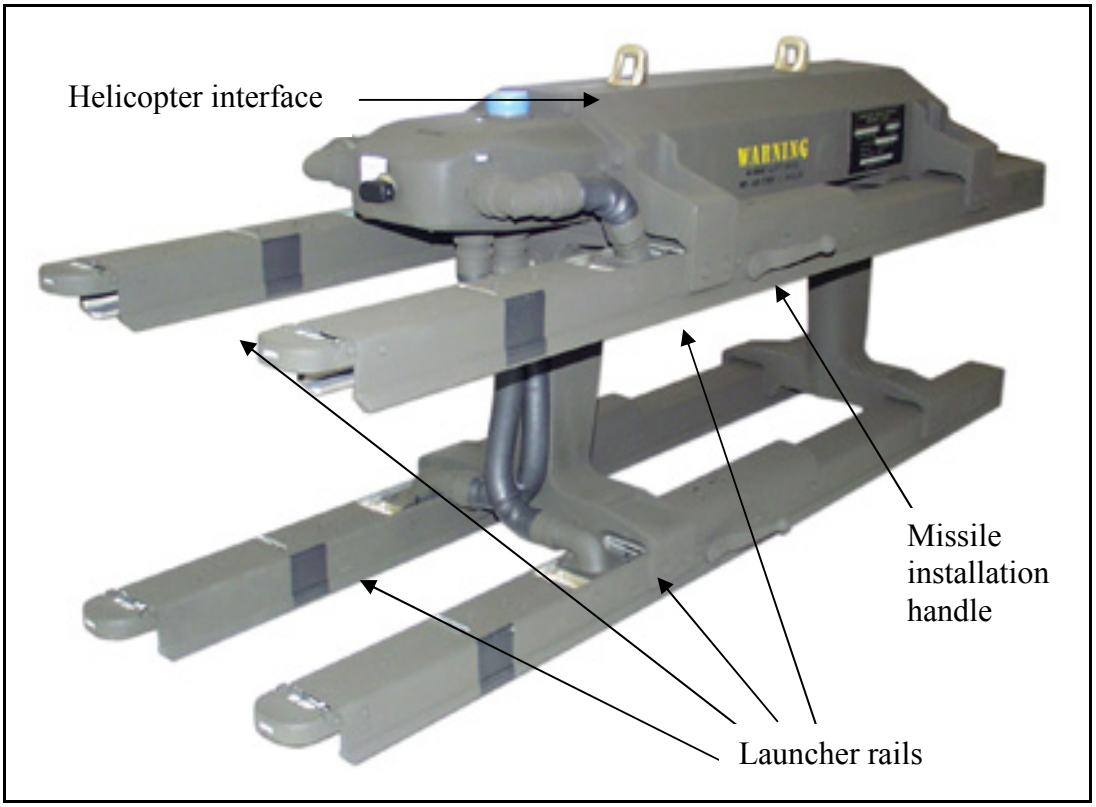

Figure 1-1 A view of Hellfire M299 launcher [1]

The M299 launcher is composed of four rails which carry missiles. It is an aluminum construction. Moreover, there is an installation handle on the launcher. This is used to activate the release mechanism in the launcher rail. As seen in Figure 1-2, the missiles are hanged on the rails by the help of shoes on them. Hellfire is a 178 mm diameter missile with a weight of approximately 45 kg [2].

The maintenance and life-time are two major parameters that determine the usability of a helicopter launcher. Since they are operational weapons which are used in harsh environments, reliability is also important for helicopter launchers. It should be guaranteed that missiles leave the launcher safely for all firings in the desired life time of launcher.

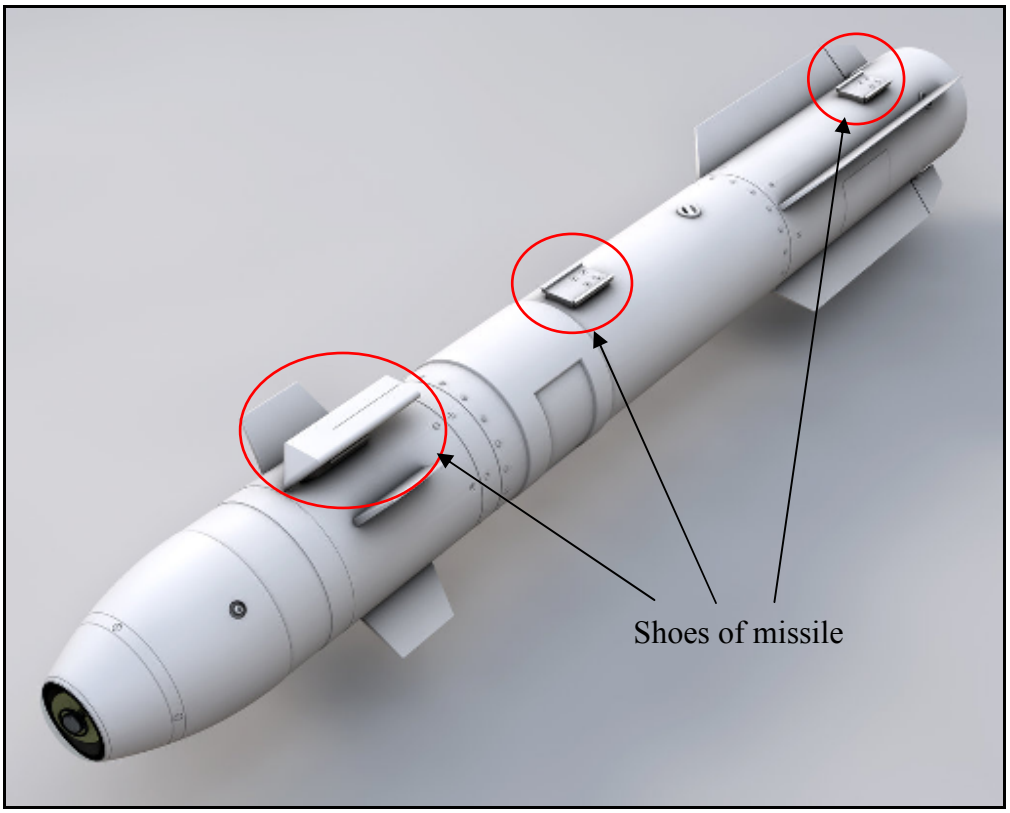

Figure 1-2 A view of Hellfire missile [3]

1.2 WEAR ON LAUNCHERS

The launcher exit velocity of the missile is very important for its ballistics because the flight performance is strongly depended with the exit velocity. To increase velocity of the missile, thrust of rocket motor should be enhanced. However, promoted thrust will have restrictions caused from rocket motor. Moreover, it would affect flight velocity, maneuver capability of the rocket etc.

In literature, studies about launcher wear are generally made on gun-bore wear and wear in artillery systems because guidance is more critical problem for unguided weapons than guided weapons because unguided weapons are generally fired from a tube-shaped launcher. Wear of launcher will cause unpreventable aiming errors. Exhaust gases and heat dissipation are serious parameters for these types of launchers. B. Lawton states that [4],

> *It has long been known that the performance of a gun is limited by the wear rate of its barrel. In the 16th century, Biringuccio*

discussing the lack of range in a cannon says: "if the defect comes from the powder, you must give it more so that it serves, although I do not recommend this because of the danger of wearing out the gun".

Today, gun designers share concerns of Biringuccio and use parts which are called erosion rings in gun barrels in order to decrease wear rate. In Figure 1-3, section view of a gun and erosion ring can be seen.

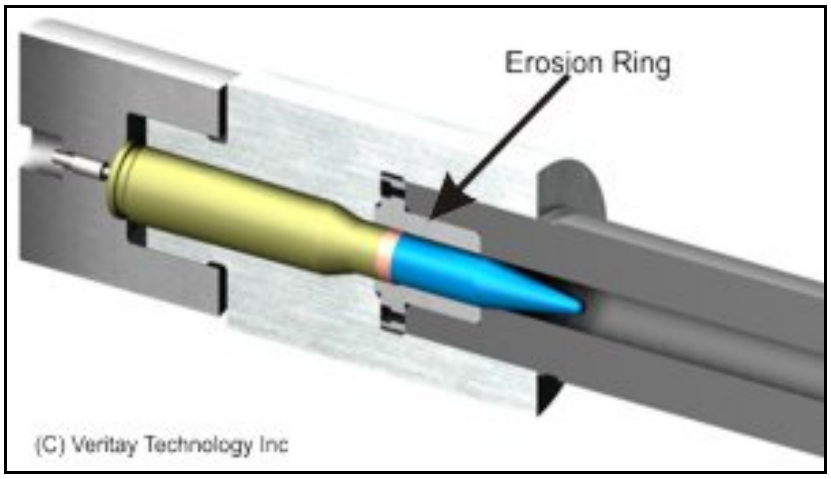

Figure 1-3 A view of Gun-bore and the erosion ring [5]

Wear on launchers does not depend only on contact forces between materials. As they will be mentioned in the proceeding chapters, there are lots of parameters which affect wear.

As it is seen on Figure 1-4, mechanical removal of material is one cause of wear. There are also temperature gradients due to exhaust gases of the rocket motor or bullet powder, radiation effects, surface melt by rising contact surface temperature between two materials [6] and effects of ablation products.

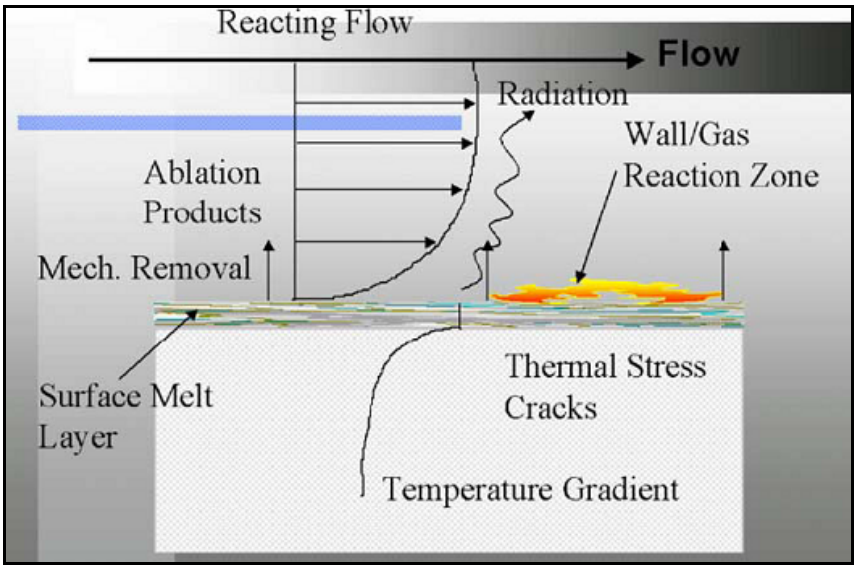

Figure 1-4 Thermal-Chemical-Mechanical wear zones [7]

1.3 AIM OF THE STUDY

During firing, rockets are trusted by a large amount of force depending on their masses. This thrust force is needed to raise velocity of rockets to the desired launcher exit velocity. Generally, the distance of rocket travel in launchers is small because of ergonomic prerequisites. Therefore, rockets apply large sliding forces to the launchers in a small interval of time.

Despite a rocket is fired for only one turn, rocket launchers are used repeatedly. Thus, wear is not a problem for missiles but it has a critical role in designing launchers.

It is known that only wear generally does not cause failure of the material. Wear generates surface cracks on the materials and these cracks are propagated under additional loading as seen in Figure 1-5. Then, as a result of crack growth, failure of the material occurs. Figure 1-6 is given in order to provide a size scale to the phenomenon of fatigue crack development. In Figure 1-6, it is seen that crack initiation corresponds approximately 20% of the total life to fracture. The graph changes with respect to applied loading, environmental conditions, material properties, etc. but it shows that crack initiation covers an important region in life-time of components.

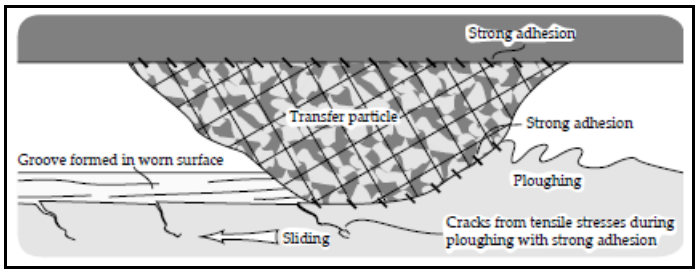

Figure 1-5 A schematic view of surface crack development during wear [8]

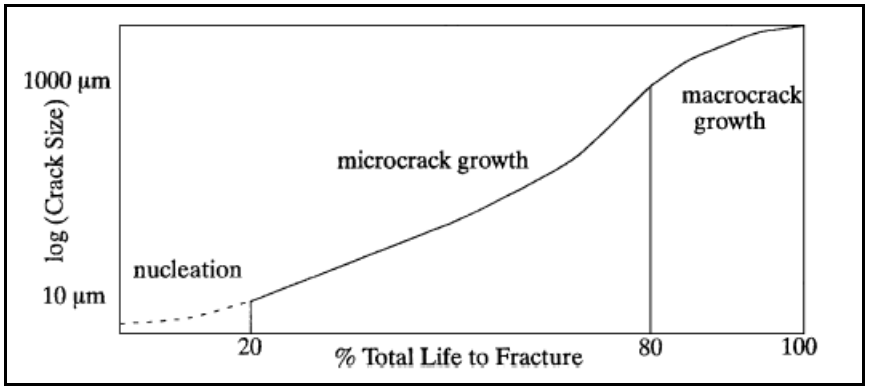

Figure 1-6 A typical fatigue crack development graph for metals [9]

The aim of this thesis study is to simulate wear and compute the crack initiation time of launcher components. For this purpose, numerical wear models are supported by some experimental studies. So that, without additional experiments the wear performance of launcher components are simulated.

1.4 RUNNING CONDITIONS

Wear occurs between moving mechanical parts. When the rail launcher used in thesis work was inspected, it was realized that two components of the launcher are critical for wear examination. One of them is rail, and the other is release latch. These two parts are the only components which have interaction with missile. Missile shoes slide on the rail of the launcher and dry sliding takes effect between them. Release latch prevents missile movement up to a certain thrust force in order to increase the launcher exit velocity of the missile.

In this thesis study, the launcher used for measuring wear is similar to Hellfire M299 launcher. It has four missile rails and missiles are hanged on rails by the help of their

shoes. Each missile has three shoes. There is no lubrication on rails since all surfaces are open to atmosphere. The locations of missile shoes are represented in Figure 1-7.

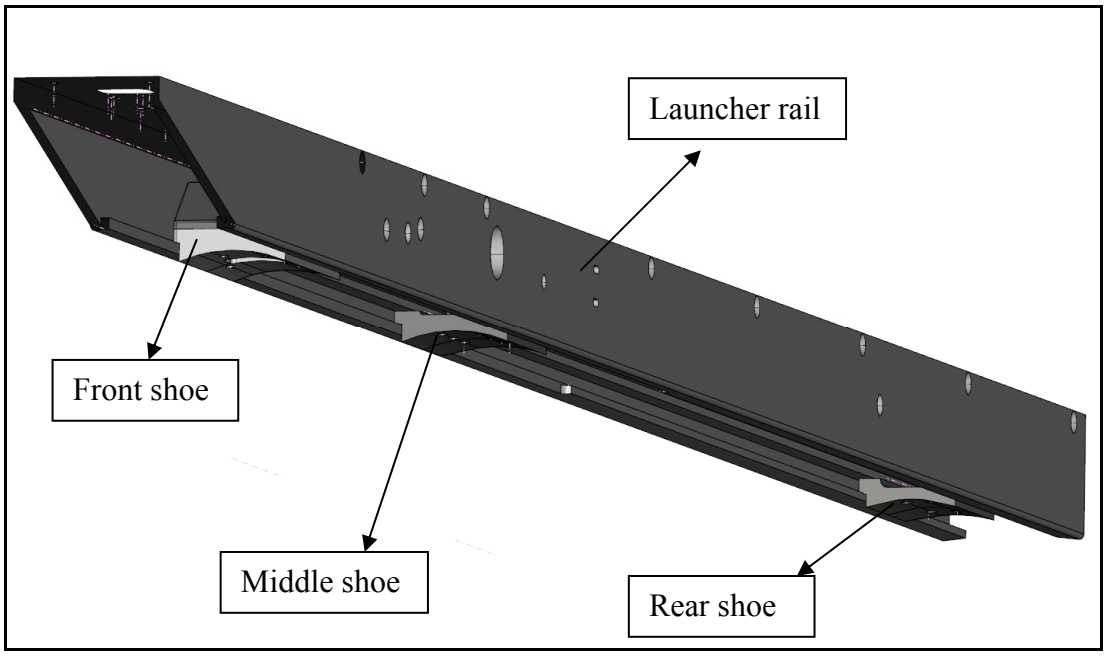

Figure 1-7 Shoe locations on launcher rail

When missile is launched, it slides along the launcher for about 500 (five hundred) millimeters. Since speed of missile increases very rapidly, missile leaves launcher after approximately 0.1 seconds.

Launcher rails are made of aluminum; the front and the rear shoes of missile are aluminum and the middle shoe of missile is made from steel. In order to prevent excessive wear on rail, aluminum is plated with hard-anodized plating. Brief information will be given in the preceding chapters.

As mentioned before, the most precise machined surface of launcher rail is the interface between the missile and the launcher rail. To supply safe flight and accuracy on target, launcher rail surface should be 0.3 mm planarity as seen in Figure 1-8.

Moreover, firing experiences showed that after 100-120 μm wear depth, surface cracks arise on the surface of the rail material. Surface cracks are generated earlier than planarity requirement limit.

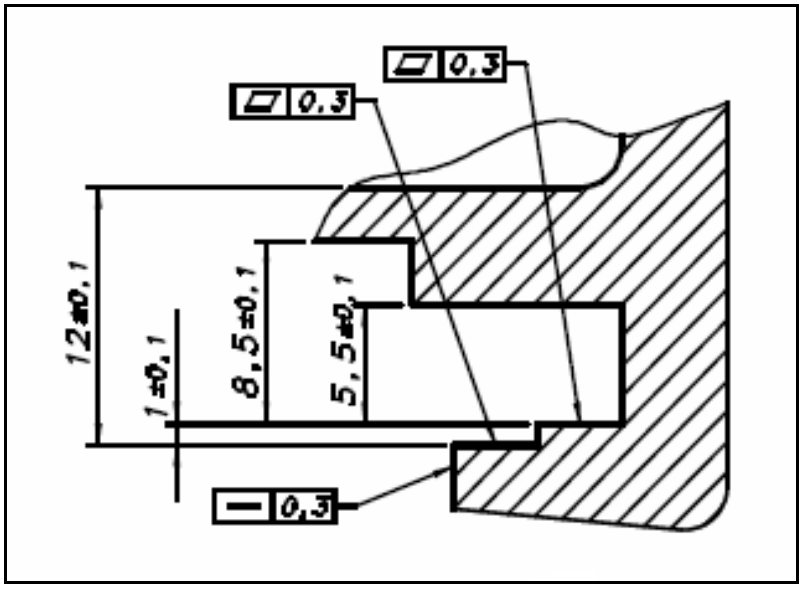

Figure 1-8 A detailed technical drawing of launcher rail and missile interface

In Figure 1-9, the interface between missile shoe and release mechanism is shown. Shoe of the missile is used only for one firing but release mechanism latch is used permanently. Therefore, deformation on the latch affects the performance of the launcher. Experiences show that, after approximately 60-80 µm wear depth the surface cracks arises on the contact surface of release latch material. Thus, it will be taken as limit wear depth in evaluating crack initiation time of release latch.

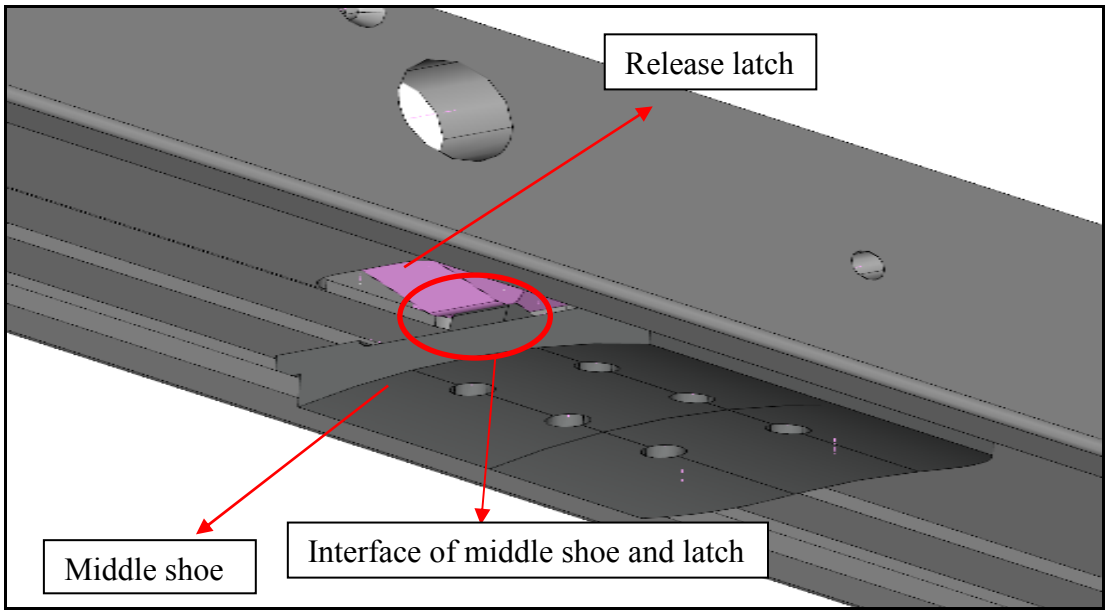

Figure 1-9 A view of interface between middle shoe and release mechanism latch

1.5 SCOPE OF THE THESIS

Crack initiation or failure depending on wear take long time to arise. In other words, this type of failures requires longer time than static failures. Therefore, longer experimental studies are needed in order to see these effects of wear. The experimental study made to evaluate wear performance in launcher components is firing tests because the real usage environment of the launcher can only be created during firing tests. However, the main aim of firing tests is to see the flight performance of missiles/rockets and they are very expensive tests. Doing huge amount of firing tests only to inspect wear performance of launcher is impractical. Thus, the need to simulate wear arises. The scope of this thesis study is to investigate wear performance of launcher components with a few firing tests and to construct a simulation of wear for annihilating the demand of more firing tests. Below, brief descriptions about chapters of thesis are given.

In chapter 2, wear theory, wear mechanisms and parameters affecting wear will be introduced. The effect of surface roughness on wear will be mentioned and contact between rough surfaces will be explained by the help of contact mechanics. Then, the bearing area curves of rough surfaces which are used to figure out the amount of wear will be described.

In chapter 3, experimental work of thesis work will be explained. A description of the experimental setup and the results of experiments will also be given in this chapter.

In chapter 4, simulation study of wear will be explained. The details of simulation study and the results of analyses will be given in this chapter.

In chapter 5, the discussion and comparison of the experimental results and modeling results will be given. Moreover, the recommendations for future works will be mentioned for those who are interested in developing the topic of thesis study.

CHAPTER 2

WEAR ANALYSIS AND MODELLING ON ROUGH SURFACES

2.1 THEORY OF WEAR

Wear can be defined as damage to a solid surface, generally involving progressive loss of material, due to relative motion between the surface and a contacting substance or substances [10]. It is an undesired case for machines or mechanisms. Therefore, all over the time, it is tried to be prevented.

Wear takes place when surfaces of mechanical components contact each other. The investigated question is, how much of the material will be lost during the given operation time. Wear and plastic deformation cause surface profiles change and pressure distribution is strongly depended on the phenomena.

There can be many causes for wear. First of all, it is caused by material fracture under stresses in the process of friction. This widespread type of wear is classified as mechanical wear and is often taken to be a synonym of the word "wear".

Among other wear causes, chemical reactions and electrochemical processes can be mentioned. Corrosive wear is an example of this type of surface fracture. It is the main wear mechanism in moving components, operating in a chemically aggressive environment.

Some physical processes can also cause wear. For example, it is known that almost all of the energy dissipated in friction is converted into heat. An increase of the surface layer temperature can change the aggregate state of the material. In such a case the wear is provided because of melting and flowing of the melt out of the interface (ablation wear) or because of evaporation (breaks, high speed guides, plane wheels, etc.). High temperature accelerates diffusion processes which can influence wear in some cases (cutting tools). For these cases, wear occurs at the atomic and molecular levels.

Wear rates of materials change between 10^{-15} and 10^{-1} mm^3/Nm, depending on operating conditions and material selections [11]. Figure 2-1 shows wear volume curves. Type I is a constant wear volume on the whole process. Type II is an initially high to steady wear rate which is quite seen in metallic materials. Type III is an initially low to high wear rate case which is seen in ceramics.

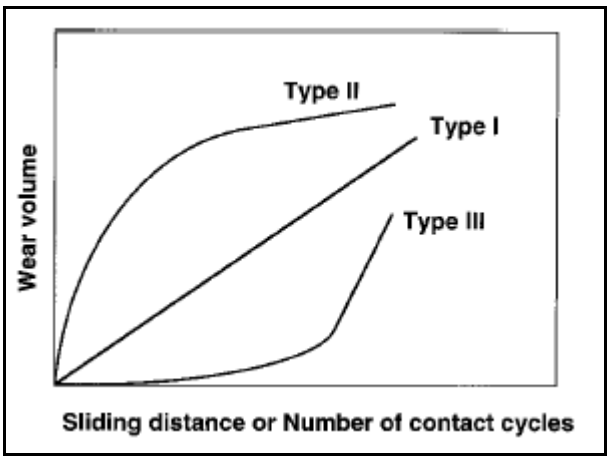

Figure 2-1 Wear curves in repeated contacts [12]

The most important thing about wear is to know that "Wear is not a material property, it is a system response" [13]. Therefore there are lots of system parameters to distinguish wear. These parameters can be seen on Table 2-1.

Table 2-1 Parameters affecting wear

WEAR PARAMETERS		
OPERATING PARAMETERS	**MATERIAL PARAMETERS**	**ENVIRONMENTAL PARAMETERS**
CONTACT PRESSURE	HARDNESS, YIELD AND ULTIMATE TENSILE STRENGHT	RELATIVE HUMIDITY
SLIDING SPEED	TOUGHNESS	HEAT RADIATION LEVEL
SLIDING DISTANCE	MELTING POINT	
SURFACE TEMPERATURE	THERMAL CONDUCTIVITY	
SURFACE FINISH	ELECTROCHEMICAL POTENTIAL	
TYPE OF CONTACT		

2.1.1 BASIC WEAR MECHANISMS

Wear is described by the material removal mechanisms which are so called wear types. In different applications different types of wear can be dominant. However, generally, there is not only one type wear, but combinations of wear mechanisms are generated together.

It is common to differentiate the following fundamental types of wear according to their physical mechanisms:

- **Abrasive wear** occurs, if two bodies with distinctively different hardness are in contact or the third body contains hard particles

- **Adhesive wear** occurs even in contacts with the same or similar materials
- **Corrosive wear** is associated with chemical modifications of the surface and finally removal of the surface layer
- **Surface fatigue** is caused by repeated loading of the surface either by sliding or rolling, where in every single loading cycle, no noticeable changes in the surface stresses appear [13].

2.1.1.1 ABRASIVE WEAR

For existing abrasive wear, there should be a weaker material. Therefore, this type of wear is commonly seen in manufacturing processes such as milling, honing, etc. During abrasive wear, asperities of harder material penetrate and micro-cut the softer material as shown in Figure 2-2.

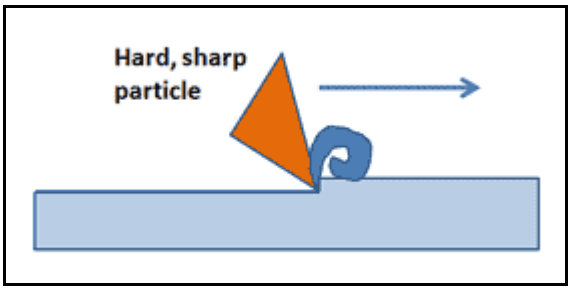

Figure 2-2 Abrasive wear mechanism [14]

In order to estimate wear volume in abrasive wear, Archard Wear Equation is used:

$$V = K_{ab} \cdot \frac{W \cdot L}{H} \tag{2-1}$$

where:

V: wear volume (mm^3)

K_{ab}: wear coefficient for abrasive wear (dimensionless)

W: normal load (N)

L: sliding distance (mm)

H: hardness value of softer material (MPa)

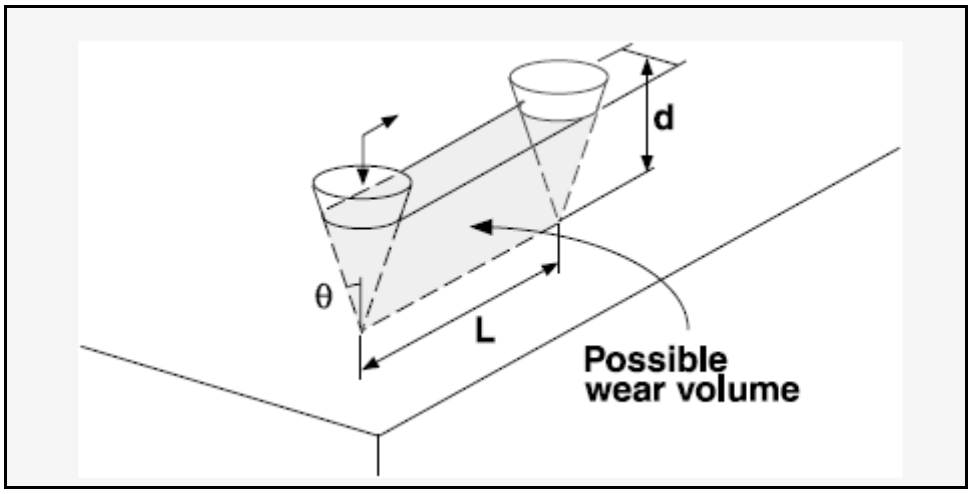

Figure 2-3 Abrasive wear volume [12]

K_{ab} is used to describe the wear rate of abrasive wear. It is strongly related with the ductility of wearing material, shear strength at the contact interface and the shape of the abrasive asperity. Wear coefficient of K_{ab} varies between 10^{-4} and 10^{-1}, depending on the contact conditions and material parameters [12].

2.1.1.2 ADHESIVE WEAR

Adhesive wear is the most commonly seen wear mechanism in applications. It can be expressed as: The action of one material sliding over another with surface interaction and welding (adhesion) at localized contact areas [14].

As it is seen on Figure 2-4, adhesive wear is caused by surface roughness of two sliding material. Load need not to be very high for adhesive wear to occur. Because of contacting rough surfaces, the interface area is very small between mating parts. This causes large stresses on material surfaces even applying small amount of loads.

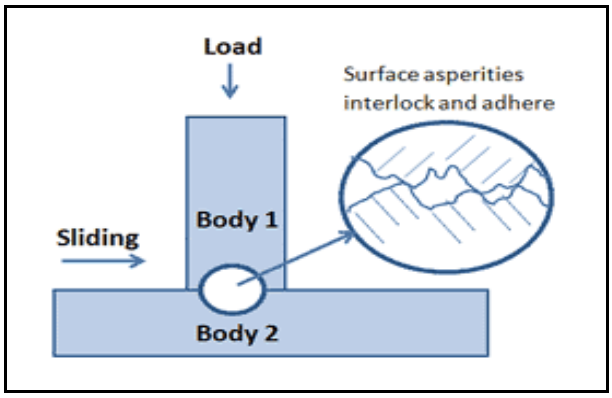

Figure 2-4 Adhesive wear mechanism [14]

According to Popov [13], the adhesion is the result of exceeding the elastic limit of two contacting materials under pressure. If tension loads are applied to materials, after a certain elastic limit (depending on mechanical properties) the materials will deform. However, in the case of contact, when materials are pressed to each other, after elastic compression limit is exceeded, the materials are welded to each other in microscopic scale which is called adhesion.

Table 2-2 Adhesion force of various metals against iron in vacuum [15]

Metal	Solubility in Iron [atomic%]	Adhesion force to iron [mN]
Iron		>4.0
Cobalt	35	1.2
Nickel	9.5	1.6
Copper	<0.25	1.3
Silver	0.13	0.6
Gold	<1.5	0.5
Platinum	20	1.0
Aluminum	22	2.5
Lead	Insoluble	1.4
Tantalum	0.20	2.3

It is evident from Table 2-2 that in all cases the adhesion or separation force is greater than the contact force. The greatest adhesion occurs for a combination of same materials, i.e. iron to iron, but many other combinations of unlike metals also show quite high adhesion.

In order to estimate wear volume of adhesion, similar to abrasive wear, Archard's Equation is used in the following form:

$$V = K_{ad} \cdot \frac{W \cdot L}{H} \tag{2-2}$$

However, this time K_{ad}, wear coefficient for adhesive wear, is used instead of K_{ab}. The physical meaning of K_{ad} is the wear volume and it is strongly affected by the material properties and the geometry of the zone in compression and shearing.

K_{ad} of metals varies between 10^{-7} and 10^{-2} depending on the operating conditions and material properties [12]. It can easily be realized that abrasive wear is more severe with respect to adhesive wear by comparing wear coefficients.

2.1.1.3 FATIGUE WEAR

The results of many experiments show that most of the failures are caused by fatigue. For abrasive or adhesive wear, there is no need to be repeated cycles of contact. However, fatigue wear occurs in cycling loading conditions as shown in Figure 2-5. When the number of contact cycles is high, the high-cycle fatigue mechanism is expected to be the wear mechanism. When it is low, low-cycle fatigue mechanism is expected.

It is known that in elastic contact case of rolling elements, the main wear mechanism is high-cycle fatigue. According to Lundberg and Palmgren, the critical rolling cycles N_f is inversely proportional to the normal load (W) applied to the surfaces:

$$N_f \propto \frac{1}{W^n} \tag{2-3}$$

where “n” is a constant which depends on the shape of the rolling element.

One of the types of fatigue wear is fretting wear caused by cycling sliding of two surfaces across each other with small amplitude (oscillating). The friction force produces alternating compression-tension stresses, which result in surface fatigue.

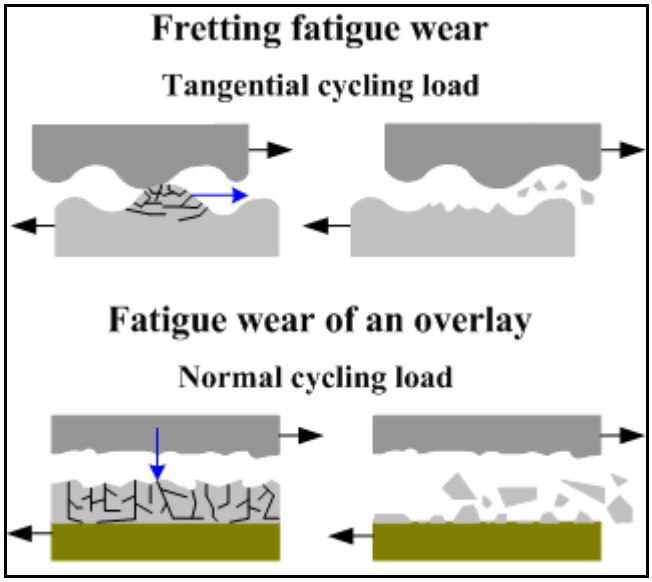

Figure 2-5 Fatigue & Fretting wear mechanism [16]

2.1.1.4 CORROSIVE WEAR

Corrosive wear occurs as a result of a chemical reaction on a wearing surface. The most common form of corrosion is due to a reaction between the metal and oxygen (oxidation); however, other chemicals may also contribute. Corrosion products, usually oxides, have shear strengths different from those of the wearing surface metals from which they were formed. The oxides tend to flake away, resulting in the pitting of' wearing surfaces.

Koji Kato and Koshi Adachi claim that [12],

> *In corrosive wear, tribochemical reaction produces a reaction layer on the surface. At the same time, such layer is removed by friction. Therefore, relative growth rate and removal rate determine the wear rate of the reaction layers and, as a result, of the bulk material. Therefore, models of the reaction layer growth and those of the layer removal become very important.*

2.2 SURFACE ROUGHNESS

Solid surfaces, irrespective of their method of formation, contain irregularities or deviations from the prescribed geometrical form [17]. No matter how it is produced, every workpiece has micro defects on their surfaces. These defects can be grouped into errors, waviness and roughness. Errors are deviations of the surface from its ideal geometrical form (convexity, concavity, taper, etc.). Waviness is a group of errors that makes a pattern and is referred to as macro roughness [12]. Vibration during machining, chattering or heat treatment may cause waviness. On the other hand, surface roughness indicates irregularities of the surfaces which are as small as 0.03 to 400 μm and as narrow as 2 to 800 μm [18].

Roughness value which is used in technical drawings defines a mean value of all irregularities of the surface. To examine wear phenomenon, more detailed information about the surface is needed. Therefore asperities of the surface should be examined. Surface texture, like roughness, is the repetitive or random deviation from the nominal surface of materials. In Figure 2-6, a pictorial display of surface texture is given.

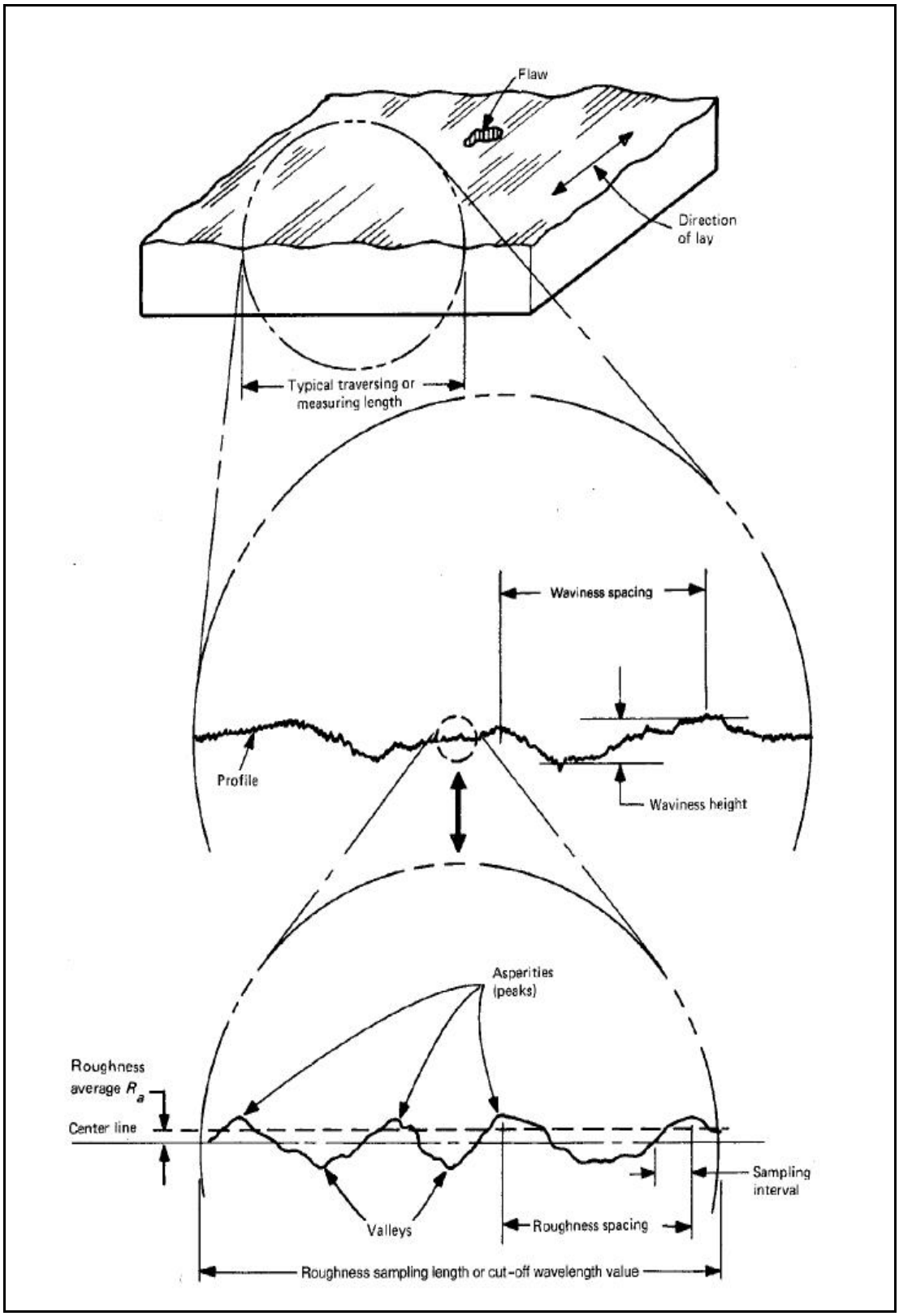

Figure 2-6 Pictorial display of surface texture [19]

Beside the asperities of surfaces, solid surface contains several zones that are the resultant of manufacturing processes. These zones can be seen on Figure 2-7.

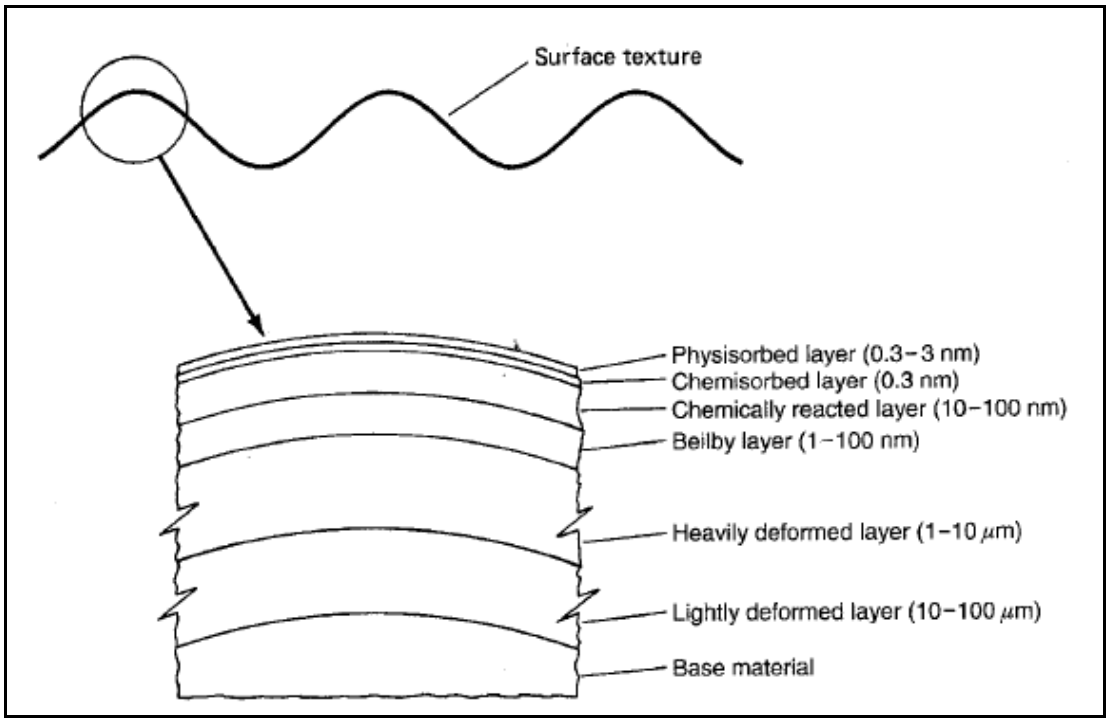

Figure 2-7 Solid surface zones [12]

These zones are highly important because mechanical behavior of their surface is affected by the amount and depth of deformation of surface layers.

Surface texture is measured by a number of parameters. There are lots of them for defining a specific texture. In Table 2-3, the most important and frequently used surface roughness height parameters are mentioned. “n” specifies number of points taken to analyze surface and y_i is the height of the points from the mean line of the surface as shown in Figure 2-8. Mean line is a line that satisfies the area between surface profile and mean line is equal for above and below the mean line.

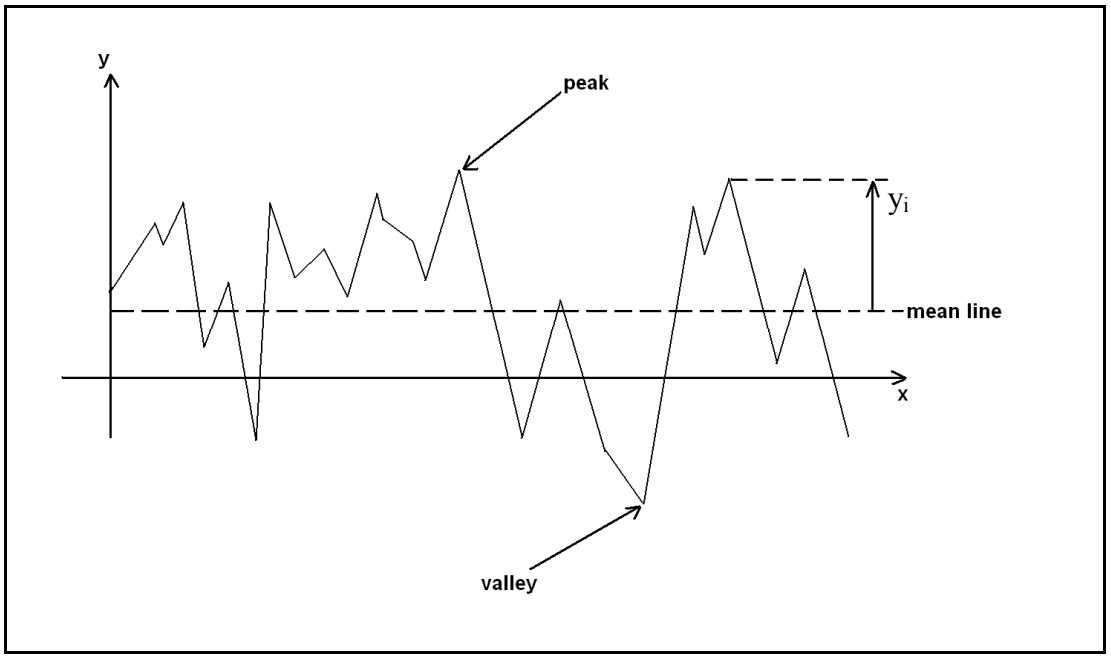

Figure 2-8 Schematic view of a random surface profile

Table 2-3 Roughness height parameters [2]

PARAMETER	DESCRIBTION	FORMULA
R_a	Arithmetic average of absolute values	$R_a = \frac{1}{n}\sum_1^n \lvert y_i \rvert$ (2-4)
R_q, R_{rms}	Root mean square	$R_q = \sqrt{\frac{1}{n}\sum_1^n y_i^2}$ (2-5)
R_v	Maximum valley depth	$R_v = \min y_i$ (2-6)
R_p	Maximum peak height	$R_p = \max y_i$ (2-7)
R_t	Maximum height of the profile	$R_t = R_v - R_p$ (2-8)
R_{sk}	skewness	$R_{sk} = \frac{1}{n \cdot R_q^3}\sum_1^n y_i^3$ (2-9)
R_{ku}	kurtosis	$R_{ku} = \frac{1}{n \cdot R_q^4}\sum_1^n y_i^4$ (2-10)

As it is mentioned before, identifying a real surface is quite hard problem. Therefore, statistics theory is used to determine random rough surfaces. Probability distribution function is a function that shows the probability of a random variable at a certain point. It is known that a mean and standard deviation of population is adequate for describing a “Normal” or “Gaussian” distribution function as shown in Figure 2-9.

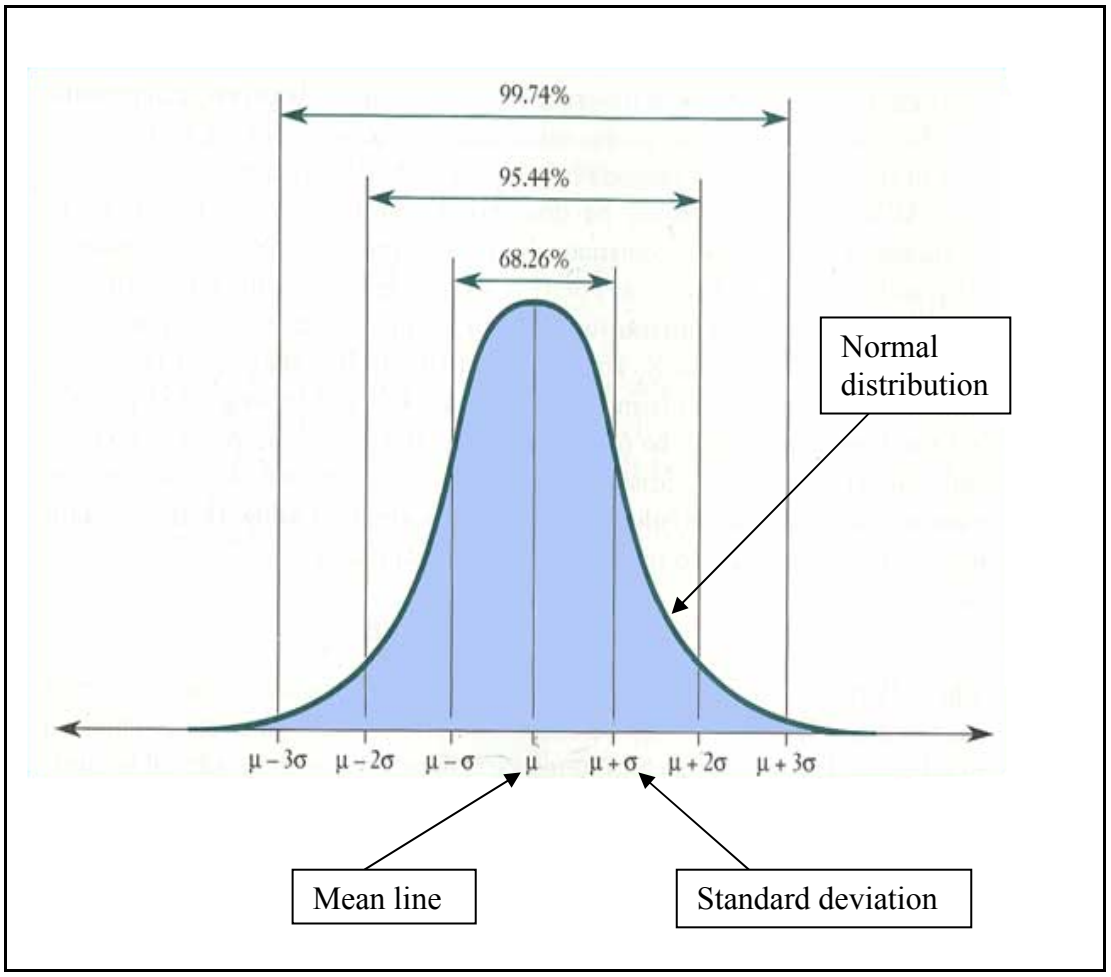

Figure 2-9 Normal (Gaussian) Distribution of data sets

If these considered data sets are surface or profile sets of a random rough surface, then probability distribution function is called as surface height distribution function or cumulative distribution function (CDF).

The shape of cumulative distribution function explains useful information about surface topography. This shape is found out by the help of moments of the function. The third moment of the function is skewness of the profile, and the fourth moment is kurtosis of the profile as showed in equations (2.9) and (2.10), respectively. In Figure 2-10, shape change of CDF is showed with changing skewness and kurtosis, respectively. Positive and negative skewness represents an asymmetric distribution of points while zero skewness shows a symmetric distribution. On the other hand, kurtosis is a measure of degree of pointedness or bluntness of distribution [12].

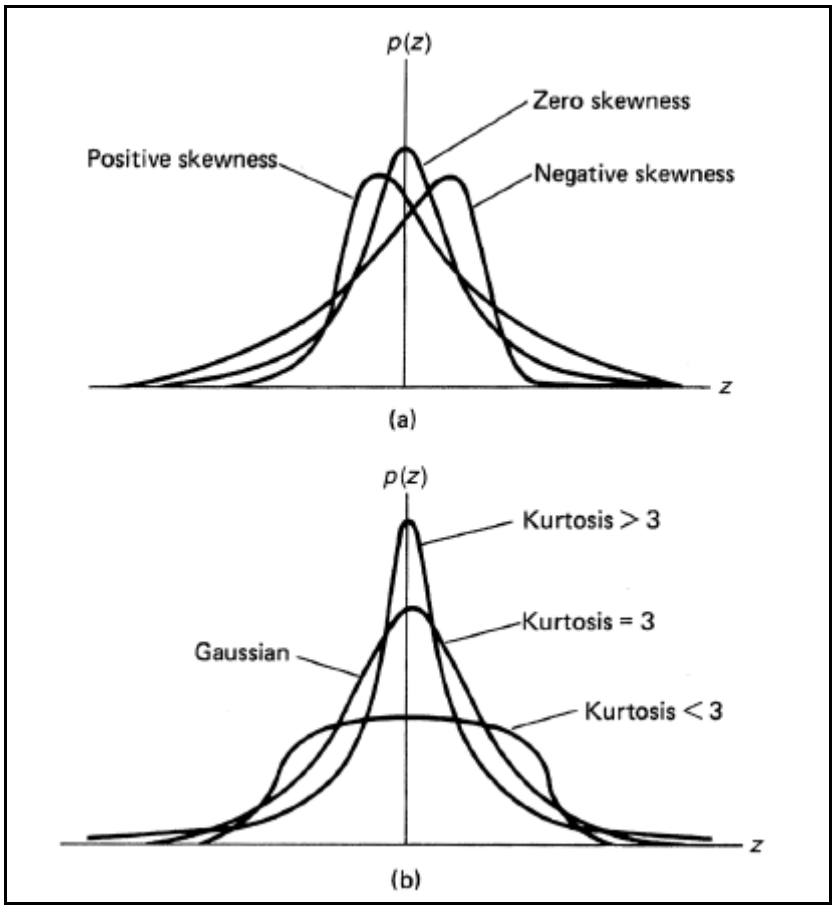

Figure 2-10 a) shape change of CDF (cumulative distribution function) with changing skewness value b) shape change of CDF with changing kurtosis value [12]

It is thought that generally surface profiles of mechanical parts have Gaussian distribution. However, this is false for some applications. For example, mechanical parts which are manufactured by grinding, honing, lapping have negatively skewed height distributions [21]. On the other hand, some milling and turning operations can cause mechanical parts have positively skewed height distributions [22].

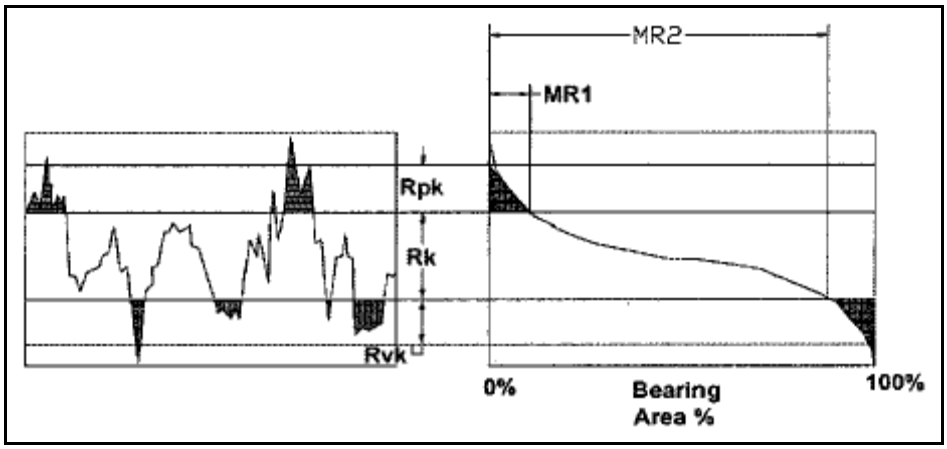

Figure 2-11 Surface roughness parameters

R_k is roughness value of a surface when peaks and valleys are excluded. For generally machined surfaces theoretical value of R_k is approximately πR_a.

R_{vk} is value of valley depth and R_{pk} is the value of peak height. In Figure 2-11, schematically representations of R_{pk}, R_{vk} and R_k can be seen.

Moreover, in Figure 2-11, some statistical parameters of surfaces are shown. MR1 and MR2 are material ratio parameters of surfaces and they are figured out by the help of R_{pk}, R_{vk} and R_k. Their importance will be described in the proceeding sections.

2.3 BEARING AREA CURVE (BAC)

It should be noted that the functional properties of a surface is not only determined with its roughness. Structure of the profile is also important. Bearing are curve (BAC) is a statistical tool which is used to analyze structure of the surface profile. It shows the ratio of air to material on the surface profile of any material at any level. The curve starts with the highest peak of the surface and ends with lowest valley. In 1933, EJ Abbott and FA Firestone had first described the curve. BAC is also known as Material Ratio Curve or Abbott Curve in literature. According to Mike Steward, BAC is the integral of the probability distribution function or amplitude distribution function of a randomly distributed surface [23]:

$$BAC = \int ADF = \int P(y)dy \tag{2-11}$$

where y is the height measurement made across the surface.

Figure 2-12 describes schematically how a BAC curve can be figured out. Here, z is the distance perpendicular to the plane of the surface, Δz is the interval between two heights, h is the mean line of the surface, p(z) is the probability density function, P(z) is the cumulative probability function.

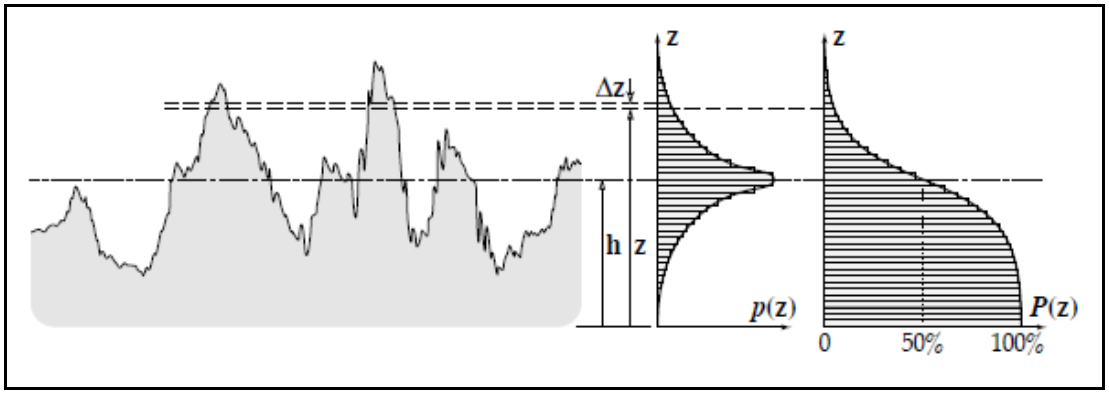

Figure 2-12 Determination of bearing area curve of a rough surface [8]

ISO 13565-2 describes definition of material ratio curve and determination of parameters of this curve. According to the standard, material ratio curve (MCC) describe the increase of the material portion of the surface with increasing depth of the roughness profile [24].

2.3.1 EVALUATION OF BAC PARAMETERS

ISO 13565-2 also specifies the parameters of bearing area curve as [24]:

Core roughness profile: roughness profile excluding the protruding peaks and deep valleys,

R_k (core roughness depth): depth of the roughness core profile,

Mr1 (material portion): level, in percent, determined for the intersection line which separates the protruding peaks from the roughness core profile,

Mr2 (material portion): level, in percent, determined for the intersection line which separates the deep valleys from the roughness core profile,

R_{pk} (reduced peak height): average height of the protruding peaks above the roughness core profile,

R_{vk} (reduced valley depths): average height of the projecting through the roughness core profile.

As it is mentioned above BAC has five parameters which are R_k, Mr1, Mr2, R_{vk} and R_{pk}. To evaluate these parameters from BAC, equivalent straight line should be calculated first. It is calculated for the central region of the BAC which includes 40% of the measured profile points. This "central region" lies where the secant of the BAC over 40 % of the material ratio shows the smallest gradient as in Figure 2-13. This is determined by moving the secant line for $\Delta Mr = 40$ % along BAC, starting at the Mr = 0 % position. The secant line for $\Delta Mr = 40$ % which has the smallest gradient establishes the "central region" of the BAC for the equivalence calculation. If there are multiple regions which have equivalent minimum gradient, then the one region that is first encountered is the region of choice. A straight line is then calculated for this "central region" which gives the least square deviation in the direction of the profile ordinates.

The equivalent straight line intersects the abscissa Mr = 0 % and Mr = 100. From these points two lines are plotted to the x-axis, which determine the roughness core profile by separating the protruding peaks and valleys. The vertical distance between these intersection lines is the core roughness depth R_k. Their intersections with the BAC define the material ratios Mr1 and Mr2.

The areas above and below the region of the BAC which delimits the core roughness R_k are shown hatched in Figure 2-13. These correspond to the cross-sectional area of the profile peaks and valleys which protrude out of the core roughness profile.

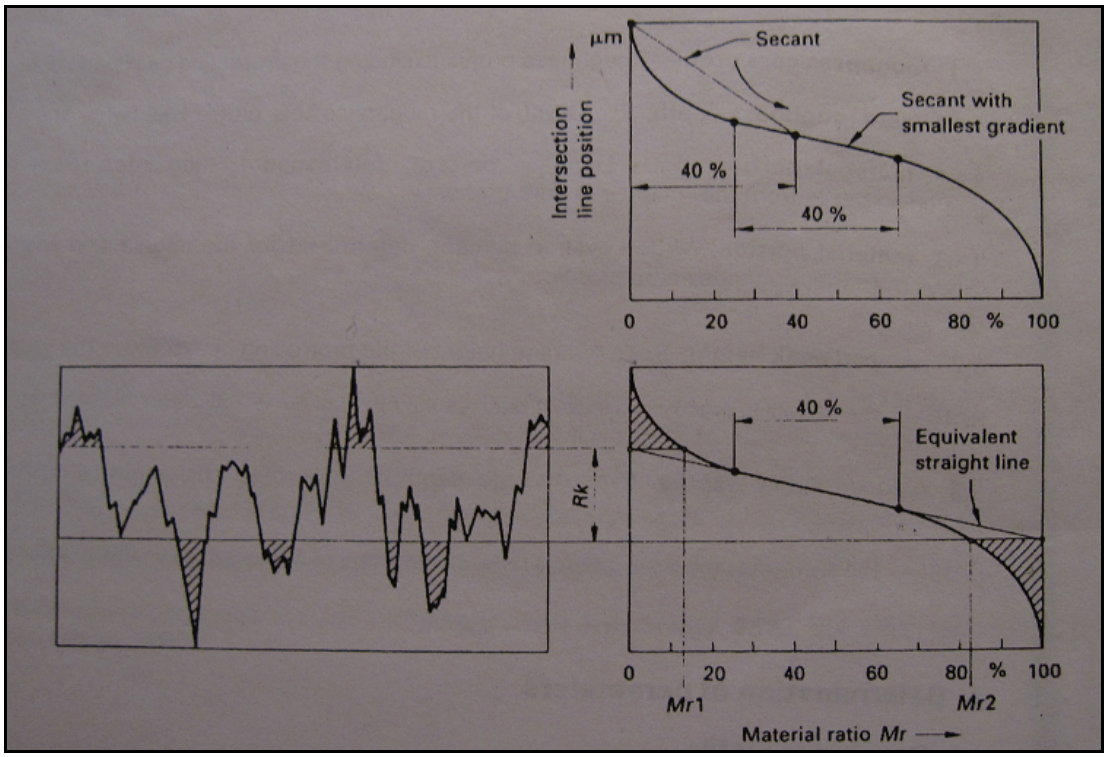

Figure 2-13 Determination of R_k, Mr1 and Mr2 parameters from BAC [24]

The parameters R_{pk} and R_{vk} are each calculated as the height of the right-angle triangle which is constructed to have the same area as the "peak area" or "valley area" respectively as in Figure 2-14. The right-angle triangle corresponding to the "peak area A1" has Mr1 as its base, and that corresponding to the "valley area A2" has 100 % - Mr2 as its base.

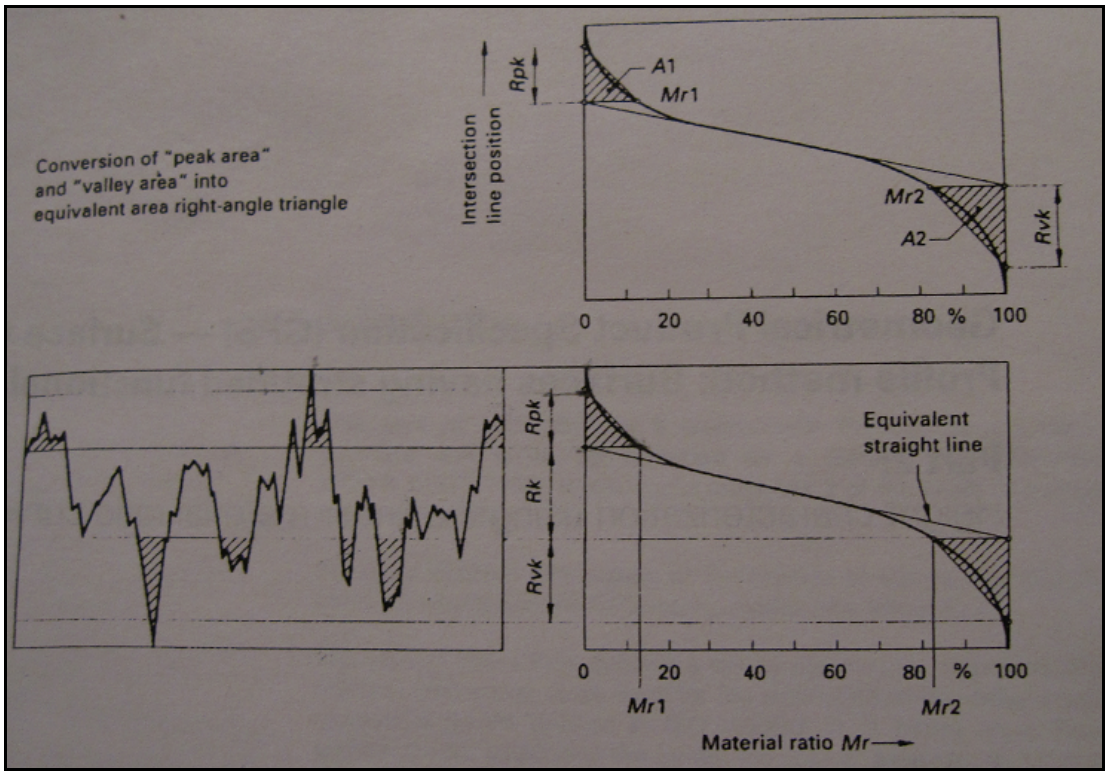

Figure 2-14 Determination of R_{vk} and R_{pk} parameters from BAC [24]

2.3.2 WEAR CALCUATION USING BAC

As specified before, BAC gives a detailed description about the surface morphology. Therefore, it is also used to calculate amount of wear between mating parts. Difference of areas under BAC between unused and used parts gives amount of worn material. According to a study made on "cylinder liner surfaces [25]", wear can be calculated by the help of areas under bearing areas curves as shown in Figure 2-15.

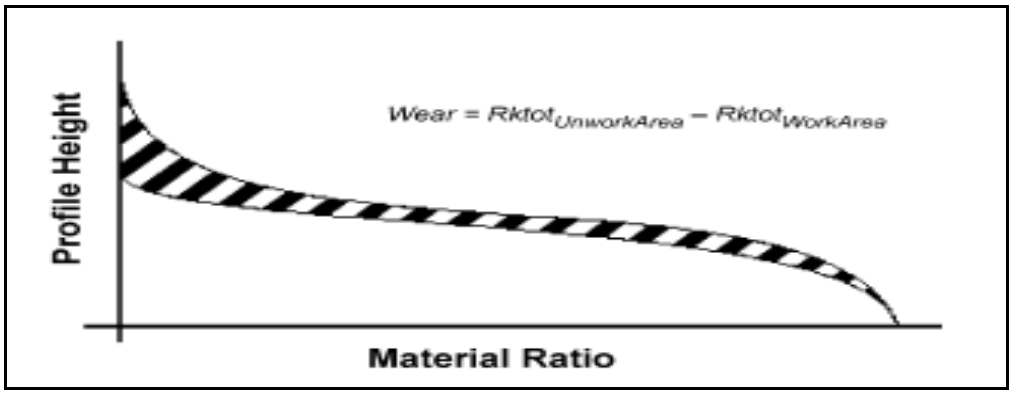

Figure 2-15 Calculation of wear amount using BAC [25]

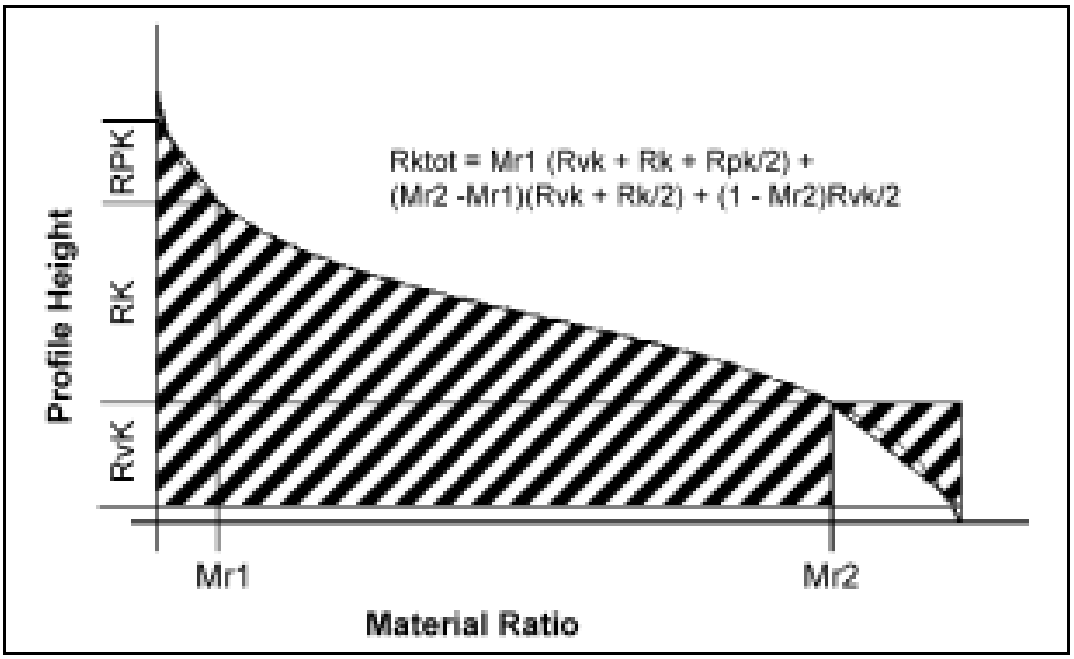

Figure 2-16 BAC parameters and area under BAC curve [25]

To calculate the amount of worn material a new surface roughness parameter is introduced which is called R_{ktot}. Figure 2-16 shows how R_{ktot} is calculated by the help of BAC parameters. R_{ktot} is a simplified integral of BAC curve as showed in Figure 2-16 and it can be defined as [25],

$$R_{ktot} = M_{r_1} \cdot \left(R_{vk} + R_k + \frac{R_{pk}}{2} \right) + \left(M_{r_2} - M_{r_1} \right) \cdot \left(R_{vk} + \frac{R_k}{2} \right) + \left(1 - M_{r_2} \right) \cdot \frac{R_{vk}}{2} \quad (2\text{-}12)$$

Therefore, the amount of worn material can be expressed as,

$$WEAR = R_{ktot_{unusedarea}} - R_{ktot_{usedarea}} \quad (2\text{-}13)$$

2.4 CONTACT OF ROUGH SURFACES

Area of contact which is dependent on properties of solid surfaces affects friction, wear and lubrication. Flat solid surfaces do not contact each other as they were seen on macroscopic scale. As it is mentioned in the above sections, all theoretical flat surfaces have asperities on them. Because of these asperities, two contacting surfaces contact on only peak asperity points as seen in Figure 2-17. This situation inevitably

creates high stresses on contact points. Deformation occurs on the asperities so that with high contacting load, more contacting surface is reached. Therefore, while examining contact of solid surfaces, it should be noted that there are two different areas between contacting surfaces, contact area and true contact area.

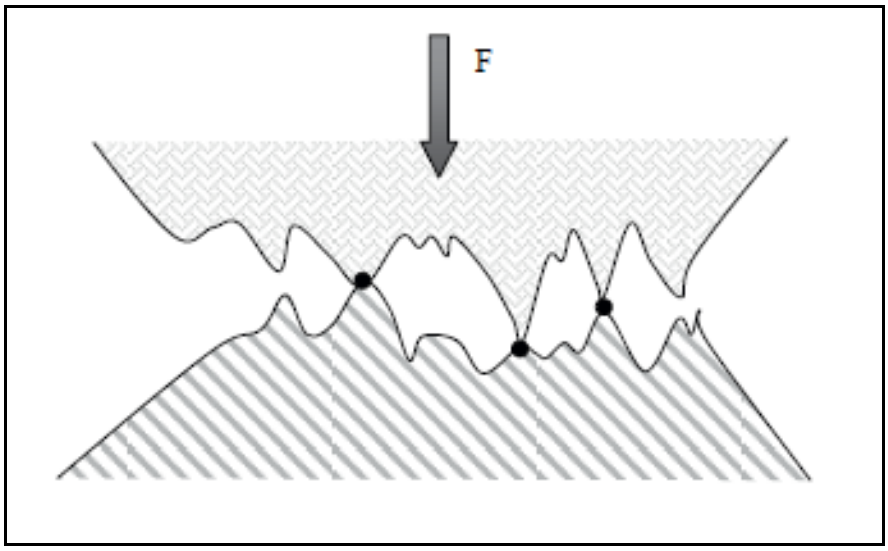

Figure 2-17 Contact of surface asperities [18]

According to Kragelsky, two contacting rough surfaces are firstly get in touch by their opposite peaks which have the largest sum of heights [18]. When more amount of load is applied to the mating parts, the number of contacting peaks increase. These peaks are deformed more with increasing load. At the beginning, the deformation on the peaks is elastic. However, with increasing number of deformed peaks, they go into plastic deformation. This will cause permanently shape changes in the microscopic structure of the surface.

The studies about contacting bodies had started by Heinrich Hertz in 1881. He had generally made calculations and experiments about elastic contact between solids. According to Hertzian contact theory, when two elastic spheres of radii "R_1" and "R_2" are got in touch with each other by applying a force "P" as shown in Figure 2-18, the half of width of contact distance can be calculated as [12],

$$a = \{3PR / 4E^*\}^{1/3} \tag{2-14}$$

where

$$\frac{1}{R} = \frac{1}{R_1} + \frac{1}{R_2} \tag{2-15}$$

$$\frac{1}{E^*} = \frac{1-\nu_1^{\,2}}{E_1} + \frac{1-\nu_2^{2}}{E_2} \tag{2-16}$$

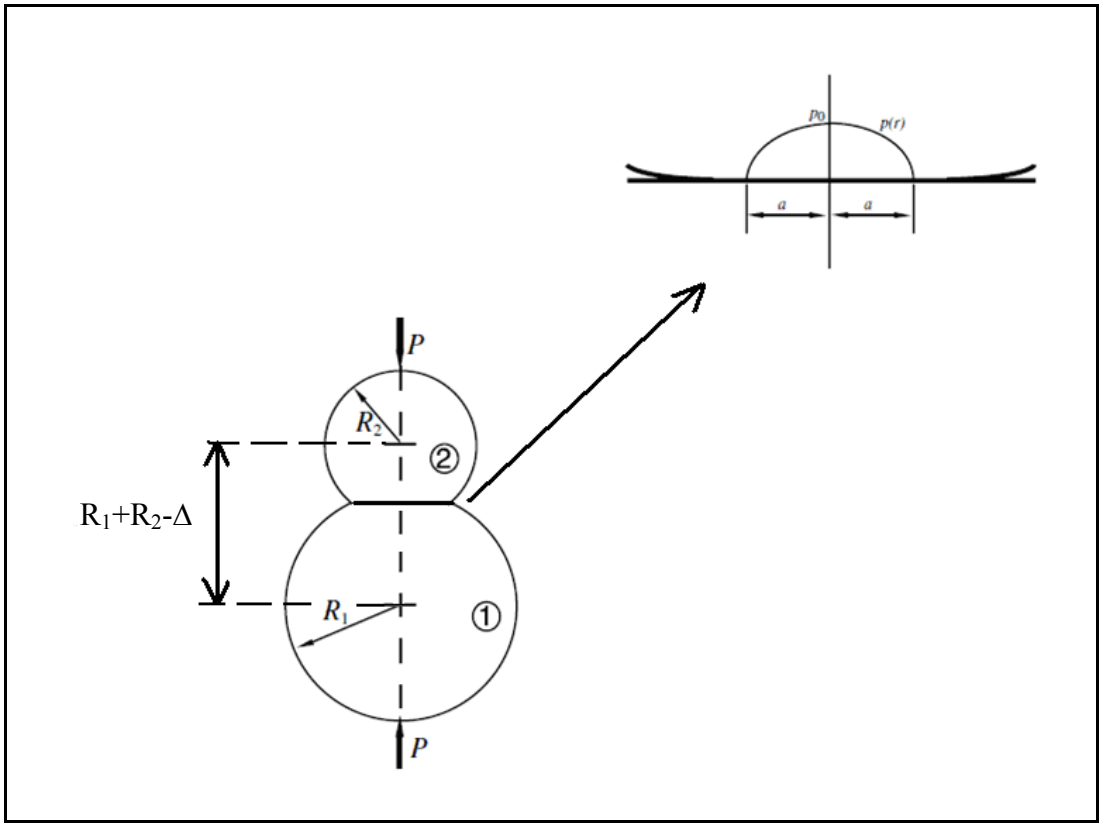

Figure 2-18 Spheres in elastic contact [12]

When two elastic spheres are in contact, there is a pressure distribution between them. As shown in Figure 2-18, maximum contact pressure "P_0" occurs at the axis of symmetry of the spherical contact and it can be calculated as,

$$P_0 = \frac{3P}{2\pi a^2} \tag{2-17}$$

Compared to sphere contact, Figure 2-19 shows the contact of two parallel axes cylinders. In this case, the half of contact with "b" and maximum contact pressure "P_0" can be computed as,

$$b = \{2PR / \pi E^*\}^{1/2} \tag{2-18}$$

$$P_0 = \left(PE^* / \pi R\right)^{1/2} \tag{2-19}$$

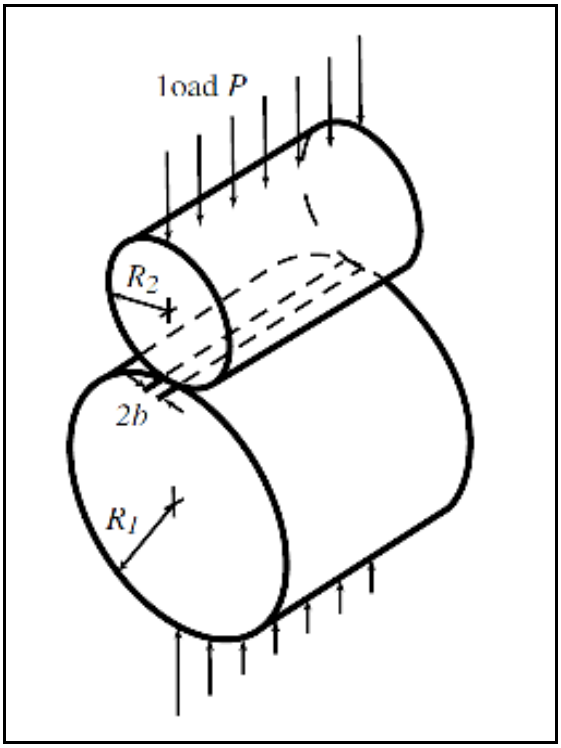

Figure 2-19 Two parallel axes cylinders in contact [12]

Hertzian theory allows calculating stress distribution in case of elastic contact. Hertz solved the problem of pressure distribution on the following assumptions [18]:

- Contacting bodies are smooth and homogeneous
- The contact forces are normal to contact surface
- The contact area is small compared with the area of contacting surfaces

Hertzian contact theory is useful to understand the reality behind the asperity contact. However, contact of two real surfaces is more complex than single asperity contact. One of the first developers of this model is Greenwood and Williamson [26]. Greenwood and Williamson assumed that all roughness peaks ("asperities") have the

same radius of curvature and that the height of the peaks is stochastically distributed around an average value as shown in Figure 2-20 [13].

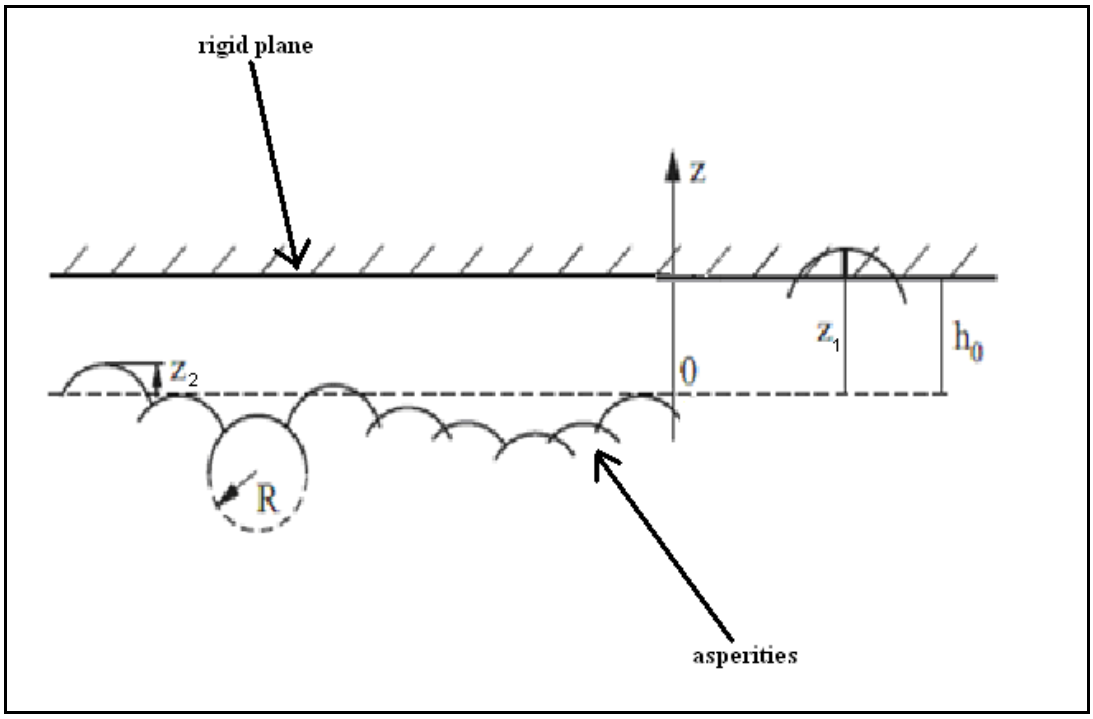

Figure 2-20 Model of Greenwood and Williamson [13]

It is obvious in Figure 2-20 that the asperities have a height bigger than h0 are in contact with the rigid plane. Therefore, total number of contacting asperities (N), area of contact (A) and total contact force (FN) are calculated as,

$$N = \int_{h_0}^{\infty} N_0 \Phi(z) dz \tag{2-20}$$

$$A = \int_{h_0}^{\infty} N_0 \Phi(z) \pi R (z - h_0) dz \tag{2-21}$$

$$F_N = \int_{h_0}^{\infty} N_0 \Phi(z) \frac{4}{3} E \times R^{1/2} (z - h_0)^{3/2} dz \tag{2-22}$$

where N_0 and E are total number of asperities and modulus of elasticity of the material, respectively. Φ(z) is the probability density function of the surface. As it

was mentioned before, height distribution of surfaces are generally considered as in normal distribution. Therefore,

$$\Phi(z) = (\frac{1}{2\pi R^2{}_q})^2 \cdot e^{\left(\frac{z^2}{2R^2{}_q}\right)} \tag{2-23}$$

Here, "R_q" is the root mean square of the distribution as it was mentioned before.

Surface roughness value of solid surfaces changes with in different types by the amount of deformed volume. As seen in Figure 2-21, type I shows steady wear in which surface roughness value does not change with worn volume. Type II shows increasing roughness value and type III shows decreasing value with increasing number of contact.

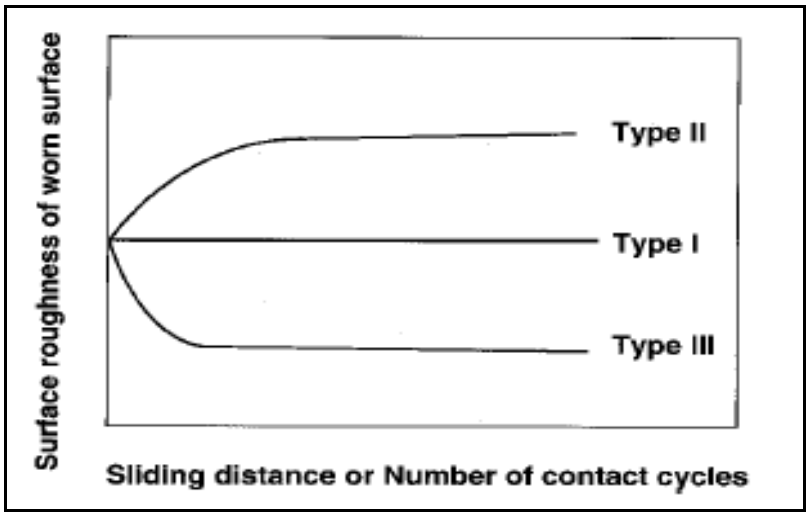

Figure 2-21 Surface roughness changes of repeated contacts [12]

CHAPTER 3

EXPERIMENTAL STUDY ON WEAR OF LAUNCHER RAIL

For inspection of material loss due to wear on the rail of launcher, a series of experimental studies and measurements are arranged. These studies are made parallel with the firing tests. There had been made a series of firing tests and all data about launcher wear is gathered from these tests.

3.1 EXPERIMENTAL SET-UP

As it is seen in Figure 3-1, test set-up is composed of a rail to aim the missile to the target, thermocouples to see temperature variations on the rail surface and strain gauges to inspect pressure of exhaust gases.

In Figure 3-1, there are 3 views which two of them are detailed view and one is side view of the missile and rail interface. As shown in Figure 3-2 and Figure 3-3, thermocouple is located near the sliding surface of the missile shoe and straingauge is located on the protective cap of the rail. The jet effect of exhaust gases would be seen most dominant on these locations.

According to Nyquist–Shannon sampling theorem, the sampling rate should be at least twice of the maximum frequency of examined data in order not to miss peak points of the gathered data [27]. Strain gauges and thermocouples give analog signal output. These analog signals are transferred to digital signal by the help of data acquisition system. Therefore, the most important equipment in test set-up is data acquisition system. Past experiences shows that temperature and pressure data signals may be gathered at about approximately 1500 Hz. Therefore, data acquisition system used in these tests is chosen to gather data in 2000 Hz. The technical specifications about the data acquisition system are given in the Appendix A.

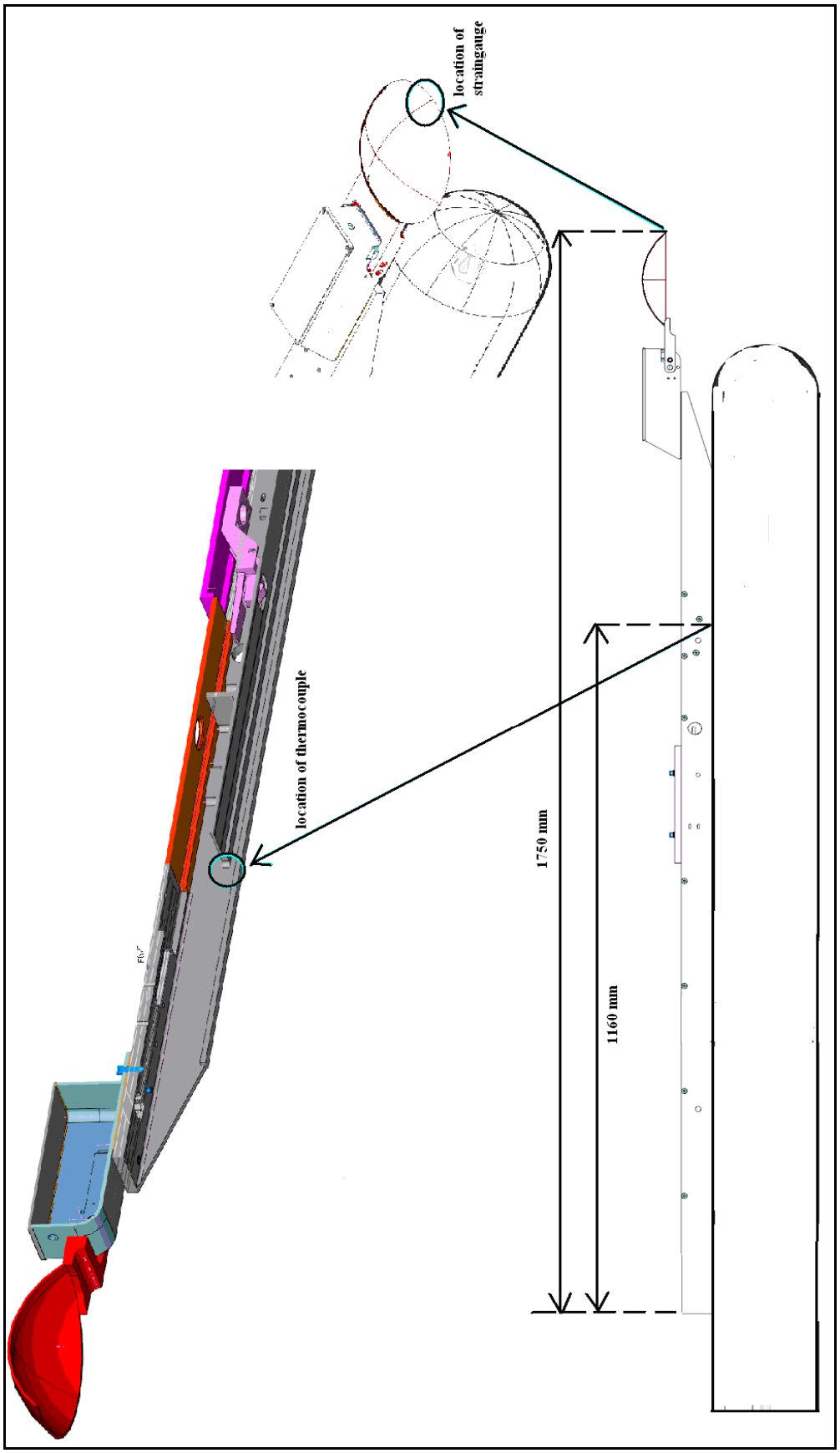

Figure 3-1 Schematic view of thermocouple and straingauges' locations on the test set-up

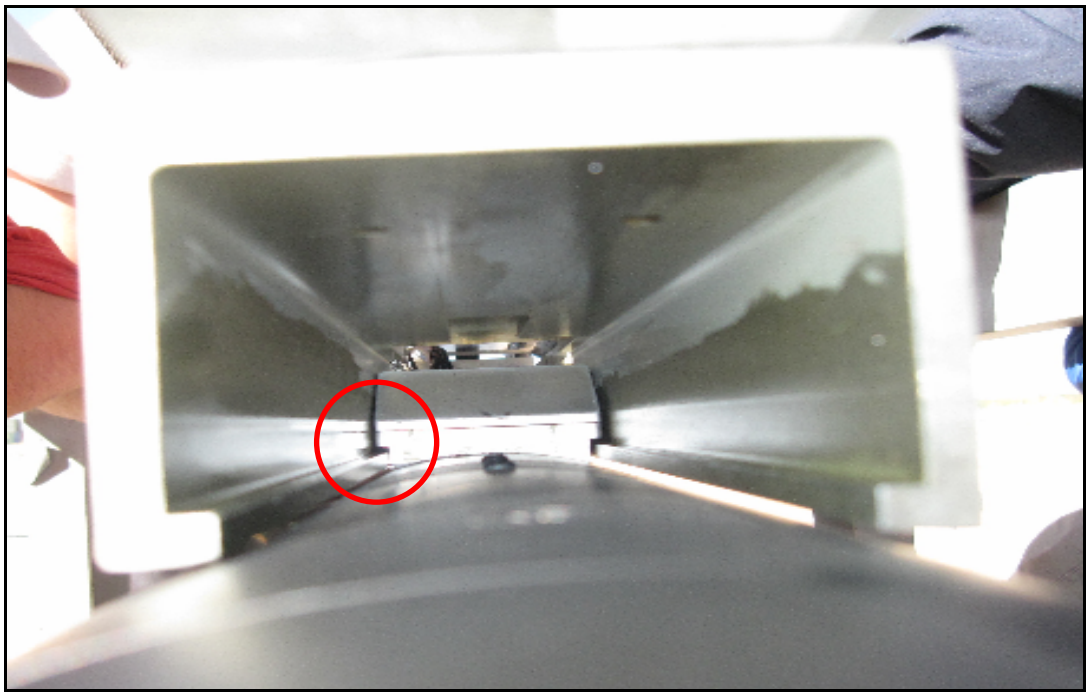

Figure 3-2 A view of thermocouple location on the rail (front view of the rail)

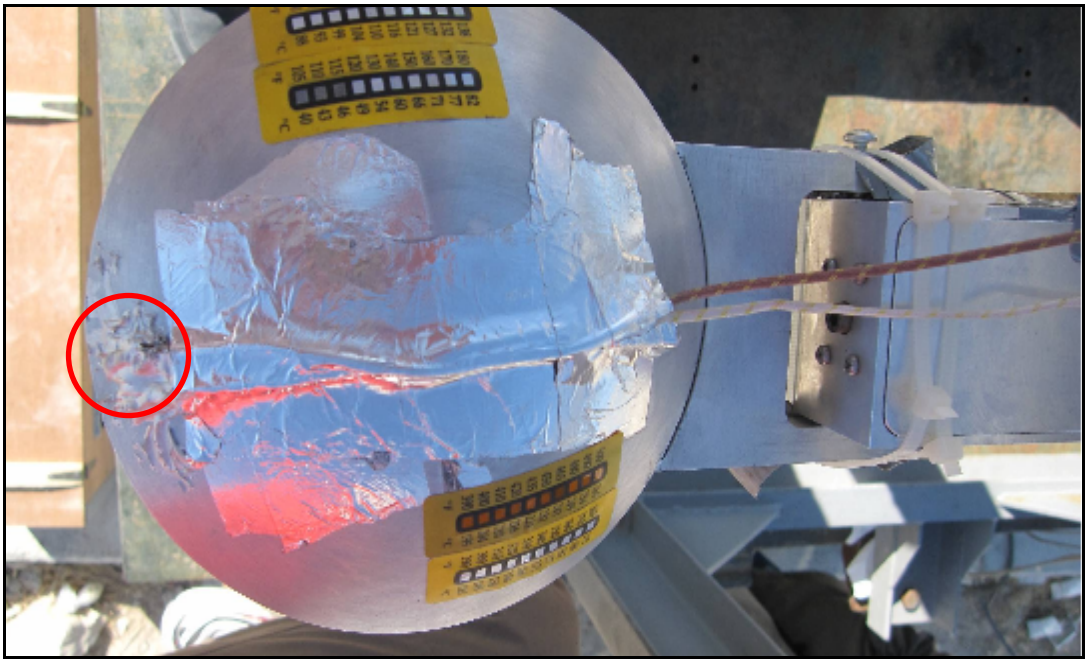

Figure 3-3 A view of strain gauge's location on protective cap (top view of the protective cap and rail)

3.2 TEST RESULTS

Totally, 3 firing tests were made to measure the surface temperature and pressure effects of rocket motor. All tests made with the same missile configuration. The average results of thermocouple measurements are shown in Figure 3-4 and the average results of straingauge measurements are given in Figure 3-5.

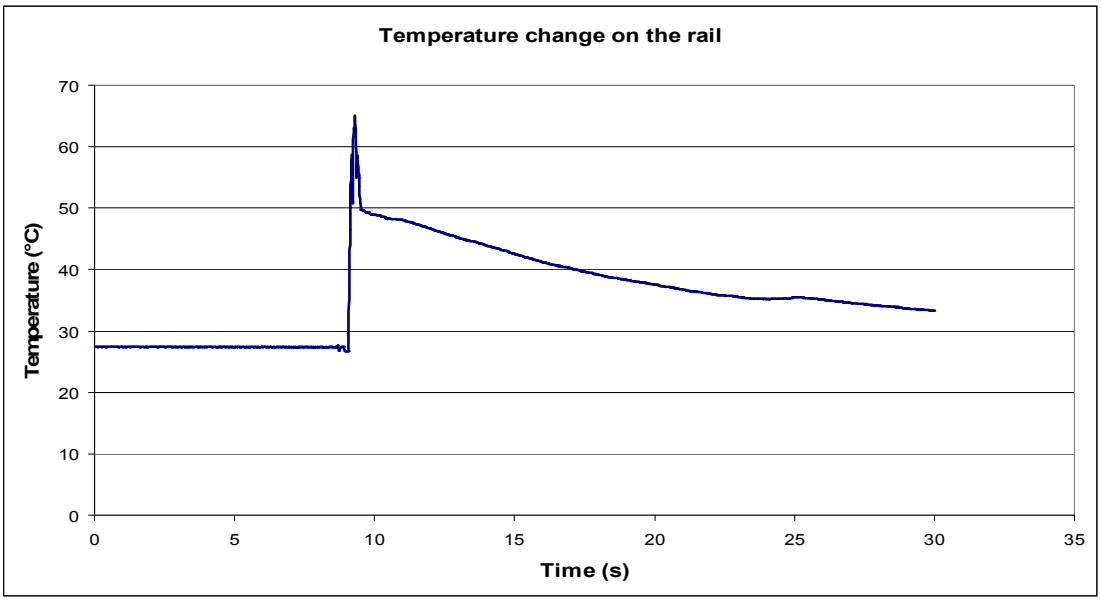

Figure 3-4 Thermocouple data after firing

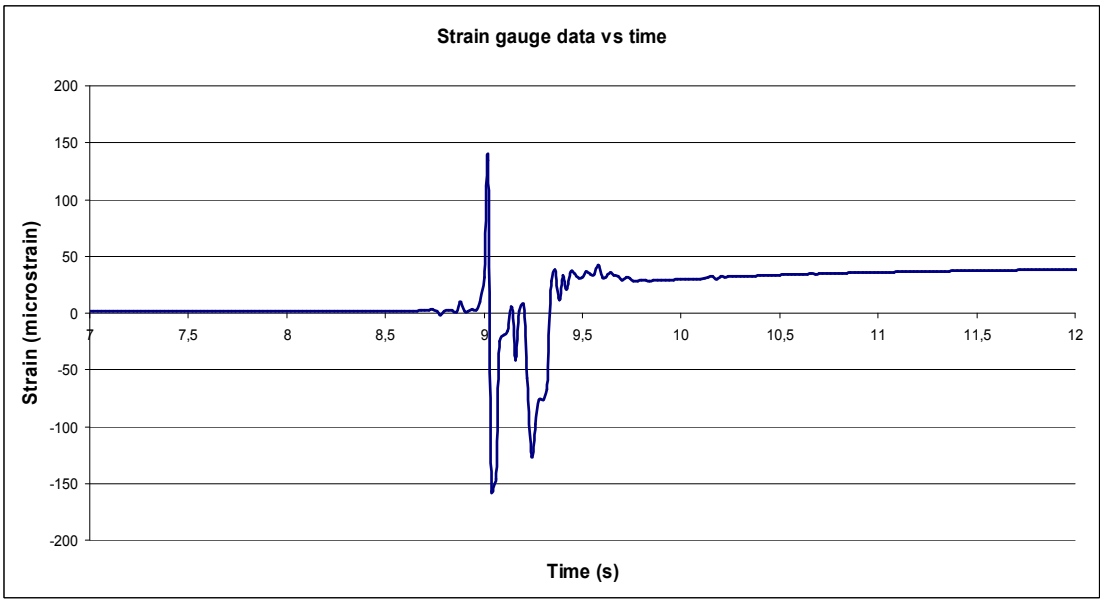

Figure 3-5 Strain gauge data after firing

As it is seen, the graphs have certain peak points. The values are approximately zero up to a time, and then they oscillate between peak points and converge to a certain degree. The reason of this is measurements began before launching time. In Figure 3-5, the straingauge data seems to converge a positive strain value after the firing of the missile. The reason for this result is certainly the thermal effect of missile jet. Thermal strain arises after firing and for a long time it affects the strain gauge measurement.

According to Figure 3-4 and Figure 3-5, the thermocouple measurements showed that the maximum temperature on the rail is about 65 ^{0}C. The strain gauge measurements were used in a commercial finite element program and the pressure which creates the maximum strain value (in Figure 3-5) on protective cap was evaluated. The results showed that the maximum 37 MPa of pressure is applied to the protective cap of the rail assembly by the rocket motor jet. It was decided that 37 Mpa of pressure could be ignored for this situation, but for at least rail material, 65 ^{0}C should be checked whether it has effect on strength of the aluminum material or not. The missile shoe and release latch are both made of steel material which is more durable to temperature changes than aluminum.

The Launcher rail is made from aluminum alloy. It is Al-2024-T851. In Table 3-1, some mechanical properties of this alloy is given. Moreover, the variation of the ultimate strength of material with temperature is given in Table 3-2.

Table 3-1 Mechanical properties of the launcher rail (Al-2024-T851) [28]

Density (gr/cm^3)	2.78
Hardness (Brinell)	128
Ultimate tensile strength (MPa)	483
Yield tensile strength (MPa)	448
Modulus of elasticity (GPa)	72.4
Poisons ratio	0.33
Melting temperature (^{0}C)	502-638

Table 3-2 Ultimate tensile strength of Al-2024-T851 at different temperatures [28]

Temperature (^{0}C)	**Ultimate tensile strength (MPa)**
371	34
316	52
260	76
204	186
149	379
100	455
24	483
-28	503
-80	510
-196	586

On Figure 3-6, a graph is shown to mention changes in ultimate tensile strength with respect to temperature. According to graph, if a temperature of 65 ^{0}C is considered, then ultimate tensile strength can be computed approximately 465 MPa.

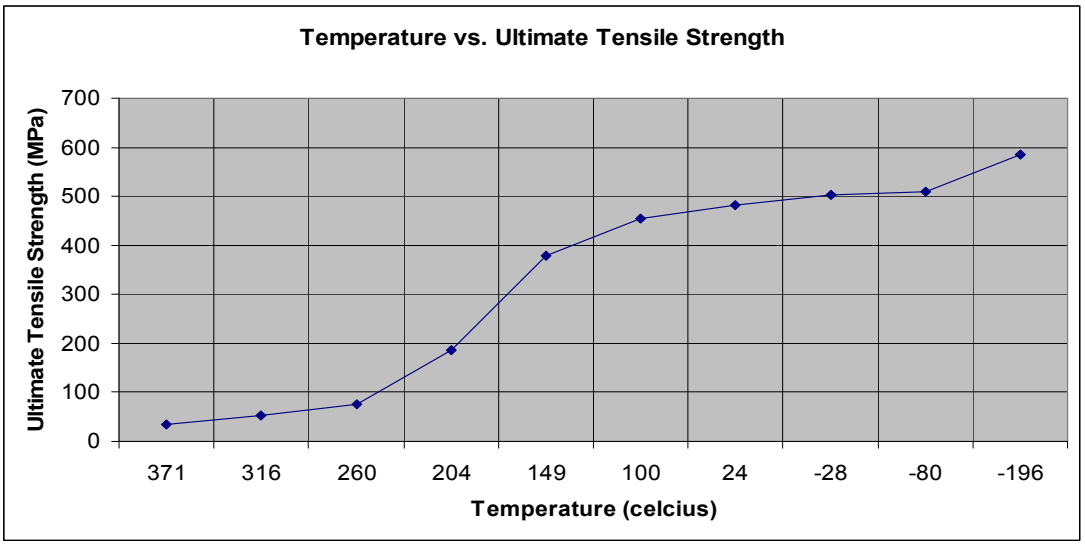

Figure 3-6 Ultimate Strength vs. Temperature of Al-2024-T851

Moreover, for changes in tensile yield strength of AL-2024-T851 at different temperatures, Table 3-3 is shown.

Table 3-3 Yield tensile strength of Al-2024-T851 at different temperatures [28]

Temperature (^{0}C)	**Tensile Yield strength (MPa)**
371	28
316	41
260	62
204	138
149	338
100	427
24	448
-28	469
-80	476
-196	538

Therefore, at 65 ^{0}C, the yield of Al-2024-T851 should be considered as 440 MPa.

3.3 WEAR MEASUREMENT METHODS

Wear measurement methods can be grouped as direct and indirect applications. Direct applications are used when it is possible to directly contact with the worn surface. However, it mostly is impossible to reach the worn surface in indirect methods.

Generally used direct measuring methods can be arranged as [29]:

- **Wear measurement by weighing:** It is the simplest method for wear measurement. However, an accurate mass balance should be made. Loss of material in wear applications is very small, in terms of milligrams, so little disturbances in mass can affect the test results. Moreover, displaced or transferred material during wear corrupts material mass data.
- **Stylus profilometry:** In stylus profilometry is a device, that creates a map of wear surface by the help of stylus on it, is used. Measurements are made before and after wear with device and the two maps of surfaces are compared by numerical techniques to compute loss of material.

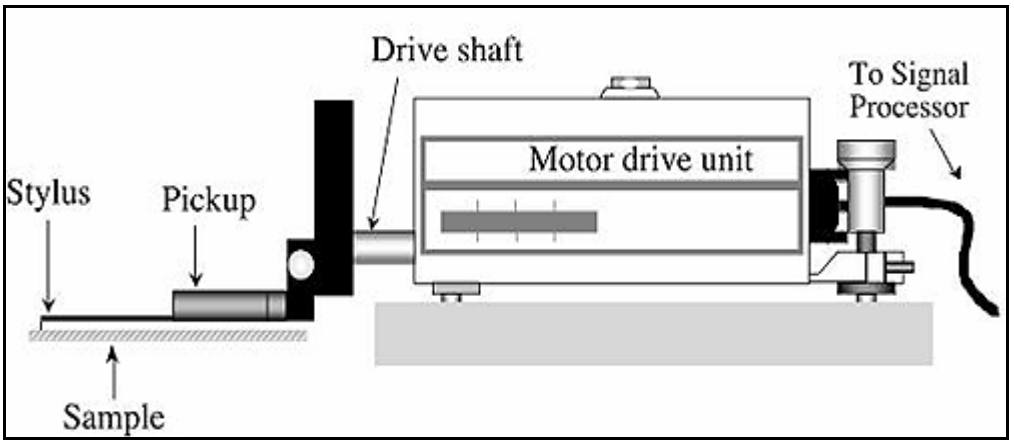

Figure 3-7 Schematic view of stylus profilometry [30]

- **Laser scanning profilometry:** As it is seen from below figure, a device that produces laser beams to the worn surface and measures the feedback of these beams from the worn surface is used in laser scanning profilometry. In the same time, lens tube is moved to supply maximum signal from the surface.

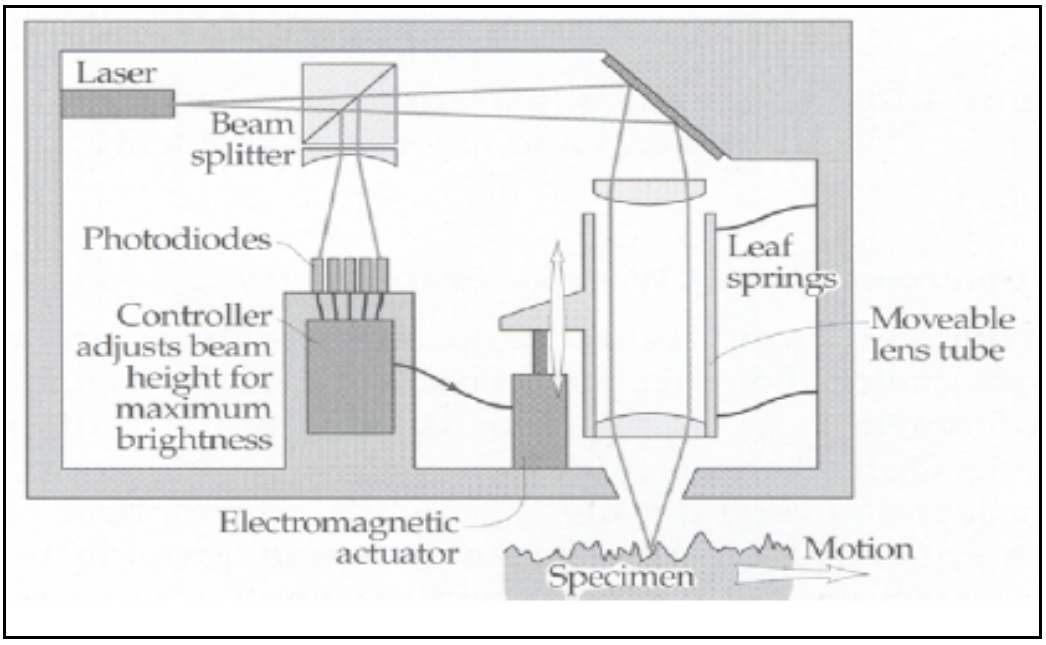

Figure 3-8 Schematic view of Laser scanning profilometry [29]

- **Optical profilometry:** This method can be expressed as reflecting an image of material surface on a screen and measuring the adjustment in dimension of

the silhouette of the worn specimen. This method is generally used for simple shape object such as pins.

- **Surface activation:** In surface activation, the interested surface is activated with radioactive rays. Then, it is allowed to wear. After wearing process, the interested surface is examined with a radioactive-ray spectrometer and the change in activity shows the amount of wear.
- **Ultrasonic interference** [31]**:** This technique requires highly specialized personnel. Real time wear can be measured by this method. While specimens are worn, ultrasonic beams are send to worn surface and the send-back data is collected to calculate loss of material. The method is very exquisite so that 1 μm dimensional changes can be realized.

The advantages and disadvantages of the above methods are shown in Table 3-4.

Table 3-4 Comparison of direct wear measuring methods [29]

Method	***Advantages***	***Disadvantages***
Weighing	*Simple and accurate*	*Data corrupted by displaced or transferred material*
Stylus profilometry	*Very accurate. Gives distribution of wear between specimens.*	*Slow and mostly suitable for the end of the test. Expensive equipment required.*
Laser scanning profilometry	*Very accurate and fast. Gives distribution of wear between specimens.*	*Expensive equipment required.*
Optical profilometry	*Simple and rapid.*	*Method impossible when the specimen has complex shape or its shape is distorted by wear or creep under load.*
Surface activation	*Possibility of simultaneous measurement of wear rates of various parts.*	*Inaccurate and difficult to ensure safety or personnel*
Ultrasonic interference	*Sensitive to small changes in dimension.*	*Specialized technique that requires expertise.*

On the other hand, measuring wear directly is not possible in all cases. Accessing contact of specimens is sometimes impossible. For these situations, indirect methods of measuring wear are used. These methods do not measure wear but they measure the resultant source of data which are caused by wear. For example, heat, noise and vibration are formed because of wear. These data can be measured and a relation can be made with wear. In fact, these relations should de made carefully because heat, noise and vibration sources can be different from wear in mechanical systems.

Wear measurement in this thesis work were made by using stylus profilometry. The measurements were made in Department of Metallurgical and Materials Engineering of Dokuz Eylül University. The stylus is Ambios XP-2 surface profile meter as seen in Figure 3-9.

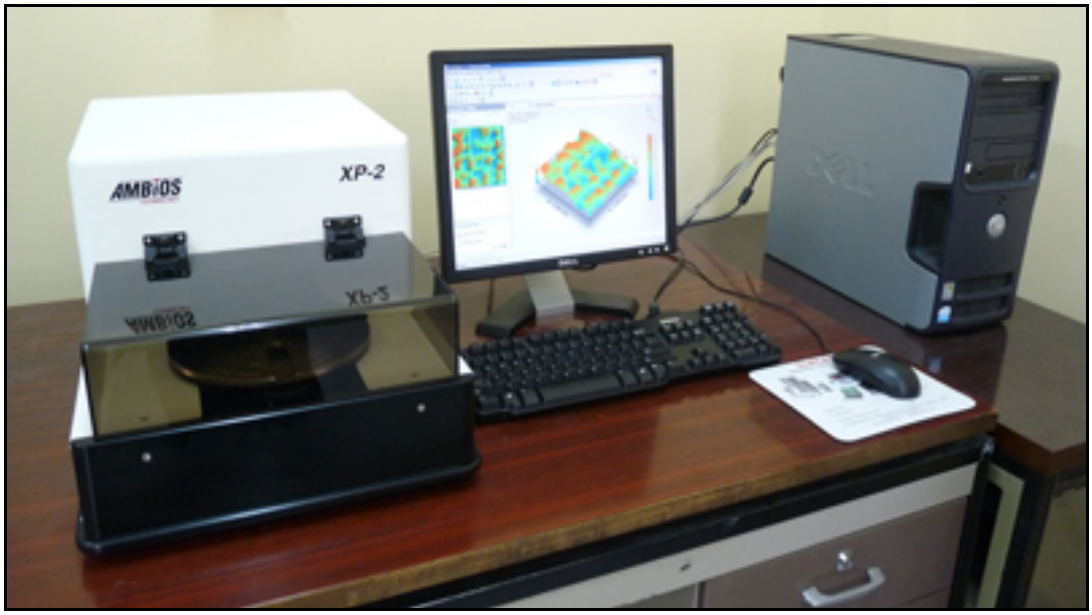

Figure 3-9 A view of Ambios XP-2 surface profile meter

The measurements were made for two different launcher rails. One is unused rail and one is used rail in firing tests. The aim is to create their surface map and compare to calculate material loss after firing of the missile.

Since the rail of launcher is approximately 1500 mm in length, it is not possible to mount it on the surface profile meter. Therefore, a prediction was made about the most worn surface on the launcher rail, and this surface is cut out from the rail to make measurements.

For making prediction, a simple free body diagram of rail is formed as shown in Figure 3-10. "W" defines the weight of the missile. "F_1", "F_2" and "F_3" are the three reaction forces on the rail due to the mass of the missile. The locations of the reaction forces are on the missile shoes which have mechanical interfaces between rail and missile.

The equations of equilibrium can be written as:

$$F_1 + F_2 + F_3 = W \tag{3-1}$$

$$(D - C)F_1 = (B + C - D)F_2 + (A + C - D)F_3 \tag{3-2}$$

where A,B,C and D represents distance between front and rear shoe, distance between middle and rear shoe, distance between rear shoe and rear face of missile and axial center of gravity of the missile with respect to rear face, respectively.

However, these equations represent an indeterminate system (two equations, three unknowns). Therefore, an approximation was made. In order to keep safety of the system, one of the shoes (F_3) on the missile was neglected. The reason why F_3 was neglected is that its main responsibility is to mount the electrical interface between the missile and the launcher, and to reduce the vibration effects caused by rail on the missile. Then:

$$F_1 + F_2 = W \tag{3-3}$$

$$(D - C)F_1 = (B + C - D)F_2 \tag{3-4}$$

The calculations on these formulas are given in Appendix B. It was realized that due to heavy load on the missile shoe, the most heavily worn part of the rail corresponds to the middle shoe of the rocket. Therefore, the measurement studies were made on this region of the rail.

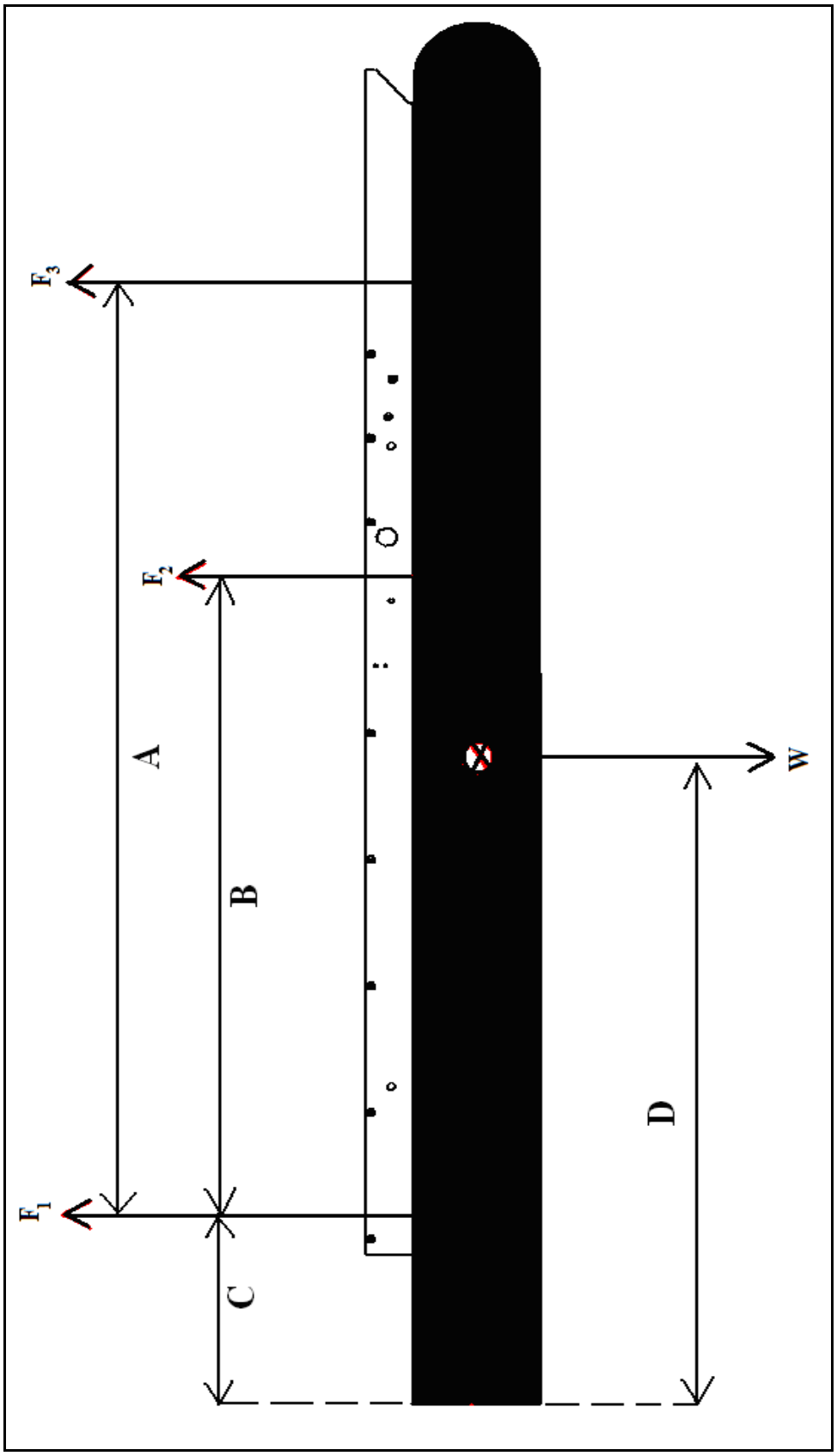

Figure 3-10 Reaction forces of the shoes on the launcher rail

3.4 WEAR MEASUREMENTS ON THE TEST RAILS

Two test rails were used in measurement works. One is a used rail and the other is unused rail. Used rail have been used in 10 (ten) firing tests. Therefore, at the end of measurements the amount of worn material measured would exist after 10 (ten) firing tests. Measurements were made on these rails and then compared in order to evaluate the amount of worn material. Unused rail is chosen randomly from manufactured rails because it is thought that all rails are manufactured in the same CNC machine with the same methods so all of them have identical surface profiles.

The specified region of the test rails were cut out as shown in Figure 3-11. Middle shoe of the missile is in contact with this region of the rail. The surface profile measurements were made on these parts. A sample cut out part is shown in Figure 3-12.

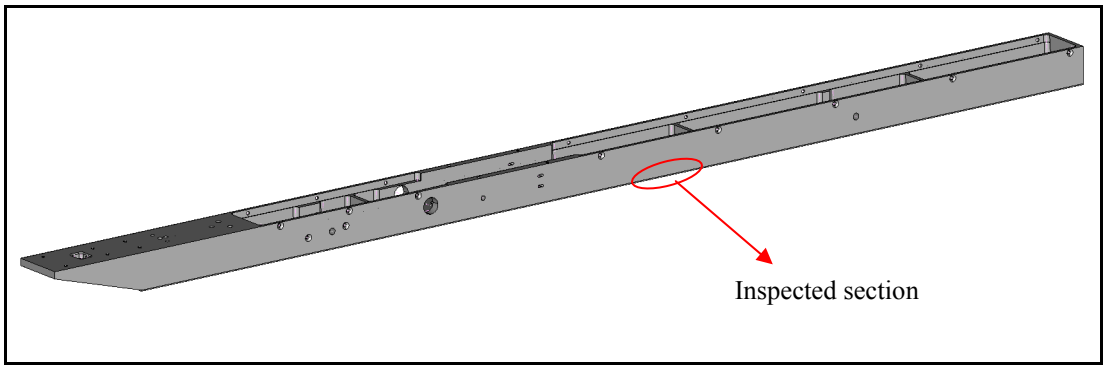

Figure 3-11 A view of inspected section on the rail

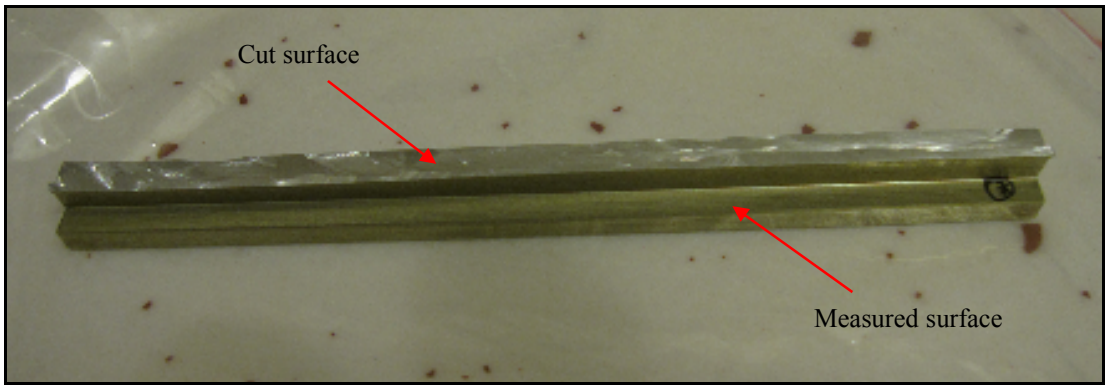

Figure 3-12 A view of measured rail part

As seen in Figure 3-13, the measurements were made for three parts. Two of them are on the right and left sides of the used rail and one of them is on the unused rail. In order to minimize the measurement errors, the measurements have been made on three locations for each part, except unused rail. It is assumed that all regions of unused rail will be in similar surface profile because there is no wear on its surface.

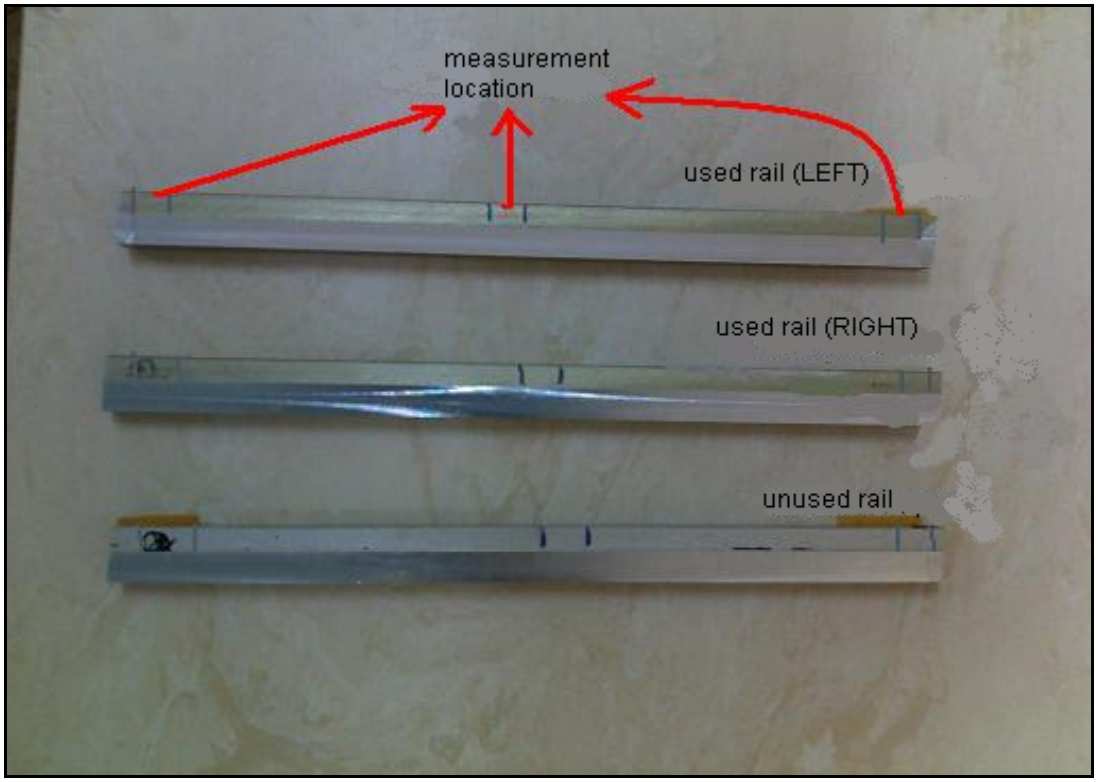

Figure 3-13 A view of measurement locations on the rails

During firing of the missile, all three measurement regions on the parts are in contact with the middle shoe. The location of the middle shoe on the measured rail region is given as a schematic view in Figure 3-14.

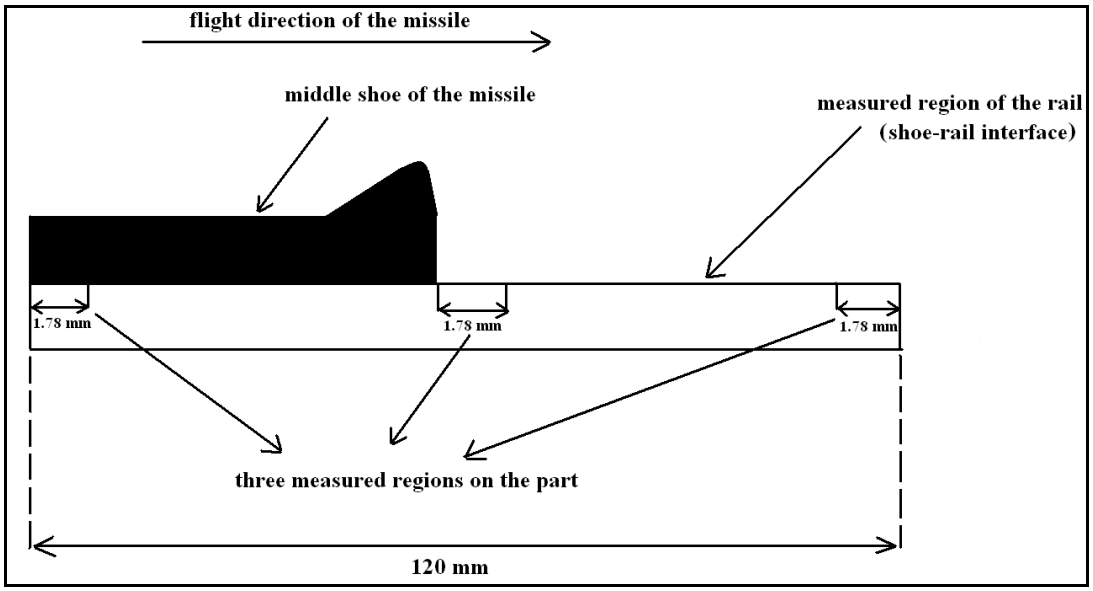

Figure 3-14 A schematic view of inspected part with middle shoe of the missile

3D surface profiles of the rails are shown below in Figure 3-15, Figure 3-16 and Figure 3-17. As seen, the measurements are taken for a 1.78 mm x 1.80 mm area. These shown measurement results are for middle region of the inspected parts. All measurement results are shown in Appendix B.

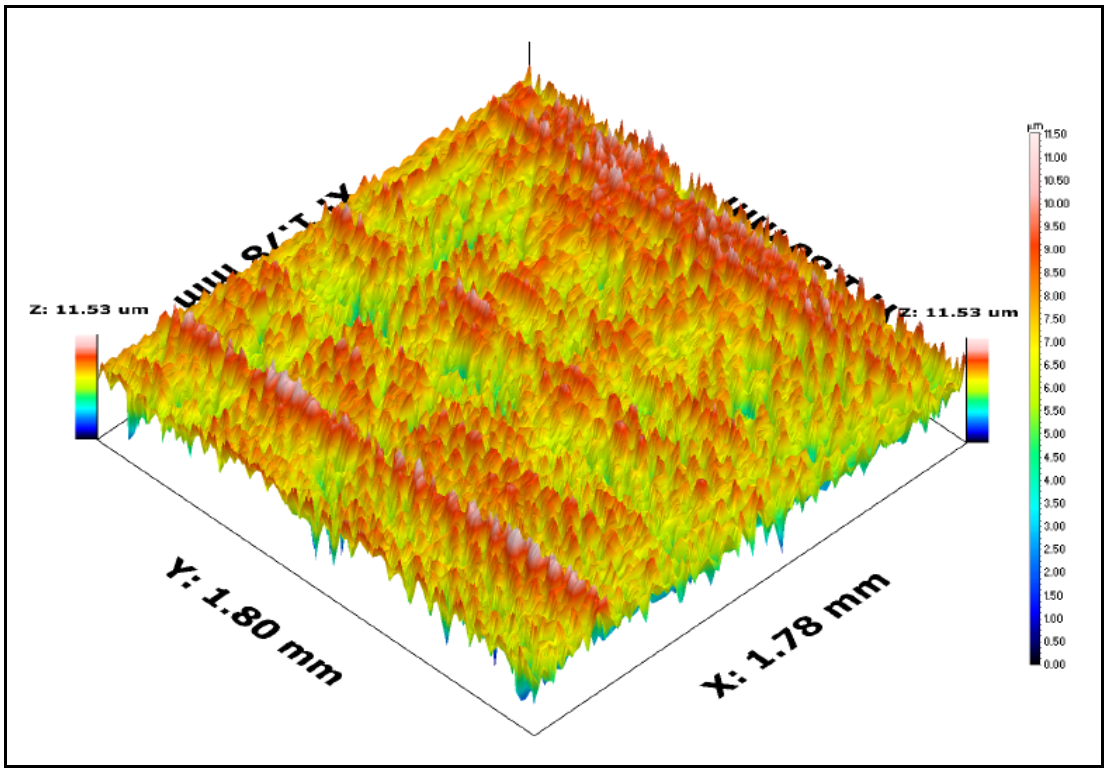

Figure 3-15 3D surface profile of the right side of the used rail

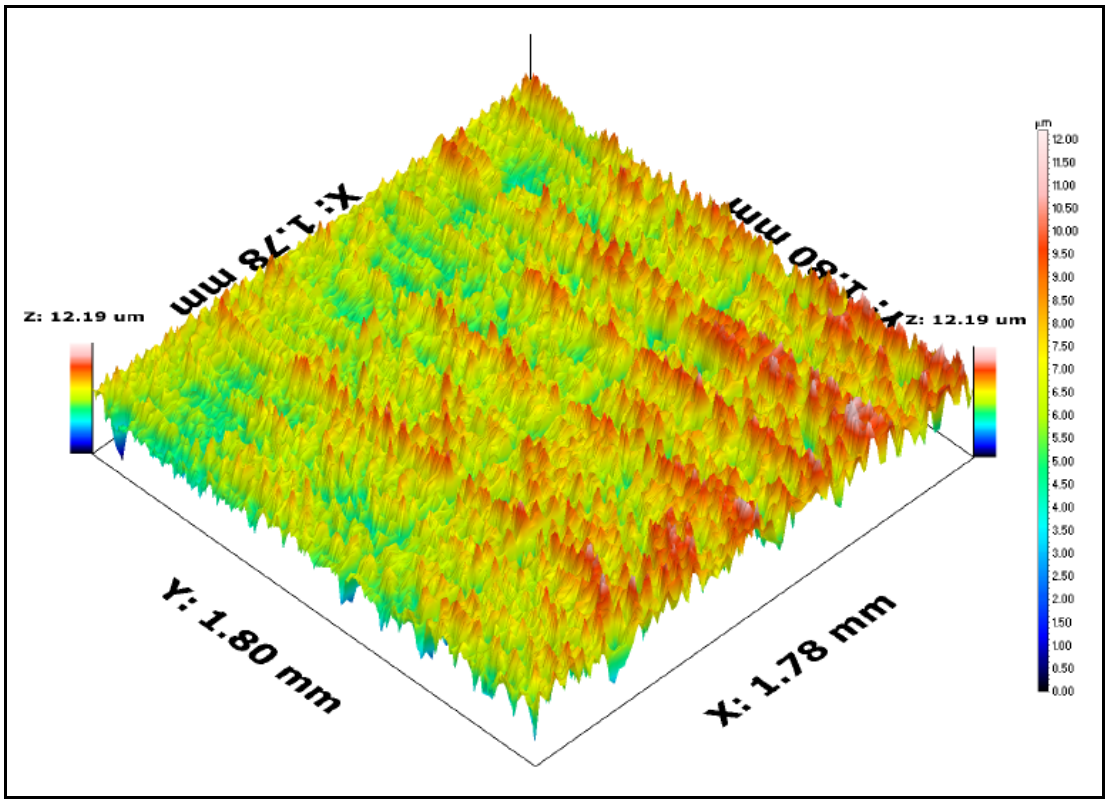

Figure 3-16 3D surface profile of the left side of the used rail

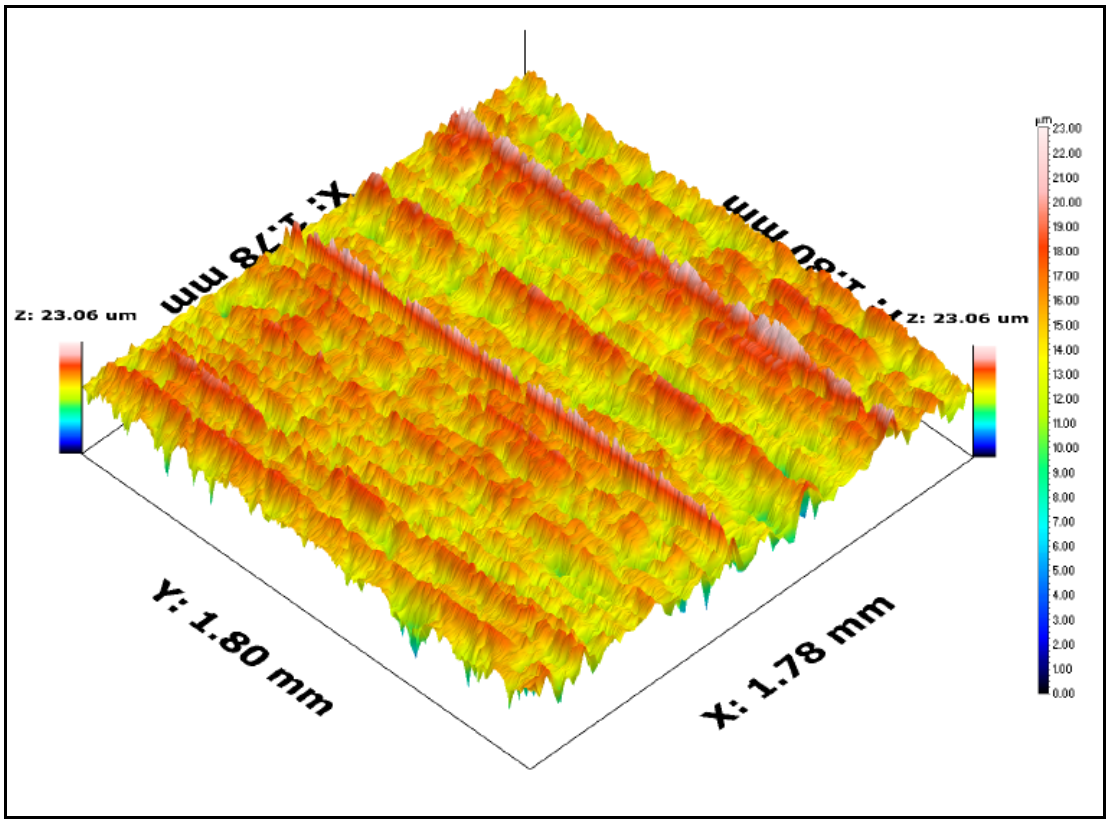

Figure 3-17 3D surface profile of the unused rail

As described in section 2.3.2, in order to calculate the amount of worn material, BAC's of the surfaces were evaluated and BAC's of the used and unused rails are compared. The results are shown in Figure 3-18, Figure 3-19 and Figure 3-20. All BAC's of measured regions are shown in Appendix B.

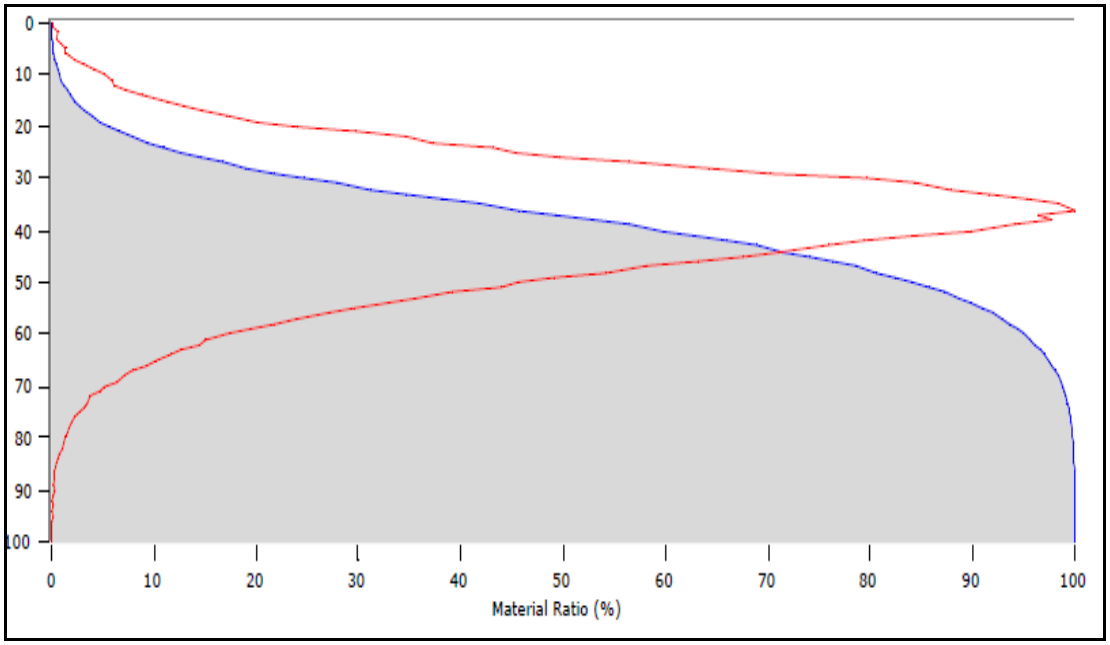

Figure 3-18 BAC of the right side of the used rail

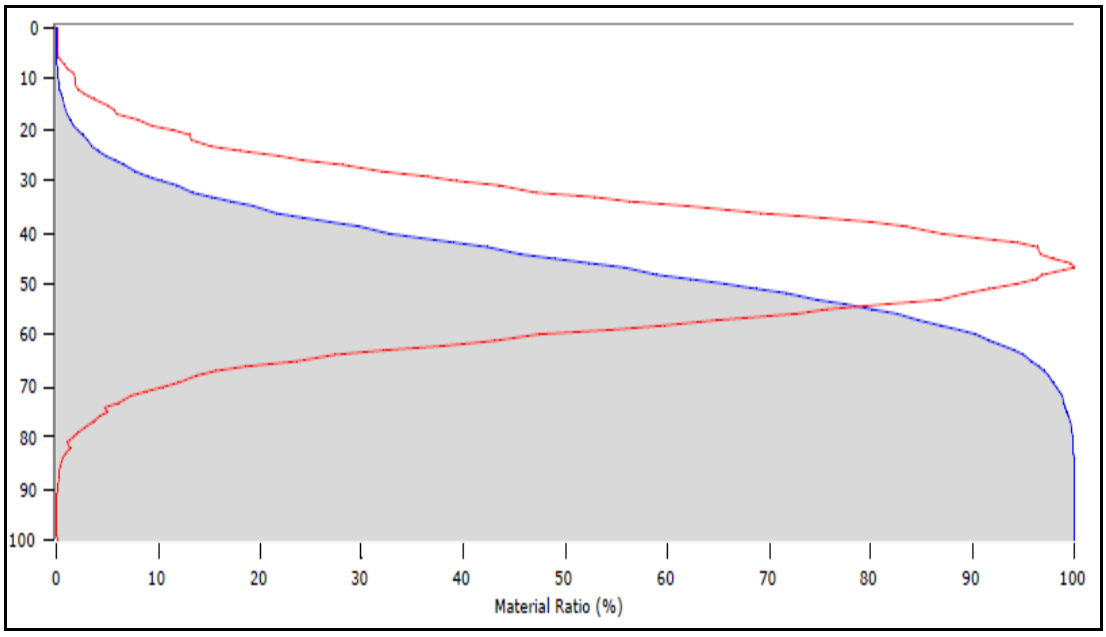

Figure 3-19 BAC of the left side of the used rail

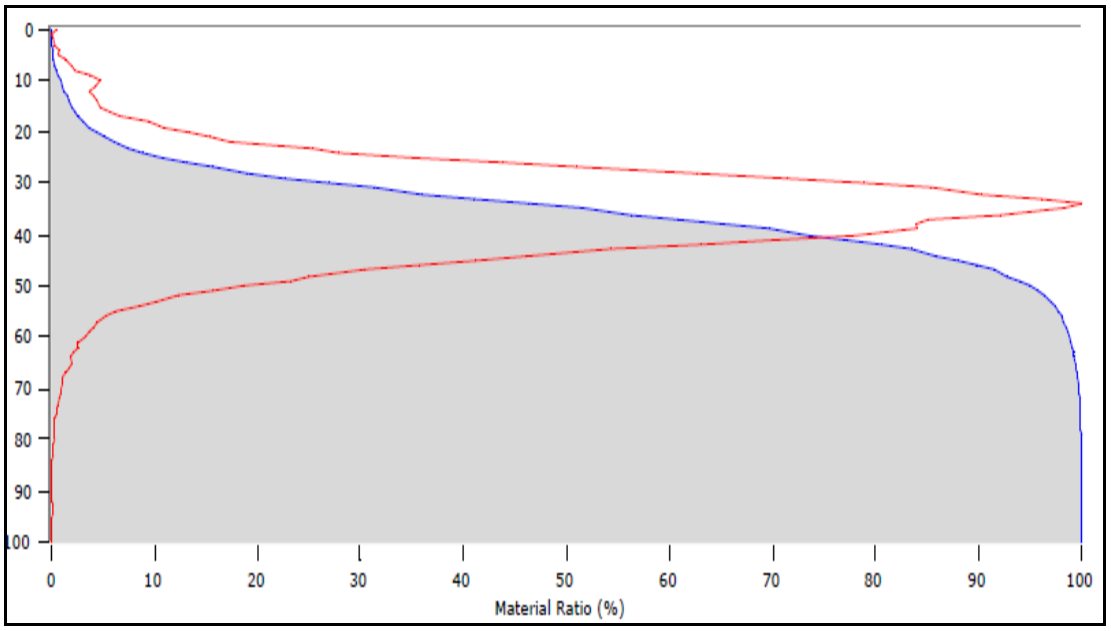

Figure 3-20 BAC of the unused rail

For evaluating integrals of these BAC's curve parameters were calculated by the help of Ambios XP-2 surface profile meter. As described in section 2.3.1, calculated BAC parameters are given in following tables. The tables of parameters for all measured regions are shown in Appendix B.

Table 3-5 BAC parameters of the right side of the used rail

PARAMETERS	VALUES	DESCRIPTION
R_k (µm)	3.34	Core roughness depth
R_{vk} (µm)	1.80	Reduced valley depth
R_{pk} (µm)	1.21	Reduced peak height
Mr1 (%)	9.045	Material ratio 1
Mr2 (%)	86.834	Material ratio 2

Table 3-6 BAC parameters of the left side of the used rail

PARAMETERS	VALUES	DESCRIPTION
R_k (μm)	3.76	Core roughness depth
R_{vk} (μm)	1.31	Reduced valley depth
R_{pk} (μm)	1.48	Reduced peak height
Mr1 (%)	10.185	Material ratio 1
Mr2 (%)	91.302	Material ratio 2

Table 3-7 BAC parameters of the unused rail

PARAMETERS	VALUES	DESCRIPTION
R_k (μm)	4.84	Core roughness depth
R_{vk} (μm)	2.75	Reduced valley depth
R_{pk} (μm)	2.55	Reduced peak height
Mr1 (%)	9.572	Material ratio 1
Mr2 (%)	88.626	Material ratio 2

As described in section 2.3.2, a quick and good estimation of worn material can be obtained by evaluating R_{ktot} value which is given in equations (2.12) and (2.13).

The related calculations are given in Appendix B. In Appendix B, these calculations are made for three regions separately. In other words, three regions of the inspected parts are compared separately. The average of the three results is considered as the amount of worn material in order to decrease measurement errors.

As shown in Appendix B, wear calculations were made for all regions of measured parts. Approximately, 1.266 μm (micrometers) wear depth was calculated on the rail surface with respect to the test results.

As shown in Figure 3-21, 1.266 μm corresponds to an average decrease in the thickness of the measured rail part. This result will be used to compute "K" (wear constant) in modeling applications in the next chapter.

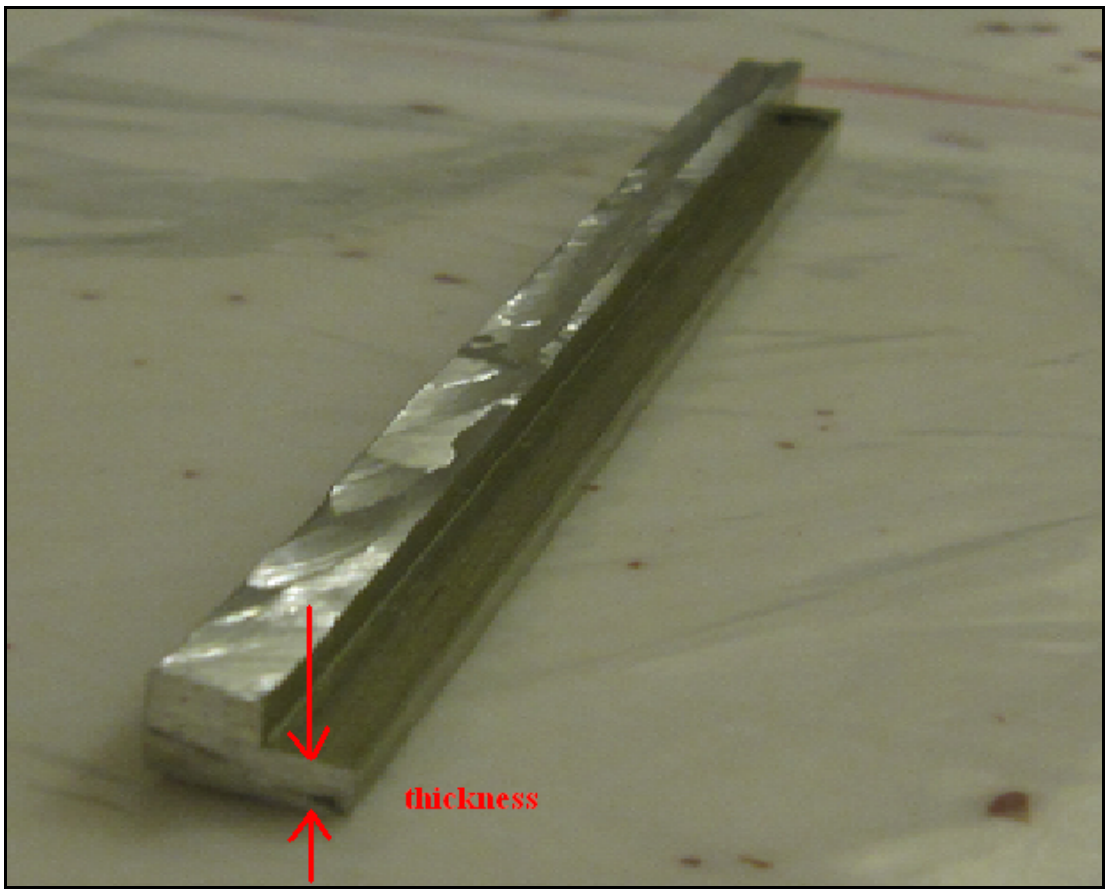

Figure 3-21 The thickness of the inspected rail part

3.5 WEAR MEASUREMENTS ON THE RELEASE LATCH

Similar to rail measurements, two release latches are used to evaluate the amount of wear. Surface profile measurements made by the used latch and unused latch. Then, the two profiles were compared in order to compute the amount of wear. However, it should be noted here that the used latch like used rail were used for 10 (ten) firing tests, so the evaluated amount of wear exists after ten firing tests.

In Figure 3-22, the inspected surface of the release latch is shown. The reason why this surface is chosen is it is the contacting surface of the latch with the middle shoe of the missile.

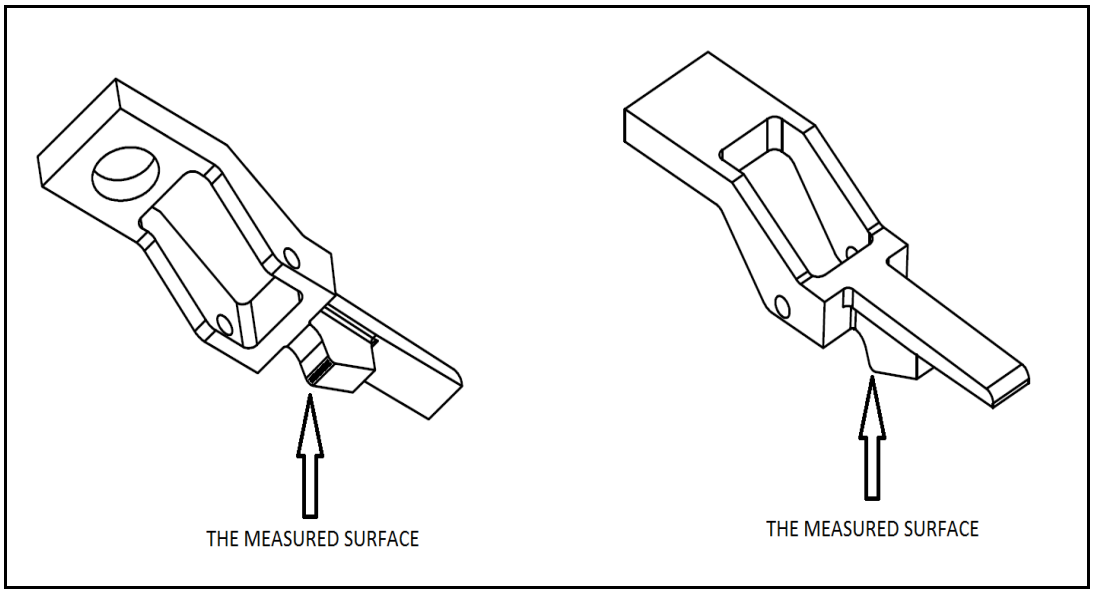

Figure 3-22 The measured surface in used and unused release latches

Firstly, the unused latch surface profile is swept by the surface profilometer. In Figure 3-23, the output of surface profilometer is shown. It should be noted that the shown graph is μm versus mm. The vertical axis shows the surface depth in terms of μm and the horizontal axis shows the length of the measured surface in millimeters.

In Table 3-8, the bearing area curve parameters of the surface are shown. As it is mentioned before, these parameters are used to compute amount of worn material.

Similar to these graph and table, in Figure 3-24 and Table 3-9 the surface profile and BAC parameters of the used latch are given, respectively.

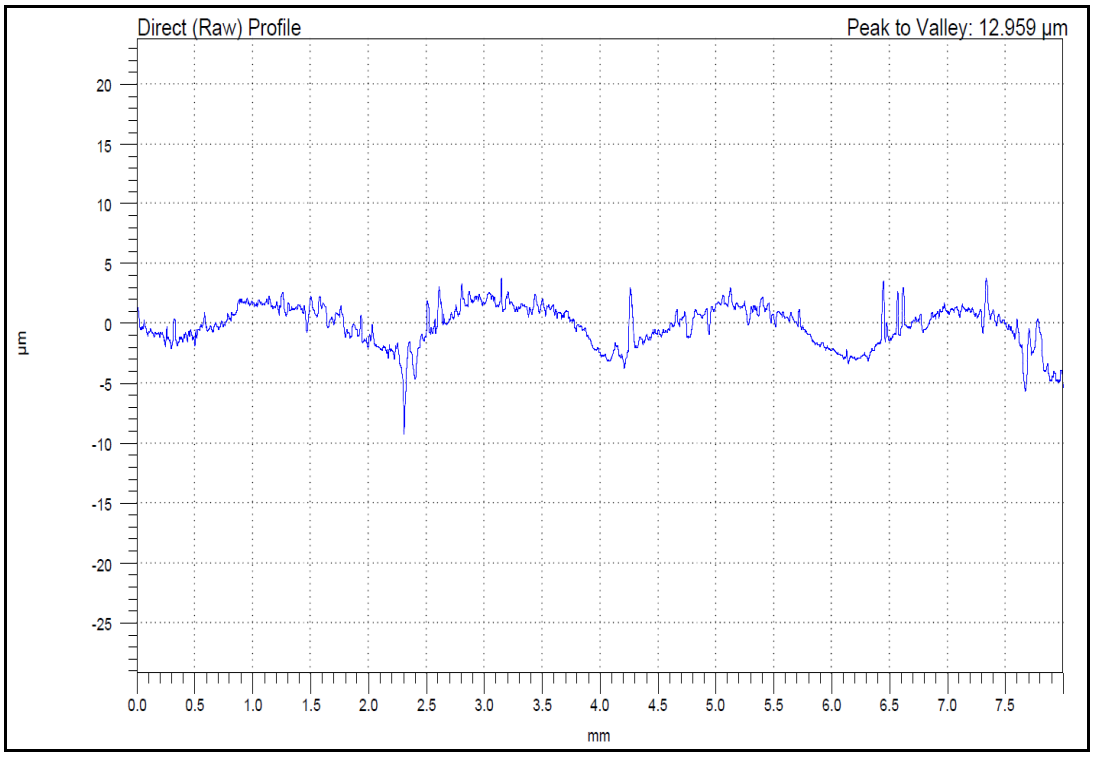

Figure 3-23 The surface profile of the unused release latch

Table 3-8 BAC parameters of unused release latch surface profile

PARAMETERS	VALUES	DESCRIPTION
R_k (µm)	4.972	Core roughness depth
R_{vk} (µm)	7.281	Reduced valley depth
R_{pk} (µm)	6.227	Reduced peak height
Mr1 (%)	11.62	Material ratio 1
Mr2 (%)	82.98	Material ratio 2

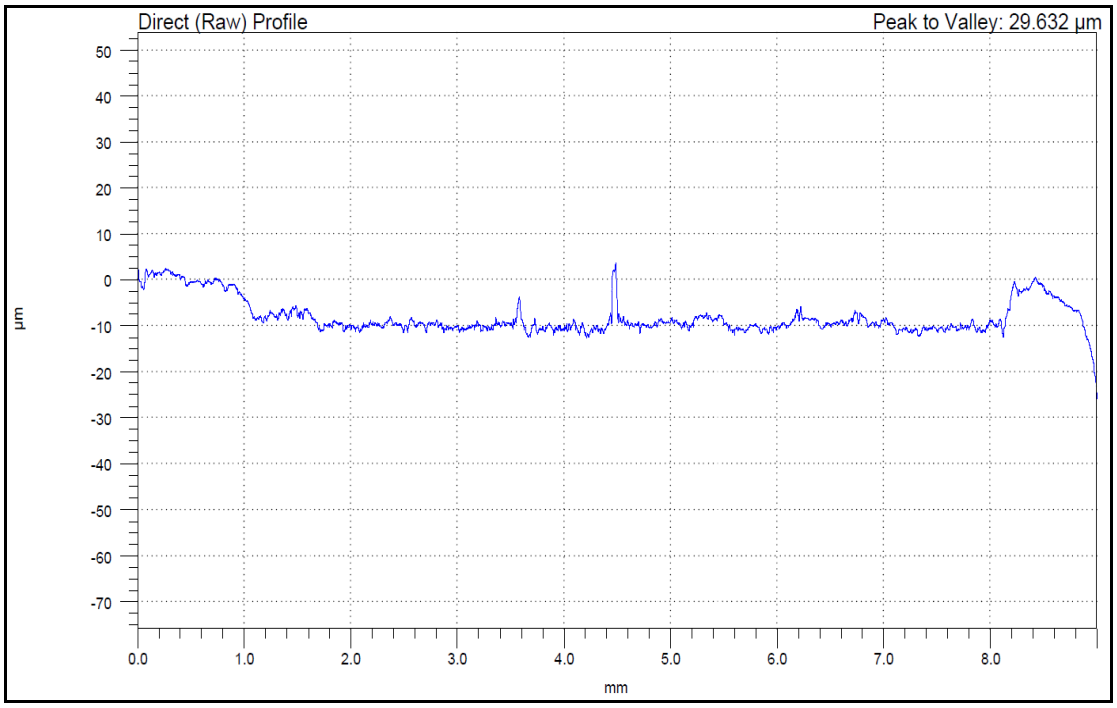

Figure 3-24 The surface profile of the used release latch

Table 3-9 BAC parameters of used release latch surface profile

PARAMETERS	VALUES	DESCRIPTION
R_k (µm)	0.784	Core roughness depth
R_{vk} (µm)	1.207	Reduced valley depth
R_{pk} (µm)	0.963	Reduced peak height
Mr1 (%)	8.98	Material ratio 1
Mr2 (%)	84.28	Material ratio 2

By using these BAC parameters of the two surface profiles, it is computed in Appendix B that the depth of worn surface in release latch after ten firing tests is approximately 8 µm.

At the end of rail and latch measurements it was obtained that the release latch is much more critical for wear because its worn depth is bigger. Thus, modeling studies explained in the next chapter was only made on the release latch.

CHAPTER 4

WEAR SIMULATION OF LAUNCHER PARTS

In the previous chapter, firing tests and measurement studies were explained. It should be noted that the main goal of firing tests are to observe the flight characteristics of rockets and missiles. The launcher performance is in second importance. Therefore, additional firing tests cannot be organized for only examining wear performance of launcher parts. At this point, the demand for wear simulation arises. If wear on launcher parts can be simulated, there will be no need for additional firing tests and wear measurements. Thus, the main goal of thesis study is to simulate wear life of launcher parts and this chapter consists of studies made for wear modeling.

4.1 WEAR MODELLING

In literature, there had been lots of work on simulating wear of materials. For example in 2001, Mona Öqvist had made a study on "numerical simulations of wear of a cylindrical steel roller oscillating against a steel plate". A special version of the finite element program NIKE2D [32] was used. Mona Öqvist had simulated wear according to flow chart given in Figure 4-1.

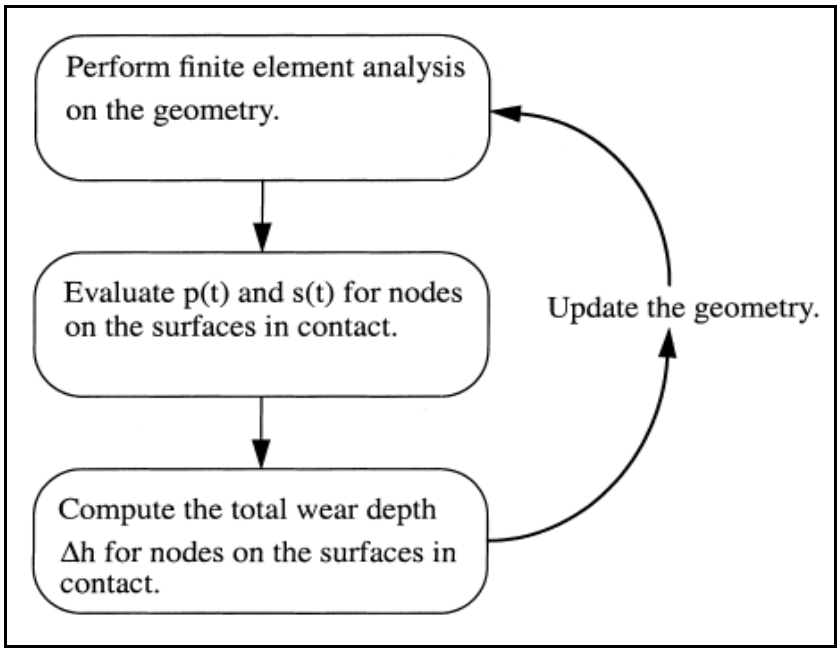

Figure 4-1 Flow chart of wear simulation made by Mona Öqvist [32]

Moreover, V Hegadekatte, N Huber and O Kraft had studied on "finite element based simulation of dry sliding wear" [33]. They claim that wear simulations can be made by using two different approaches. One is to embed a wear model into definition of a FE material model and the other one is to use FE results of a general contact problem in a wear model. They had used a finite element post-processor and Archard wear law to evaluate wear on deformable-deformable bodies.

Molinari et al. used first model to implement Archard wear law into FE analysis [34]. They had made some modifications on Archard wear law such as changing the hardness of the softer material of mating parts as a function of temperature. Moreover, surface transformation due to wear and frictional contact is also added into FE analysis.

In second method, Yan W et al. used ratchetting-based failure criterion in order to predict wear rate [35]. Ratchetting-based failure criterion is based on plastic strain accumulation in every loading. When the accumulated strain overruns a limit value, the material is considered as failed or worn out.

As it was learned from literature studies, there is no commercial FE program which is capable of simulating wear directly. The only way to calculate the worn material is to write macro. Commercial FE programs are used to compute the contact reactions of materials. The outputs of FE analysis are used as inputs for general wear models.

The most frequently used wear model in practical engineering is linear Archard wear law [36], so it was used in order to compute the amount of worn material in this thesis study. As specified in previous chapters, according to Archard,

$$V = K \cdot \frac{W \cdot L}{H} \tag{4-1}$$

where V,K,W,L and H are wear volume, dimensionless wear coefficient, total normal load, sliding distance and hardness of the target contacting material, respectively. In engineering applications, wear depth is generally more important than wear volume of materials [36], so if both sides of equation (4.1) is divided by "A" (area of contact), then,

$$\frac{V}{A} = K \cdot \frac{W \cdot L}{H \cdot A} \tag{4-2}$$

$$h = K \cdot \frac{p \cdot L}{H} \tag{4-3}$$

where, h and p are wear depth and contact pressure, respectively.

In order to find the wear depth in equation (4.3), contact pressure, sliding distance, hardness and wear coefficient should be known. Hardness is a material property so it will be taken from the literature. Contact pressure and sliding distance can be computed from FE program.

Wear coefficient is the most important parameter in Archard's wear law because it provides a contract between experimental study and simulation. Therefore, wear coefficient was evaluated by the help of experimental results explained in chapter 3. As shown in Figure 4-2, a FE analysis was made in order to calculate the contact pressure and sliding distance. Then, these results and measured wear depth are used in equation (4.3) in order to calculate wear coefficient. At this point, it should be noted that the calculated wear coefficient is for 10 firing tests. In other words, with the evaluated wear coefficient, Archard's wear law will calculate the amount of worn material for every 10 firings.

Once wear coefficient was found, it is possible to evaluate the amount of worn material for every 10 firings. As shown in Figure 4-3, a flowchart of wear simulation was constructed. By providing the requisite inputs to the FE processor, the sliding distance and contact pressure between materials were calculated. Then, by using these data in Archard's wear law, wear depth is calculated for every 10 firings. The average wear depth at the end of each simulation is compared with limit value in order to see whether total wear depth exceeds the limit or not. If the answer was no, then by updating the geometry of the FE model, all calculations were made again. When the calculated amount of worn material exceeded the limit value, it was said that this is point where crack initiation in the material begins.

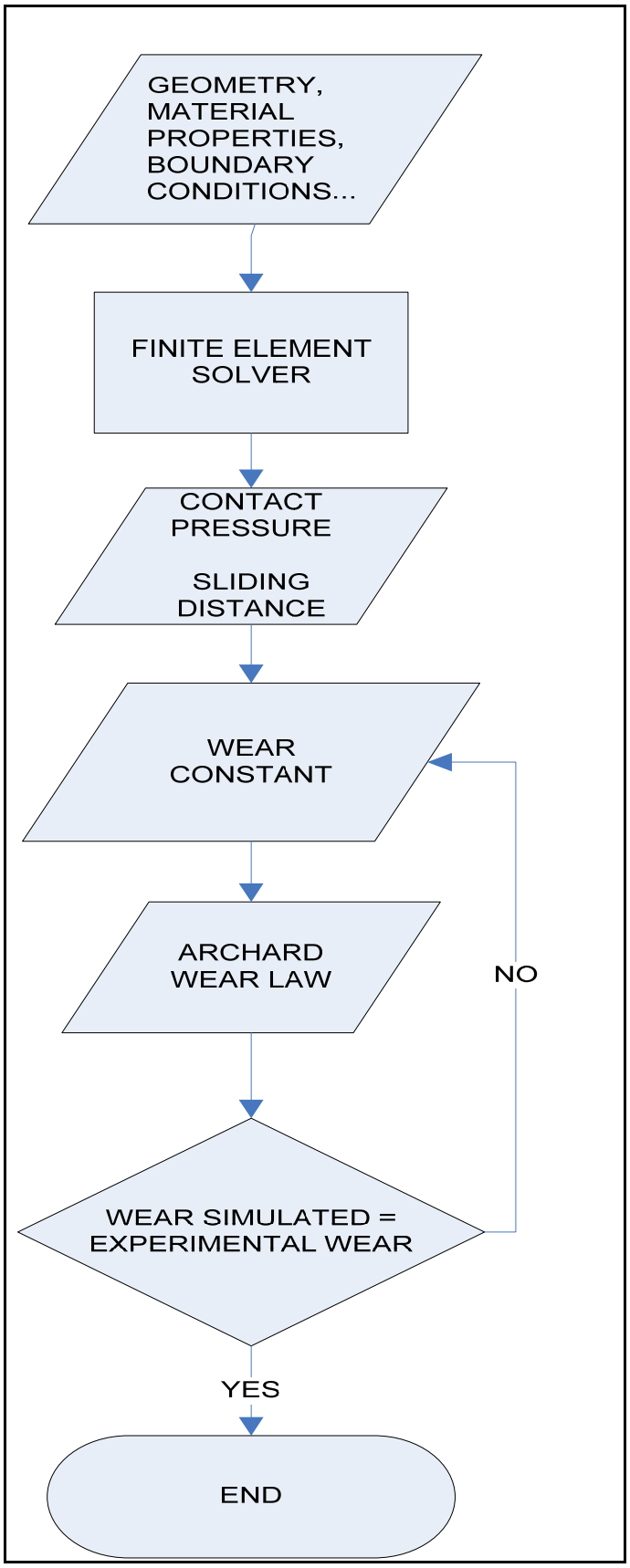

Figure 4-2 Flowchart of evaluating wear coefficient

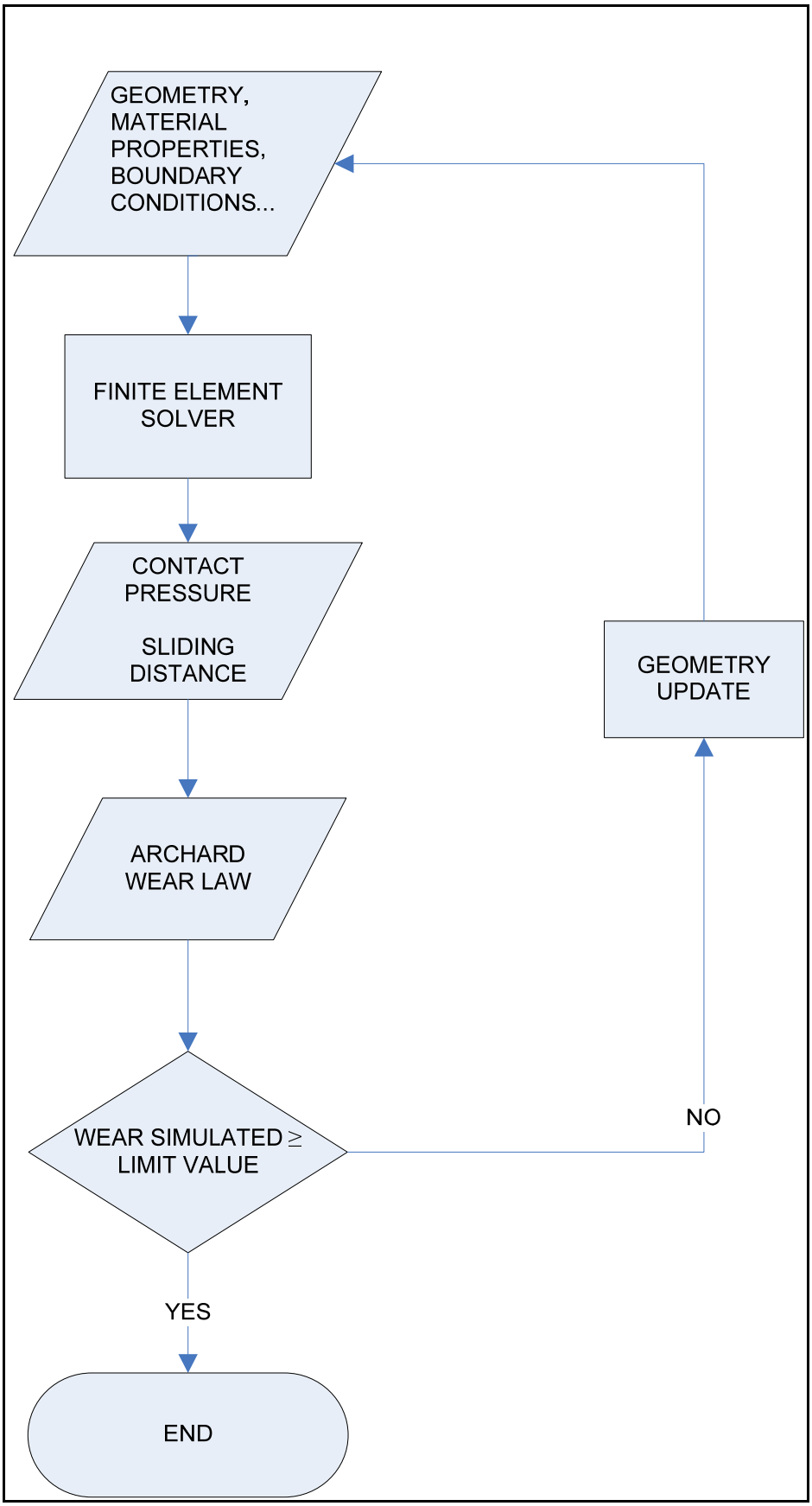

Figure 4-3 Flowchart of wear simulation

4.2 THE FINITE ELEMENT MODEL OF MISSILE SHOE-RELEASE LATCH INTERFACE

Before explaining FE model of contact interface, the real situation is explained as seen in Figure 4-4. Release latch is attached to the rail from its rotating point. It is also constrained by linear spring at the back. During firing of the missile, shoe moves on the rail and get in touch with launcher latch. As missile shoe moves, release latch compresses linear spring more, so contacting forces between shoe and latch increases up to a time when shoe loses contact. The contact between shoe and latch is lost after shoe moves approximately 5 mm in the direction shown in Figure 4-4. Figure 4-5 shows FE model of interface and boundary conditions used in the model.

3D or 2D geometries can be used in FE modeling. However, in most cases, defining a real case with 2D geometry can save significant analysis time and machine resource. Therefore, while working with models and environments that involve negligible effects from a third dimension, using 2D geometry in FE models are suggested. In order to express a 3D environment with a 2D FE geometry, the environment should satisfy at least one of the following characteristics:

- **Plane Stress:** It should be assumed that there is no stress component normal to the plane of action. This means that one of the three principal stresses is zero. If one dimension of the structure is smaller than the other dimensions, plane stress can be used. Example uses of plane stress are flat plates subjected to in-plane loading, or thin disks under pressure or centrifugal loading.
- **Axis-symmetry:** It should be assumed that a 3-D model and its loading can be generated by revolving a 2-D section 360^{o} about one of the axis of the structure. Example uses of axis-symmetry are pressure vessels, straight pipes, and shafts.
- **Plane Strain:** Plane strain assumes zero strain in one of the dimensions of the structure. It can be used when one of the dimensions is much larger than the other dimensions. Example uses of plane strain are long, constant, cross-sectional structures such as structural beams.

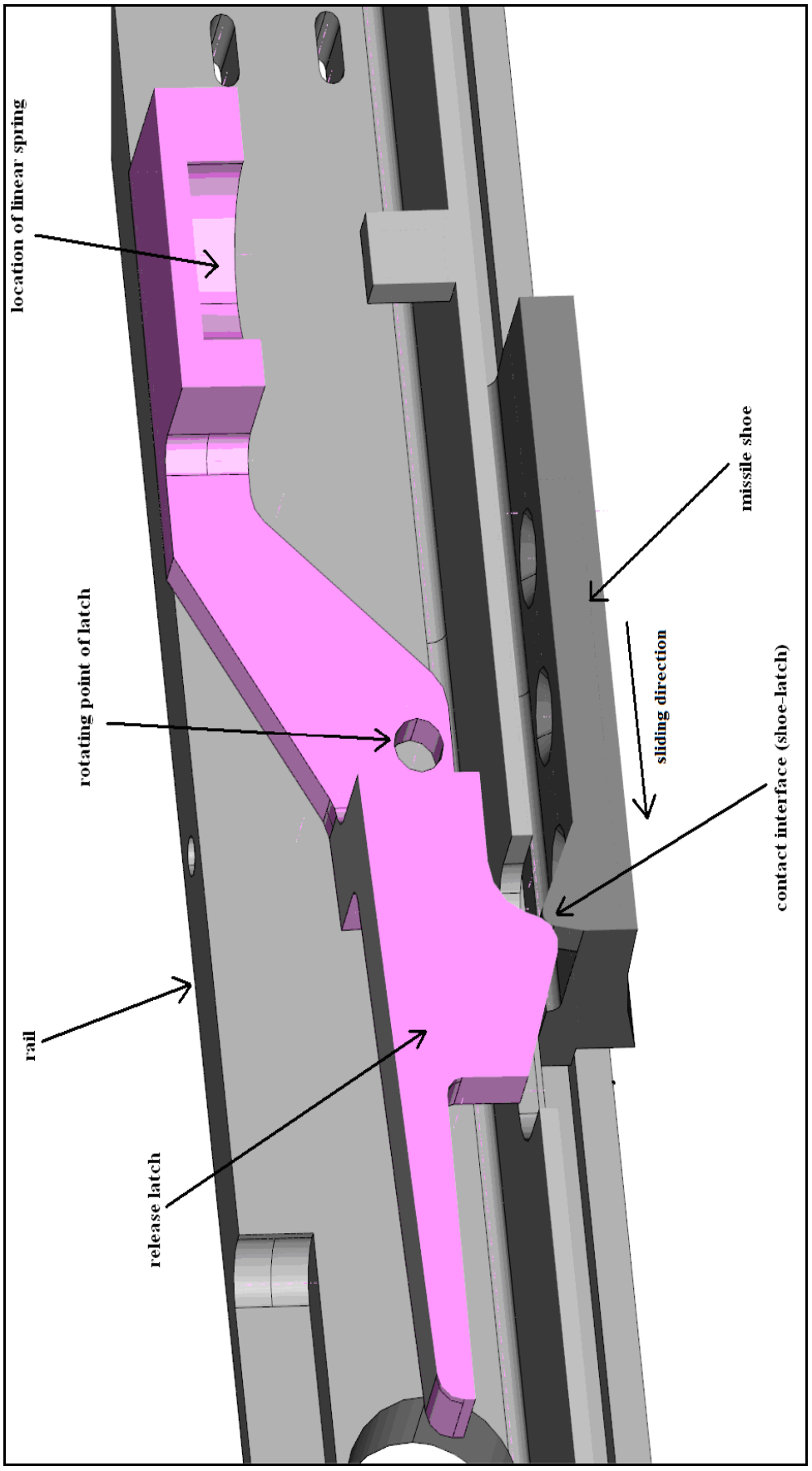

Figure 4-4 CAD model of the shoe-latch contact interface

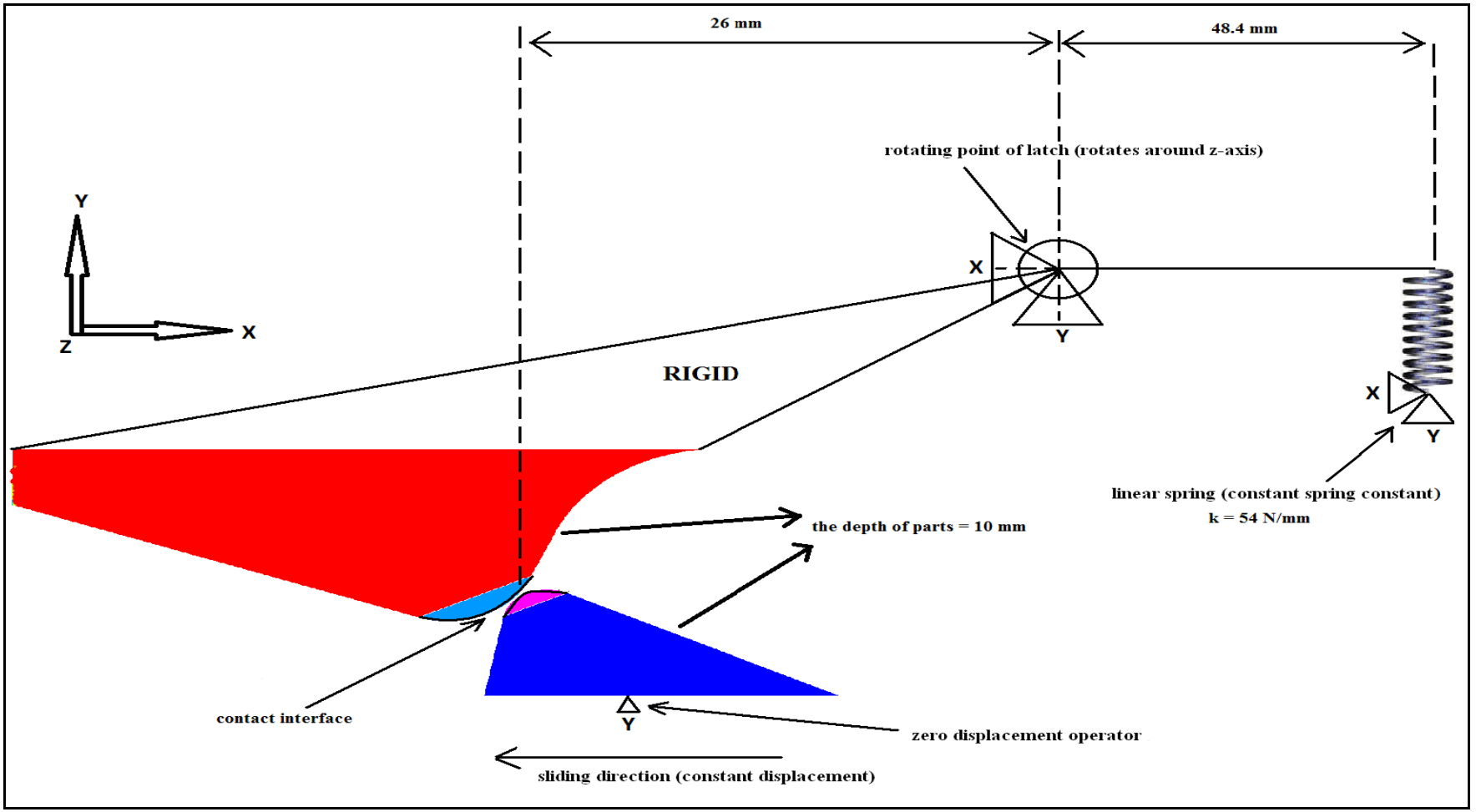

Figure 4-5 A schematic view of the missile shoe-release latch interface

The interface between launcher latch and missile shoe is a similar case to plane stress models. Since both shoe and latch have a thickness smaller than the width and length, plane stress model was used in FE modeling. In Figure 4-6, the detailed FE models are shown. In order to examine contact regions of the parts, the geometries of parts were divided into sub-areas. As it will be described in meshing section, worn regions in Figure 4-6 were meshed with smaller size elements.

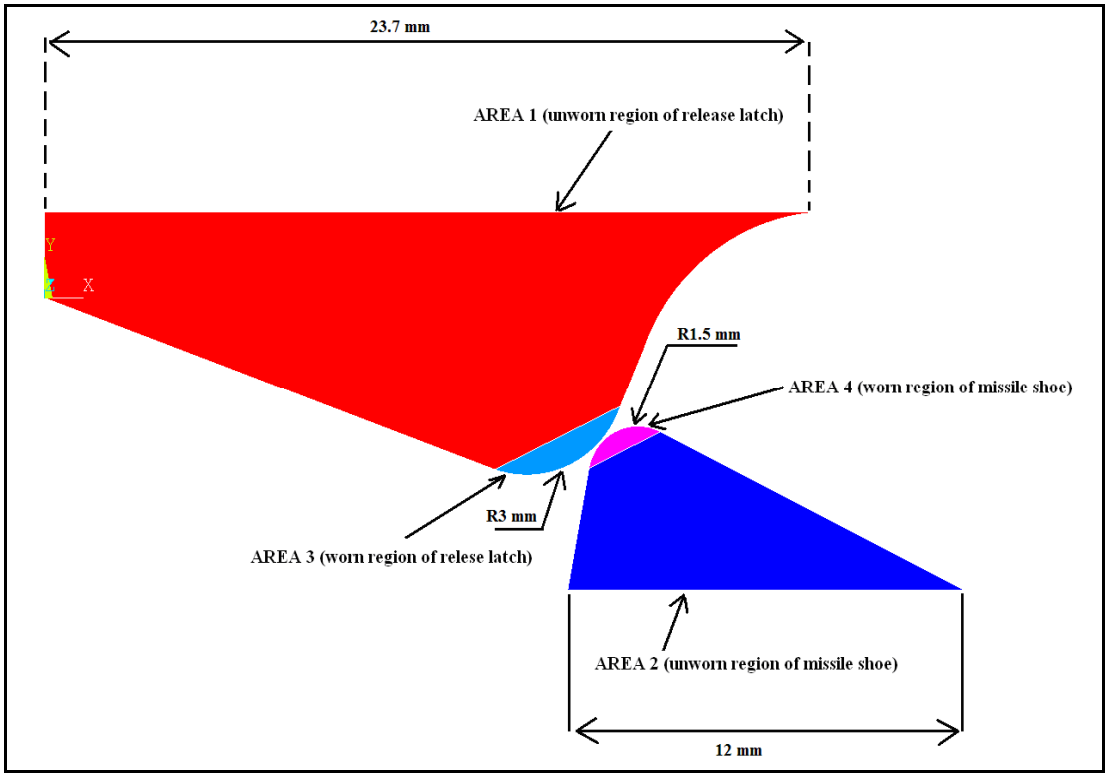

Figure 4-6 A detailed view of the release latch and the missile shoe used in FE

4.3 MATERIAL PROPERTIES OF MODELS

In structural modeling applications, materials properties of models have a high importance on results. FE material models should be convenient with material properties.

As specified in previous sections, the shoe material is AISI-1040 steel and the release latch is made from AISI-4140 carbon steel. The mechanical properties of these materials were taken from literature and given in Table 4-1 and Table 4-2.

Table 4-1 Mechanical properties of AISI-1040 steel [28]

Density (gr/cm^3)	7.845
Hardness (Rockwell C)	13
Ultimate tensile strength (MPa)	620
Yield tensile strength (MPa)	415
Modulus of elasticity (GPa)	200
Shear Modulus (GPa)	80
Poisons ratio	0.29

Table 4-2 Mechanical properties of AISI-4140 steel [28]

Density (gr/cm^3)	7.85
Hardness (Rockwell C)*	30
Ultimate tensile strength (MPa)	1020
Yield tensile strength (Mpa)	655
Modulus of elasticity (Gpa)	205
Shear Modulus (Gpa)	80
Poisons ratio	0.29

*hardness was taken as 1000 MPa in wear calculations by Archard's wear law [36].

Moreover, the kinetic friction coefficient between steel materials was taken as "0.6" in FE analysis [28].

4.4 MESHING AND ELEMENT TYPES

In FE modeling, meshing has a critical role since it determines whether the solution will converge or not. Using smaller mesh sizes generally results in more accurate answer but it requires more time to solve. Moreover, in FE models where contact occurs, element sizes in contact regions should be as small as possible because of the possibility of loosing contact. Therefore, an optimization should be made between mesh size and FE solution.

Since the main concern is wear, element size in contact region was chosen smaller than the other regions of the parts in FE model of thesis work. After some trial and error analyses, the element sizes shown in Figure 4-7 were decided.

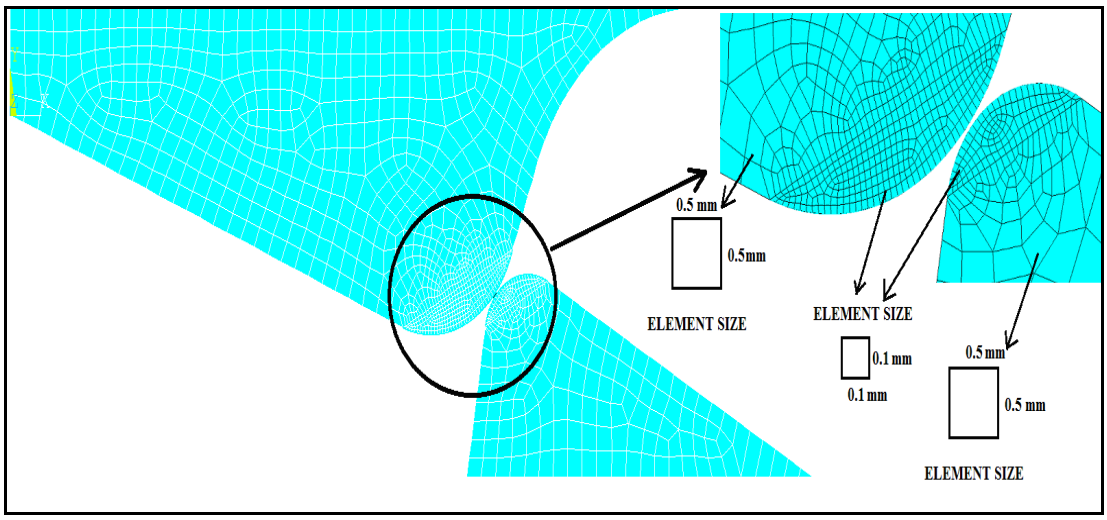

Figure 4-7 A view for meshed model of shoe-latch interface

The element types used in FE model are PLANE183, TARGE169, CONTA172, MASS21, COMBIN14 and MPC184. Below, brief descriptions are taken about elements from ANSYS software [37]:

PLANE183: PLANE183 is a higher order 2-D, 8-node or 6-node element. PLANE183 has quadratic displacement behavior and is well suited to modeling irregular meshes. This element is defined by 8 nodes or 6 nodes having two degrees of freedom at each node: translations in the nodal x and y directions. The element may be used as a plane element (plane stress, plane strain and generalized plane strain) or as an axisymmetric element. This element has plasticity, hyperelasticity, creep, stress stiffening, large deflection, and large strain capabilities.

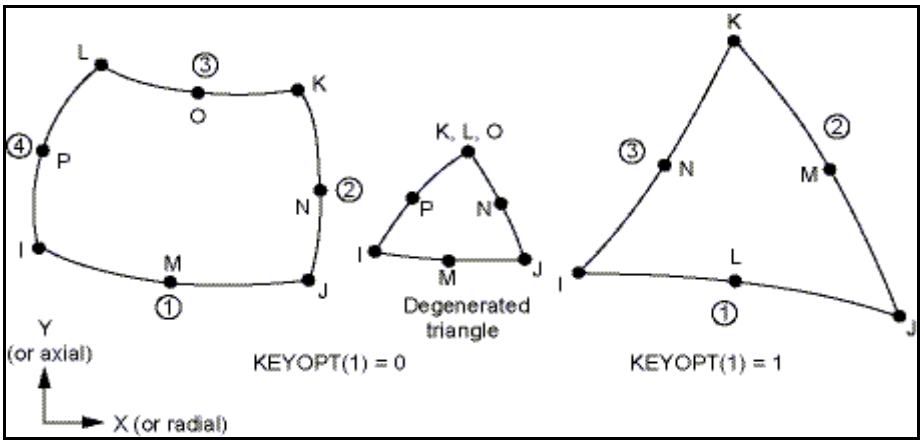

Figure 4-8 Geometry of PLANE183 element [37]

TARGE169: TARGE169 is used to represent various 2-D "target" surfaces for the associated contact elements (CONTA171, CONTA172, and CONTA175). The contact elements themselves overlay the solid elements describing the boundary of a deformable body and are potentially in contact with the target surface, defined by TARGE169. This target surface is discretized by a set of target segment elements (TARGE169) and is paired with its associated contact surface via a shared real constant set. Any translational or rotational displacement, temperature, voltage, and magnetic potential can be imposed on the target segment element. Forces and moments can also be imposed on target elements.

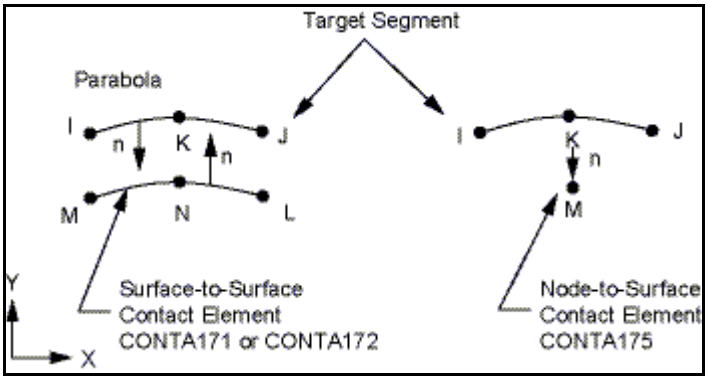

Figure 4-9 Geometry of TARGE169 element [37]

CONTA172: CONTA172 is used to represent contact and sliding between 2-D "target" surfaces (TARGE169) and a deformable surface, defined by this element. The element is applicable to 2-D structural and coupled field contact analyses. This

element is located on the surfaces of 2-D solid elements with mid-side nodes (PLANE121, PLANE183, SHELL209, PLANE82, PLANE35, PLANE77, PLANE53, PLANE223, PLANE230, or MATRIX50). It has the same geometric characteristics as the solid element face with which it is connected. Contact occurs when the element surface penetrates one of the target segment elements (TARGE169) on a specified target surface. Coulomb friction, shear stress friction, and user defined friction are allowed. This element also allows separation of bonded contact to simulate interface delamination.

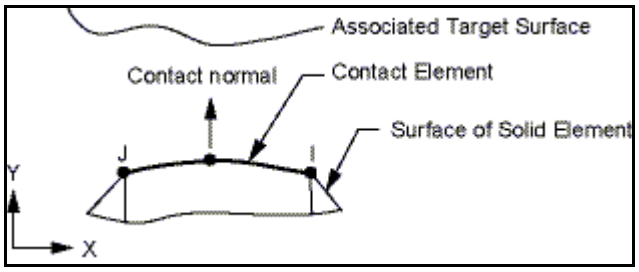

Figure 4-10 Geometry of CONTA172 element [37]

MASS21: MASS21 is a point element having up to six degrees of freedom: translations in the nodal x, y, and z directions and rotations about the nodal x, y, and direction.

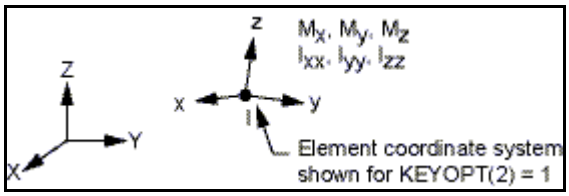

Figure 4-11 Geometry of MASS21 element [37]

COMBIN14: COMBIN14 has longitudinal or torsional capability in 1-D, 2-D, or 3-D applications. The longitudinal spring-damper option is a uniaxial tension-compression element with up to three degrees of freedom at each node: translations in the nodal x, y, and z directions. No bending or torsion is considered. The torsional spring-damper option is a purely rotational element with three degrees of freedom at each node: rotations about the nodal x, y, and z axes. No bending or axial loads are considered.

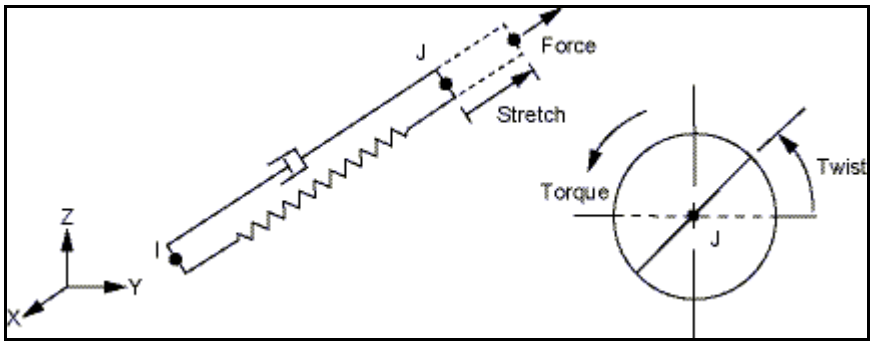

Figure 4-12 Geometry of COMBIN14 element [37]

MPC184 (rigid beam): The MPC184 rigid link/beam element can be used to model a rigid constraint between two deformable bodies or as a rigid component used to transmit forces and moments in engineering applications. This element is well suited for linear, large rotation, and/or large strain nonlinear applications.

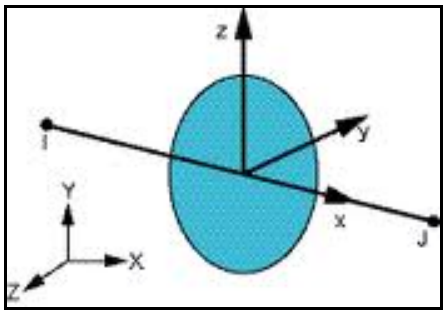

Figure 4-13 Geometry of MPC184 rigid beam type element [37]

In Figure 4-14, element types are shown on FE models. TARGE169 and CONTA72 elements are used to define contact behavior between moving parts. The rest of the moving parts are modeled with PLANE183 elements. A point mass, MASS21, is put on the rotation point of the latch and it is connected to PLANE183 by the help of constraint equations. The linear spring is modeled by COMBIN14 element and it is related to latch by MPC184 rigid beam element.

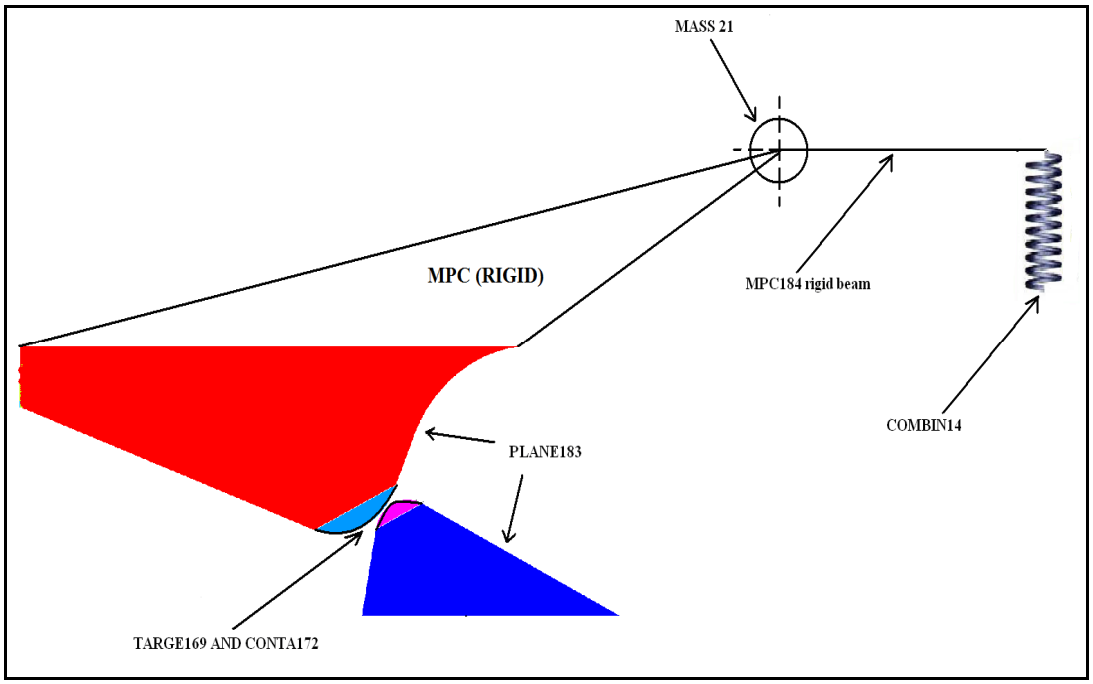

Figure 4-14 A schematic view of element types used on FE model for the shoe-latch interface

4.5 RESULTS OF SIMULATION

As mentioned in previous sections of this chapter, the first analysis study was made to evaluate wear coefficient. However, the results of first analysis had showed that stresses generated on the materials are higher than their yield strength, so it was thought that the plastic deformation should exist on the bodies.

First, the plastic deformations on the materials were calculated and FE models were updated. Then, these updated models were used to evaluate dimensionless wear coefficient. Once the wear coefficient was found, the sequential wear analysis was made in order to calculate total number of firings which exceeds the limit wear value.

4.5.1 PLASTIC DEFORMATION ON MATERIALS

In the first analysis of FE model, the elastic material properties were used. Figure 4-15 shows the graph of contact force generated between release latch and missile shoe. As it is seen on the graph, the contact force increases up to a peak value

(238 N) which contributes the maximum compression of linear spring. When the missile shoe moves approximately 5 mm, the contact between components is lost, thus the contact force drops to zero value. The stress values generated during contact of materials were examined. In Figure 4-16, it is obviously seen that the resultant stress values on materials during contact are very high with respect to their yield strength. Figure 4-16 shows the stress distribution on release latch at the time missile shoe moves 4.2275 mm. Similar to the stress values in Figure 4-16; all the contact regions had experienced high and intensive stresses through out the overall analysis time. Therefore, it is thought that in FE analysis an elastoplastic material behavior must be used.

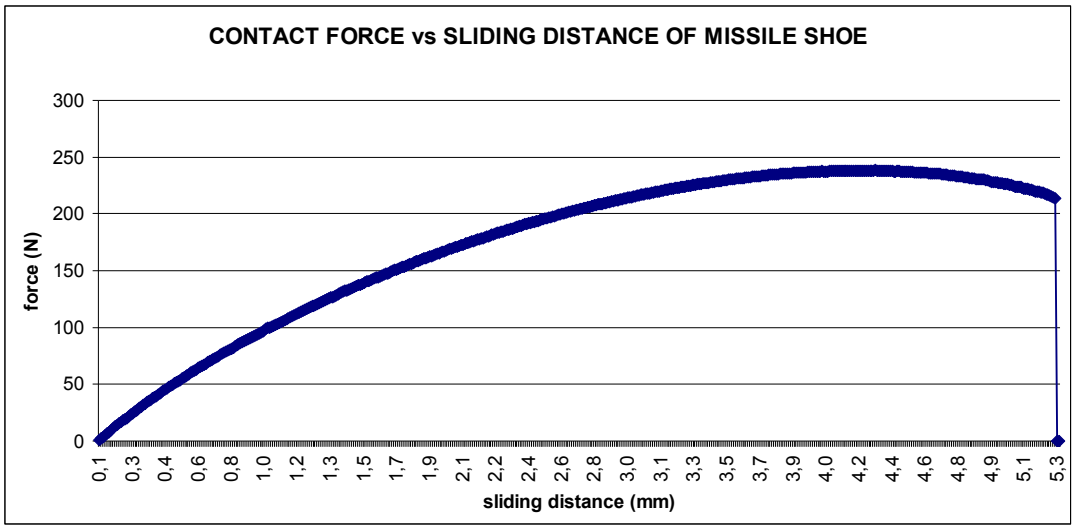

Figure 4-15 The graph of contact force vs sliding distance of the missile shoe on the contact line of release latch

By using equation (4-4) and Figure 4-15, it was calculated that the contact width between release latch and missile shoe at any instant time is approximately 0.04 mm. Thus, analyses was also made with smaller element sizes (0.01mm) than mentioned in section 4.4 in order to see whether the element size is inadequate or not. It was seen that there is no significant change (more than 10% change) in stress distribution, contact pressure or total sliding distance, but the analysis solution time increased in huge amount. Therefore, the rest of analyses were made by using element sizes given in section 4.4. The results of analyses made by using smaller element sizes were also given in Figure 4-17, Figure 4-20, Figure 4-24 and Figure 4-26 for comparison.

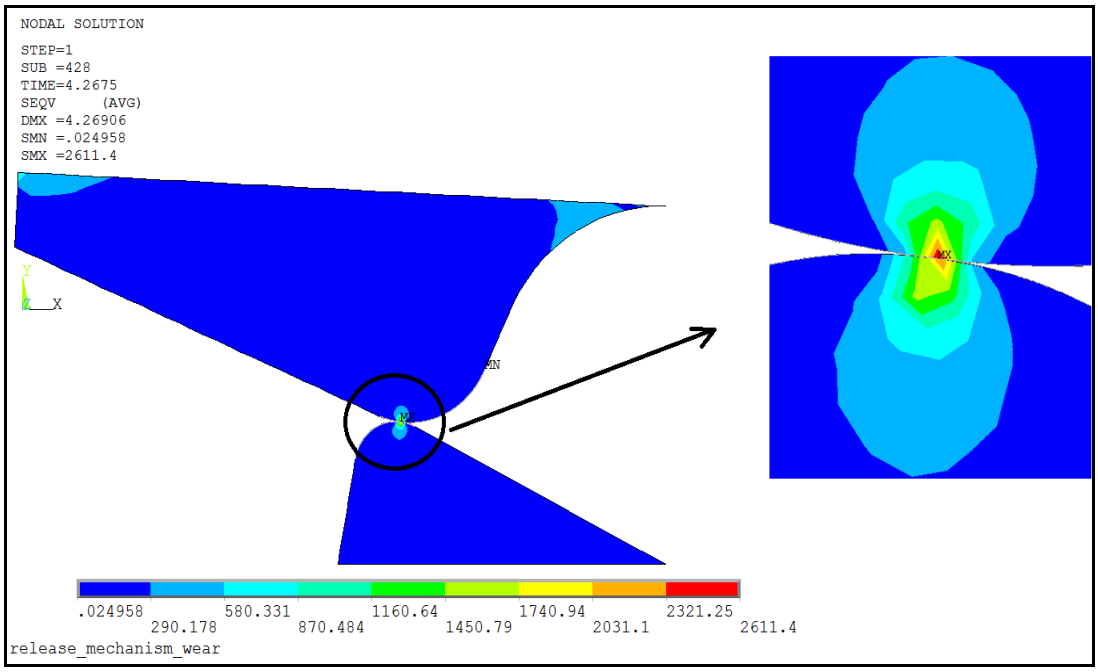

Figure 4-16 The maximum equivalent Von-Misses stress distribution during contact on FE models by using elastic material properties

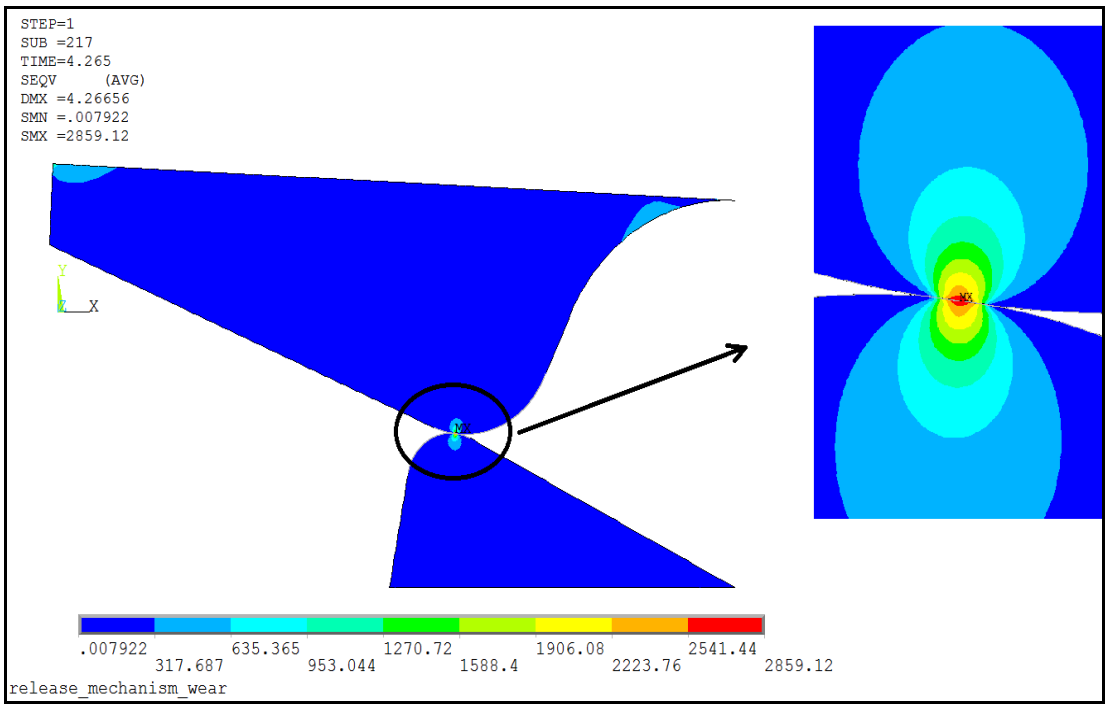

Figure 4-17 The maximum equivalent Von-Misses stress distribution by using smaller elements and elastic material model

The stress-strain curves of materials were defined in FE program for the purpose of evaluating plastic deformations on the materials, as given in Figure 4-18. The bilinear kinematic hardening material model was used to express plasticity of materials. In elastic material approach, only the elastic modulus of materials was defined in FE program. However, tangent modulus of materials was also added into FE program for plastic material approach. The tangent modulus is generally taken as 1/10 or 1/20 of the elastic modulus for steels. In this thesis study, it was taken as 1/20 of elasticity modulus.

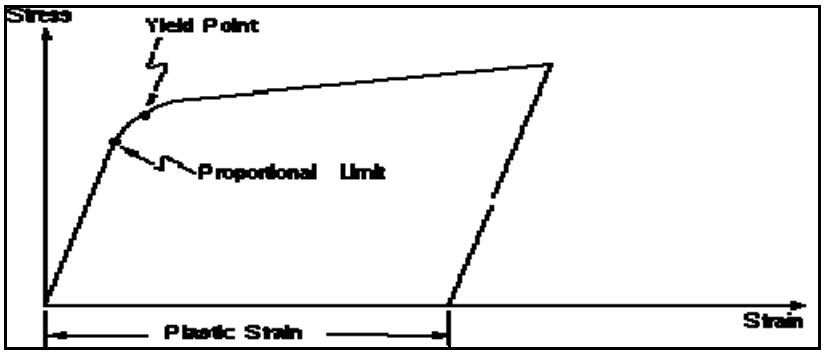

Figure 4-18 Elastoplastic stress-strain curve in ANSYS [37]

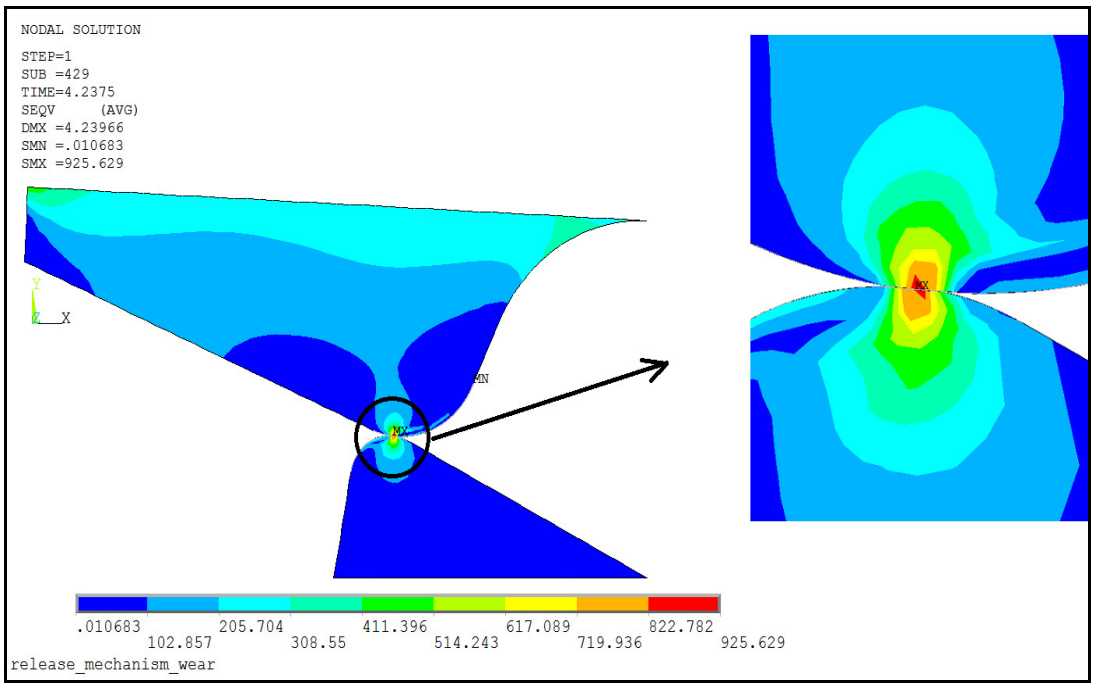

Figure 4-19 The maximum equivalent Von-Misses stress distribution during contact by using elasto-plastic material model

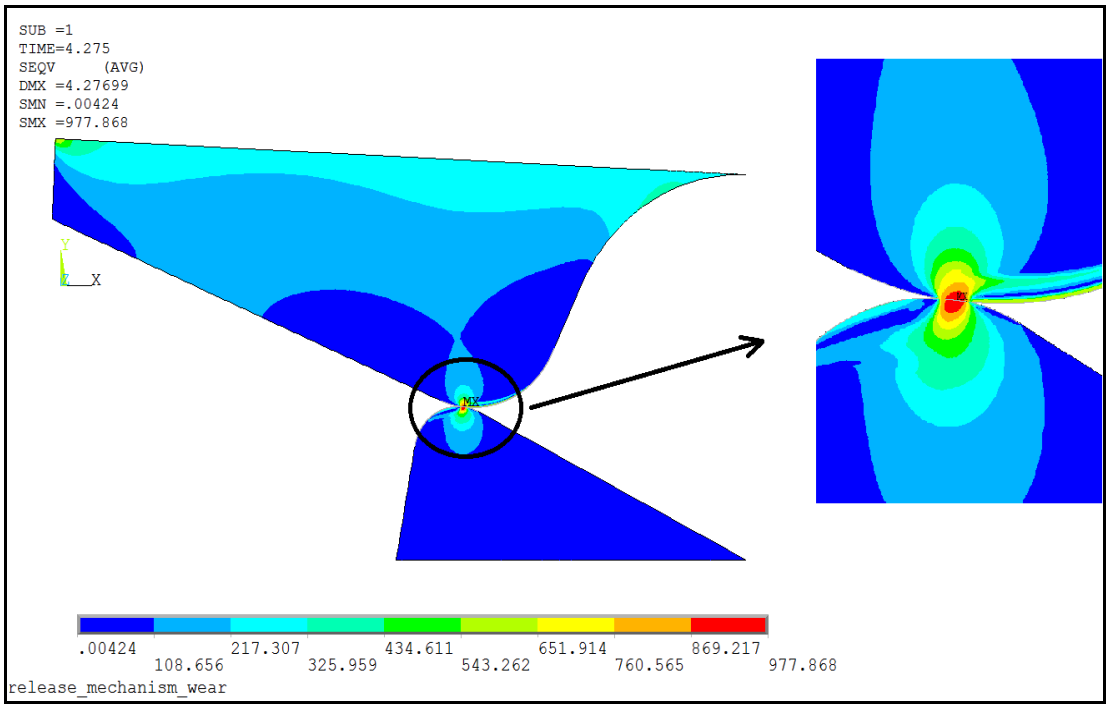

Figure 4-20 The maximum equivalent Von-Misses stress distribution by using smaller elements and elasto-plastic material model

It is obvious that the stresses generated on the contact lines shown in Figure 4-19 results in plastic deformation on the release latch. Since the shoes are used for only one fire, the plastic deformation was not considered for its contact line. In order to evaluate plastic deformation generated for every firing test on the release latch, a FE model which consists of three shoe models was used, as shown in Figure 4-21. Each shoe represents one firing tests so the result of FE model gives plastic deformations in the first three firing tests.

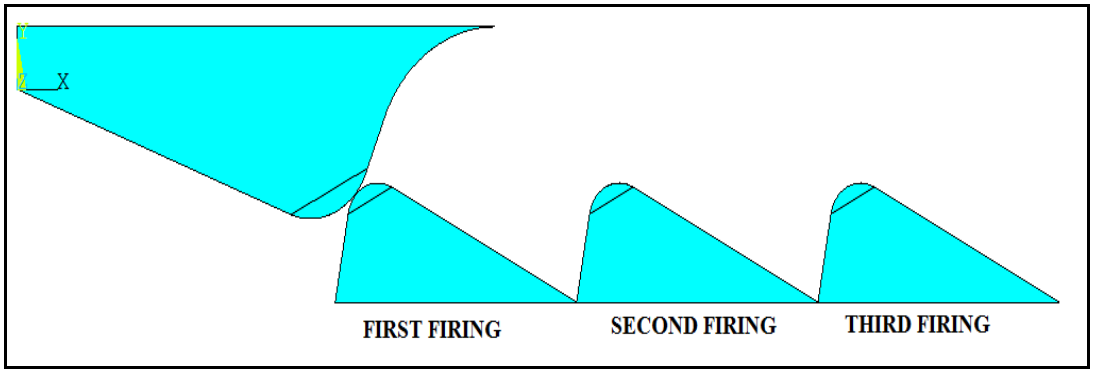

Figure 4-21 The schematic view of FE models used to observe plastic deformation values on three firing tests

As a result of analysis, it was seen that plastic deformation values are very small compared to amount of wear measured in experiments. Moreover, most of the plastic deformation composes at the end of the first firing of the missile. The results for two contacting points are shown in Figure 4-22. It should be noted that, the amount of plastic deformation for points A and B are additive results in Figure 4-22. In other words, the results for 3rd fire also cover the plastic deformation of 1st and 2nd fires.

	Plastic deformation on Point A (mm)	Plastic deformation on Point B (mm)
1st Fire	1.245e-4	1.065e-4
2nd Fire	1.314e-4	1.082e-4
3rd Fire	1.331e-4	1.087e-4

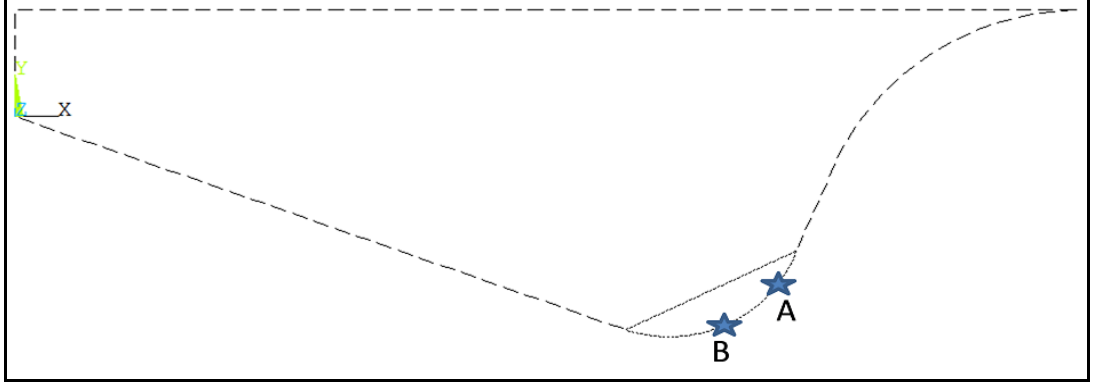

Figure 4-22 The amount of plastic deformations for two sample points on the contact line

Therefore, before going into wear analysis, a geometric update of release latch contact line was made according to the plastic deformation values of first fire.

4.5.2 ESTIMATING DIMENSIONLESS WEAR CONSTANT

As mentioned in previous sections, in order to simulate wear, first wear constant should be evaluated. If equation (4.3) is written to calculate wear constant, then,

$$K = \frac{H \cdot h}{p \cdot L} \qquad (4\text{-}5)$$

In this equation, hardness is a material property; wear depth is the result of wear measurements. Contact pressure and sliding distance are the outputs of FE analysis. After updating the geometry of contact line according to plastic deformations, an analysis was made with the updated geometry of the latch with the same boundary conditions. Figure 4-23 and Figure 4-25 shows nodal contact pressure and nodal sliding distance values of contacting nodes at the time when the missile shoe moves 4.005 mm, respectively.

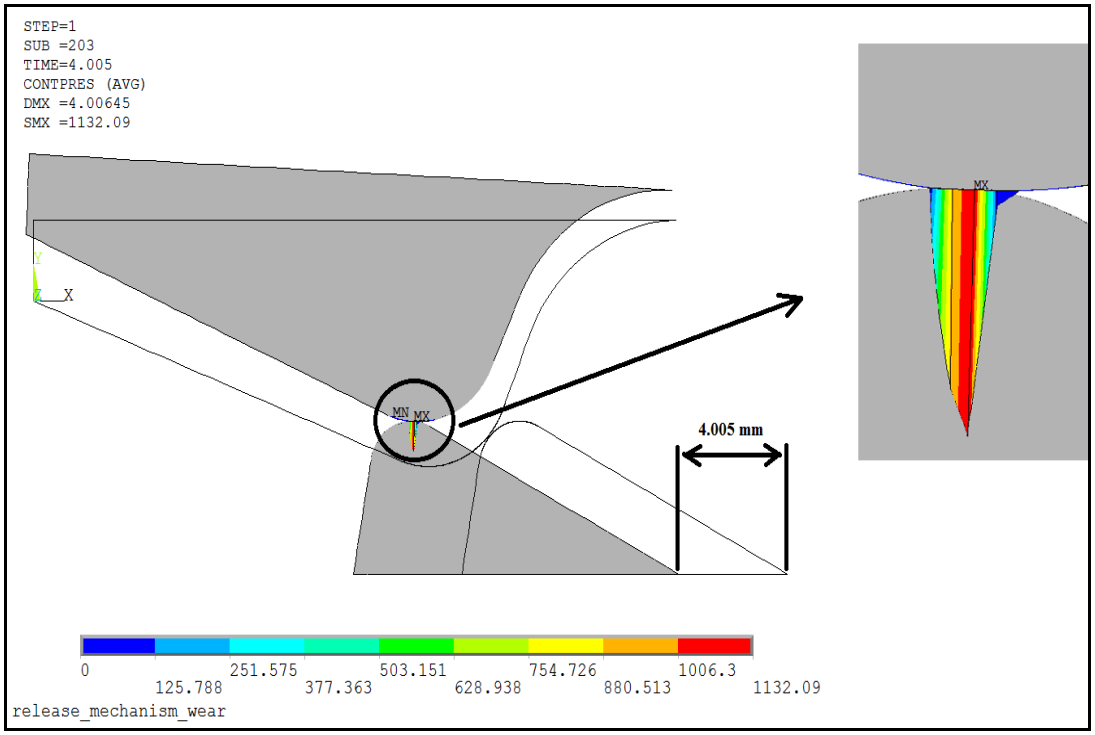

Figure 4-23 Nodal contact pressure distribution at the time when the shoe moves 4 .005 mm

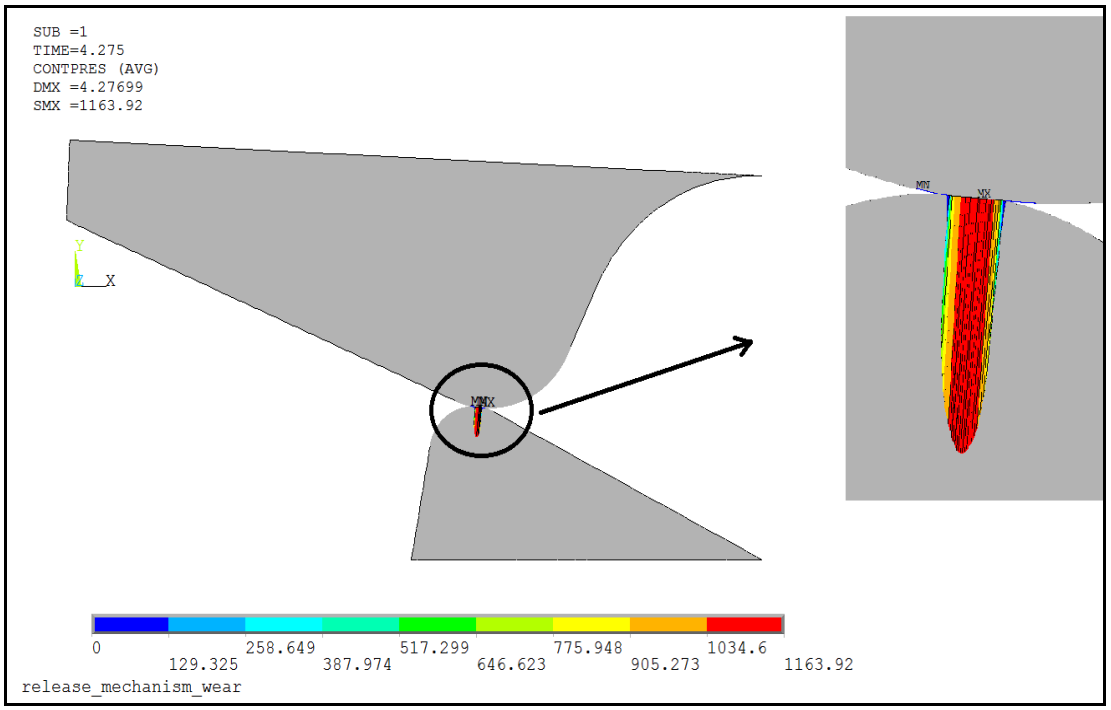

Figure 4-24 Nodal contact pressure distribution by using smaller elements

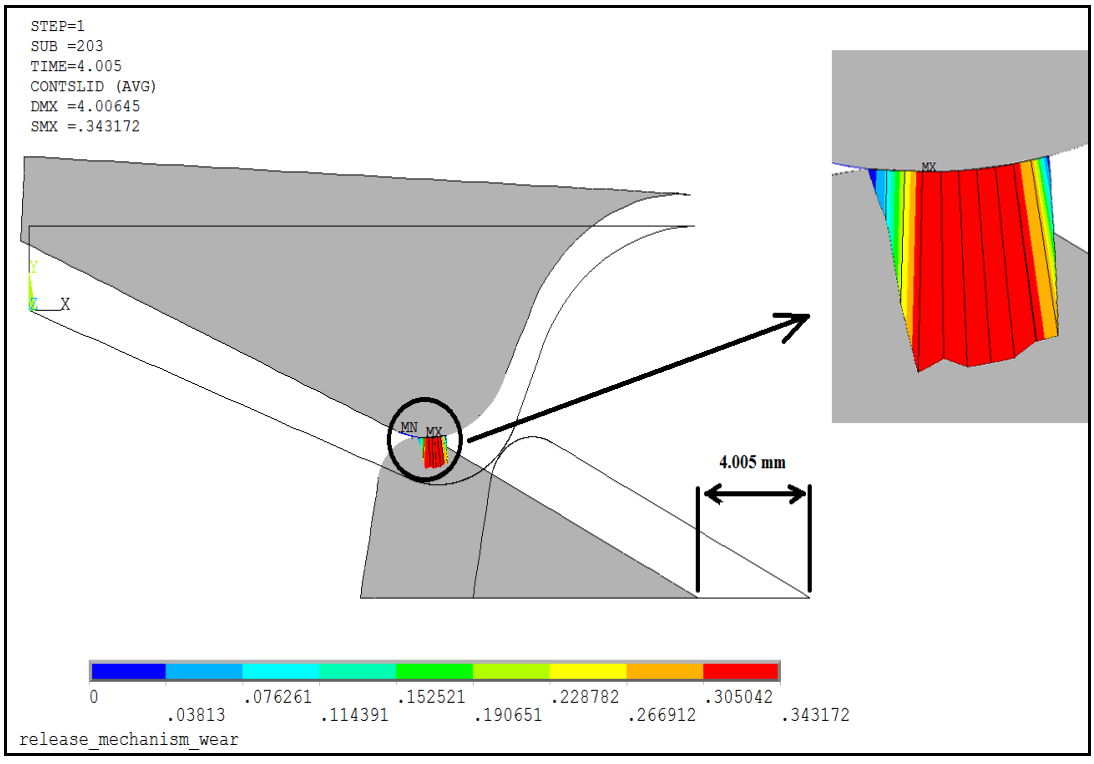

Figure 4-25 Nodal sliding distance values at the time when the shoe moves 4.005 mm

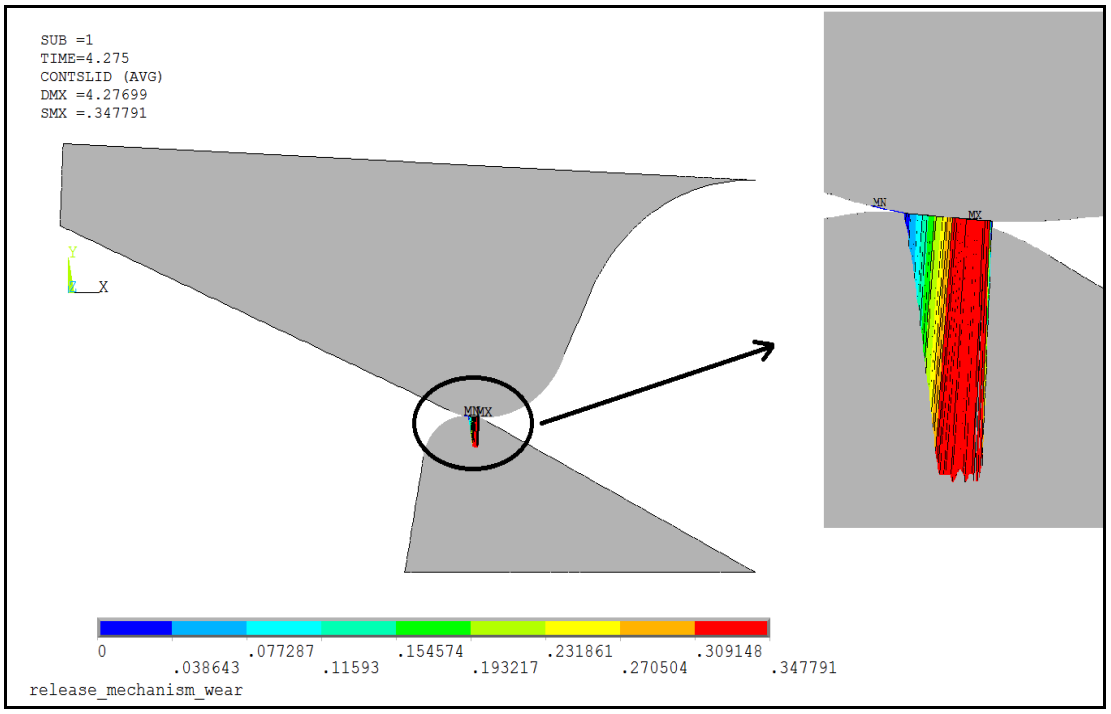

Figure 4-26 Nodal sliding distance values by using smaller elements

The contact pressure and sliding distance data were gathered for all contact nodes as seen in Figure 4-27. The sliding distance and contact pressure values are time-dependent because of the linear spring used in the system. Therefore, all data in the overall analysis time should be considered for this study. This was made by ANSYS TimeHistory PostProcessor. The contact pressure and sliding distance values of contact nodes were collected for all time-steps. Then, the peak values of contact pressure and total summation of sliding distance were used in order to evaluate wear constant. The peak contact pressure and total summation of sliding distance on the contact curve are shown in Figure 4-28 and Figure 4-29, respectively. The calculated wear depths on the contact curve are shown in Figure 4-30. After that, these nodal wear depths are averaged for calculating overall wear depth of the surface. This value is compared with the experimental result which is approximately 8 micrometers and wear constant is changed until the average wear depth of the simulation is equal to the experimental wear depth. The dimensionless wear coefficient was obtained as approximately “0.02”.

In Figure 4-28 and Figure 4-30, there is a sharp increase for the zero contact position. Since the components loose contact at this point, the max pressure on the point increases very rapidly and it results a high wear depth. If that point is admitted, a parabolic increase can be seen in three of the graphs. This is the result of Figure 4-15 which shows a parabolic increase in contact force during sliding of the missile shoe. In order to prevent the wrong effect of zero contact position, it is admitted from average wear depth calculations and geometry update.

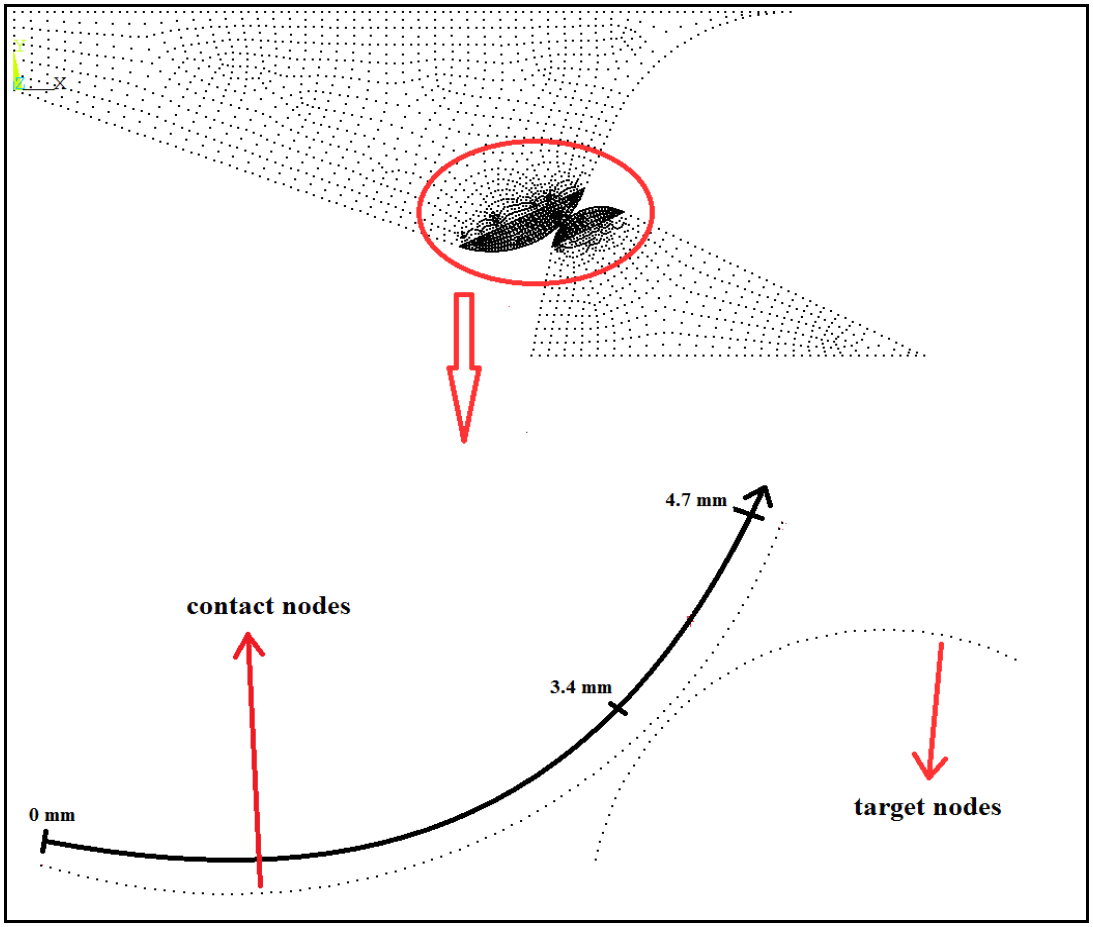

Figure 4-27 Representation of the contacting nodes of the release latch

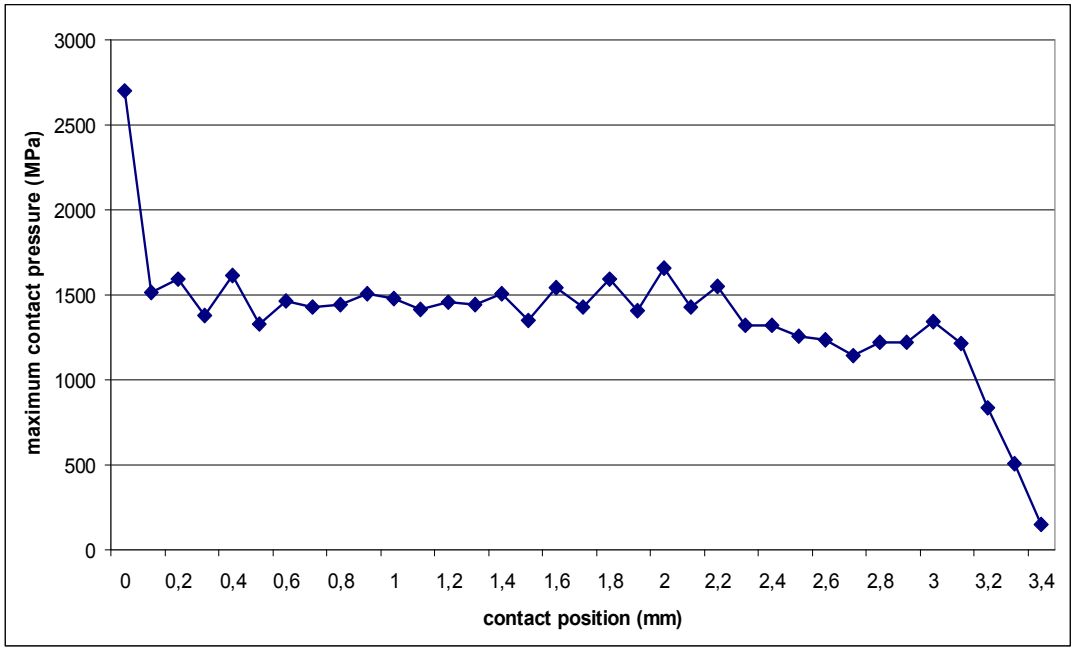

Figure 4-28 The graph of maximum contact pressure along the contact curve after 10 firings

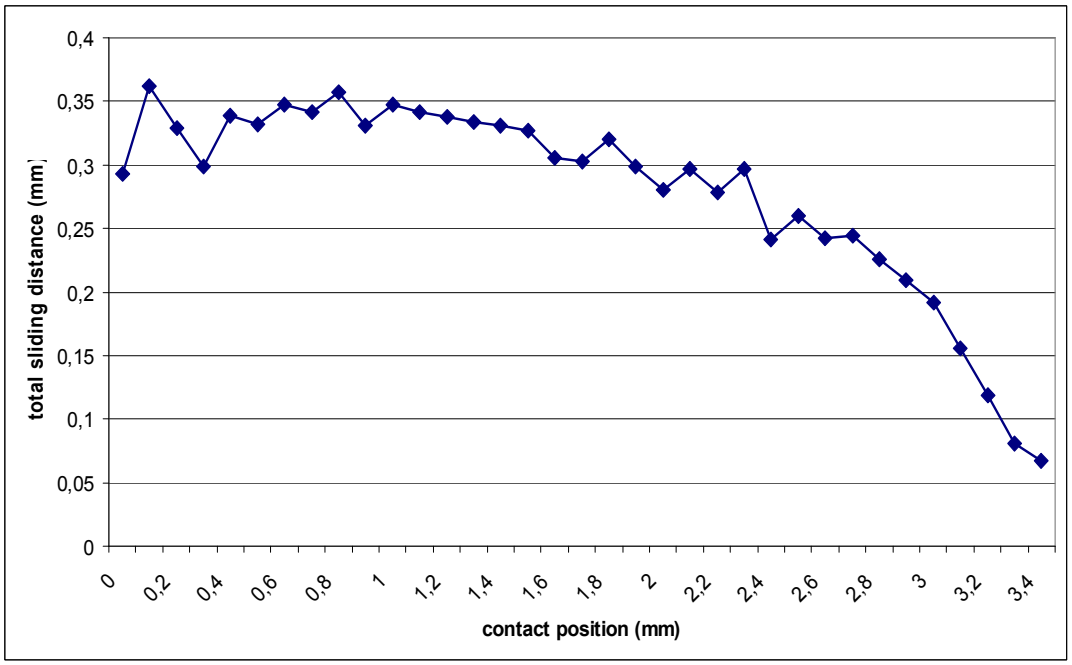

Figure 4-29 The graph of total sliding distance along the contact curve after 10 firings

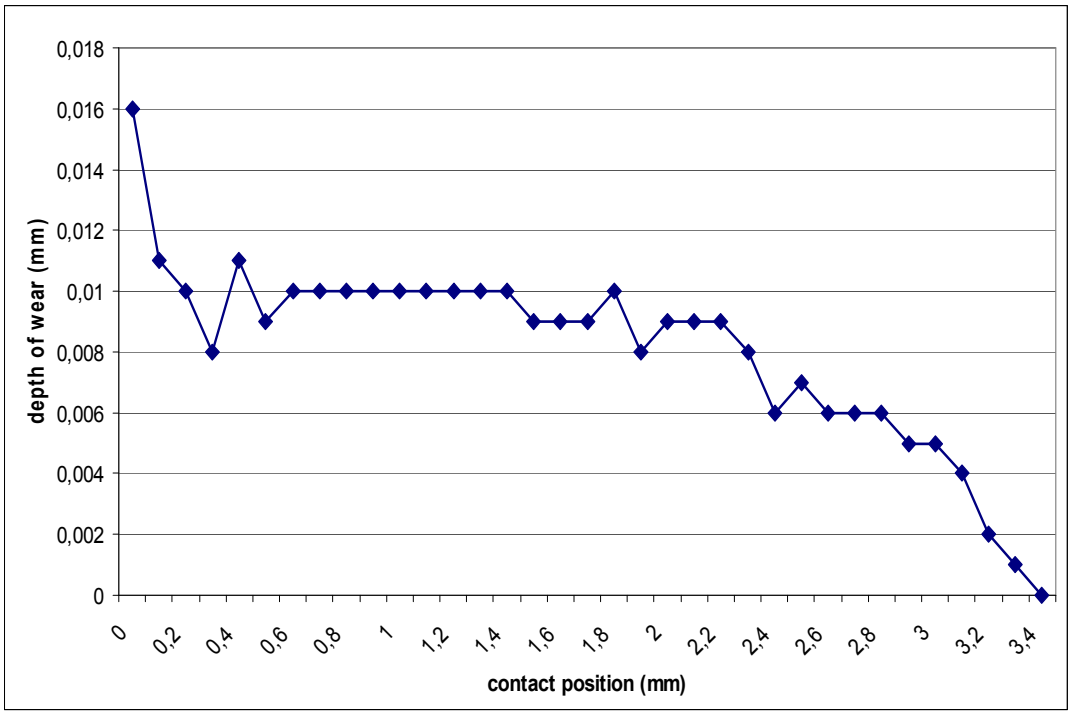

Figure 4-30 The graph of wear depth along the contact curve after 10 firings

4.5.3 SEQUANTIAL WEAR CALCULATIONS

Once the wear coefficient is obtained, it is possible to evaluate wear depths of nodes for every ten firings. As mentioned in the previous section, the wear depth for each contact node was given in Figure 4-30. Before making the second analysis for twenty firings, the geometry of the latch model was updated by using the values in Figure 4-30. Updating was made by moving the contact nodes in the direction of the contact pressure. In Figure 4-31, a schematic view of moving node number 7411 is shown. A coordinate system was constructed for each moved node. Since the contact line of release latch is defined as a portion of circle, a center node was created at the center of this circle. It was thought that the contact pressure of each contact node is applied through the center of this circle. Therefore, the coordinate system of each node was constructed as y-axes goes through the center node and the contact nodes were moved in the direction of y-axes with an amount of corresponding wear depth.

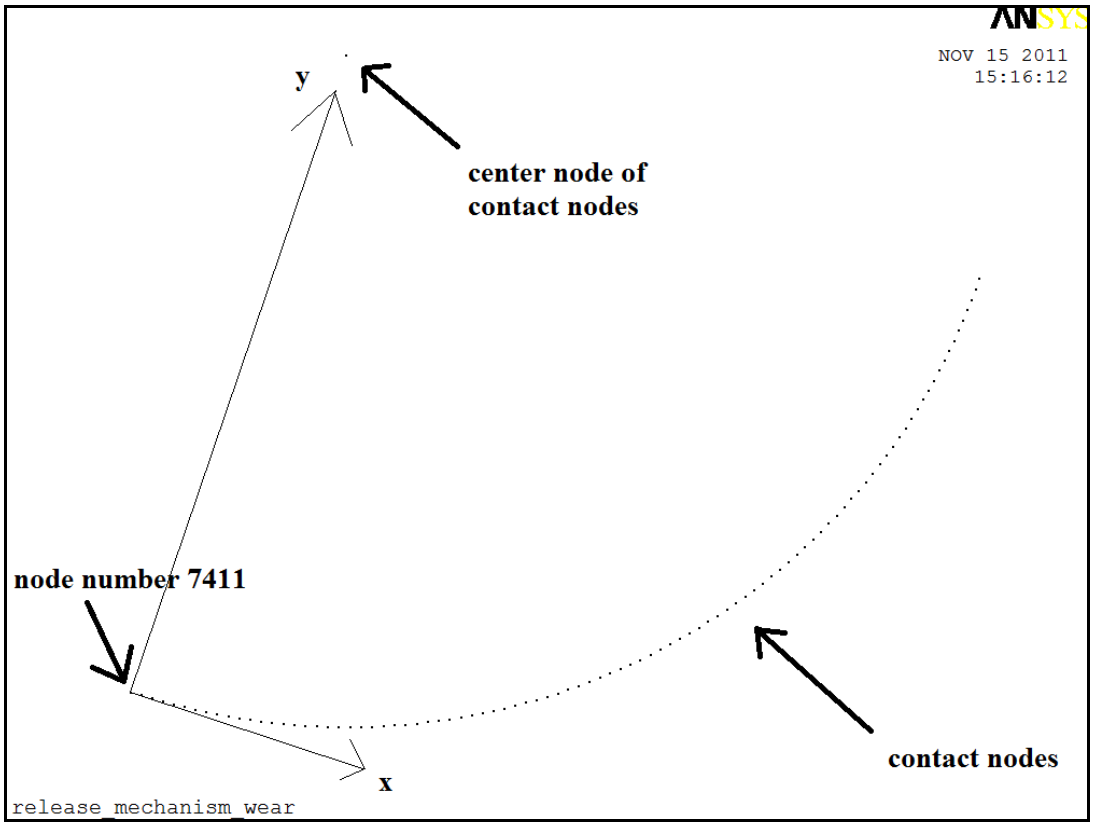

Figure 4-31 Representation of geometry update in FE model of release latch

At the end of each model updating, the analysis was run and the new contact pressures and sliding distances were obtained for each contact node. Therefore, at the end of every analysis, different wear depths of nodes were evaluated and the geometry of release latch was updated according to these results.

A total of seven analyses were made and it was seen that there is a total of 60 μm average wear depth in the release latch after seventy firings. The sequential geometry changes in release latch after each analysis is shown in Figure 4-32. Moreover, the average wear depth on contact surface of the release latch is given in Figure 4-33.

The contact pressures, sliding distances and wear depths of each contact nodes for seven analyses are given in Appendix B.

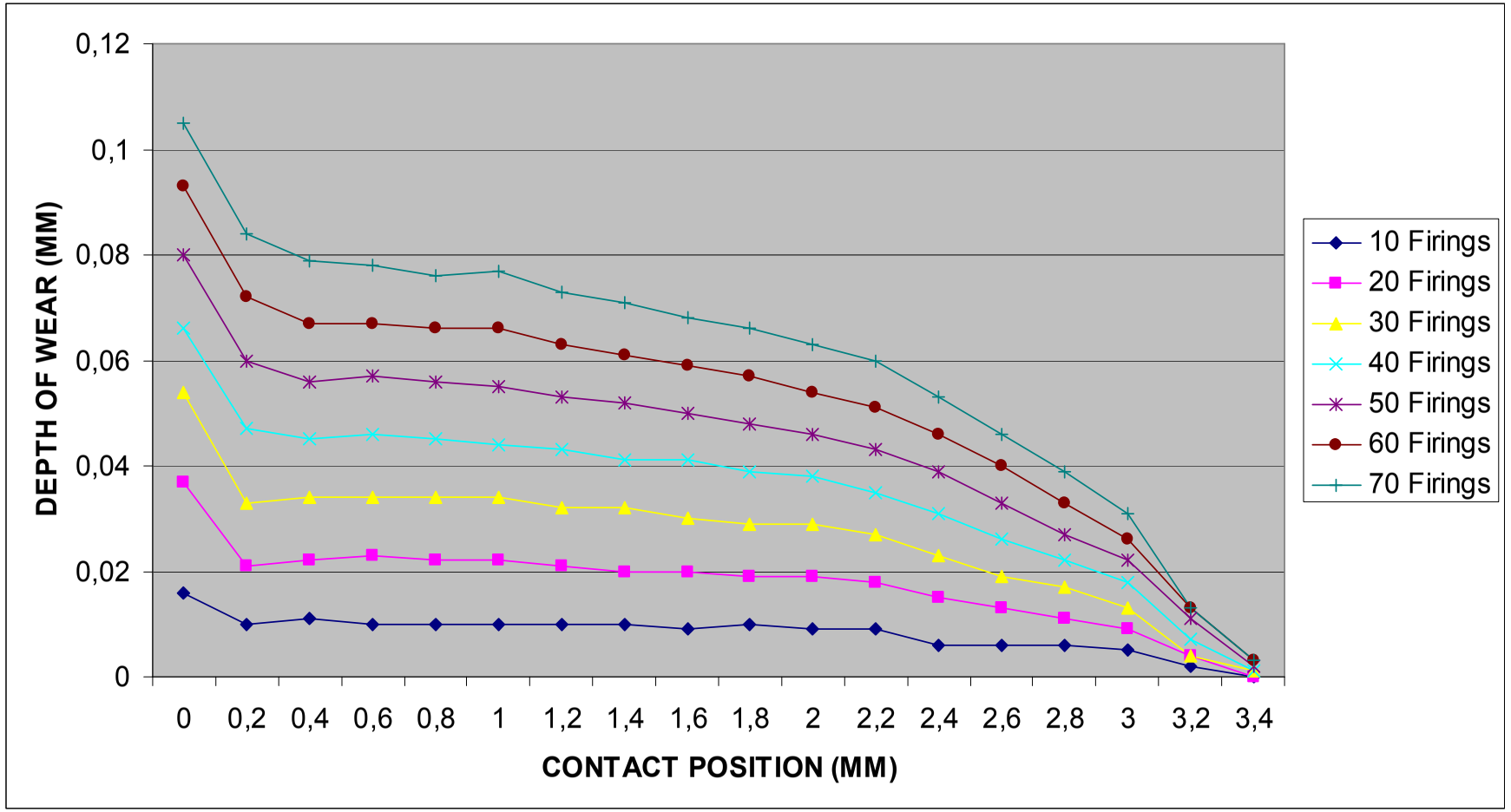

Figure 4-32 Sequential depth of wear on contact curve after each analysis

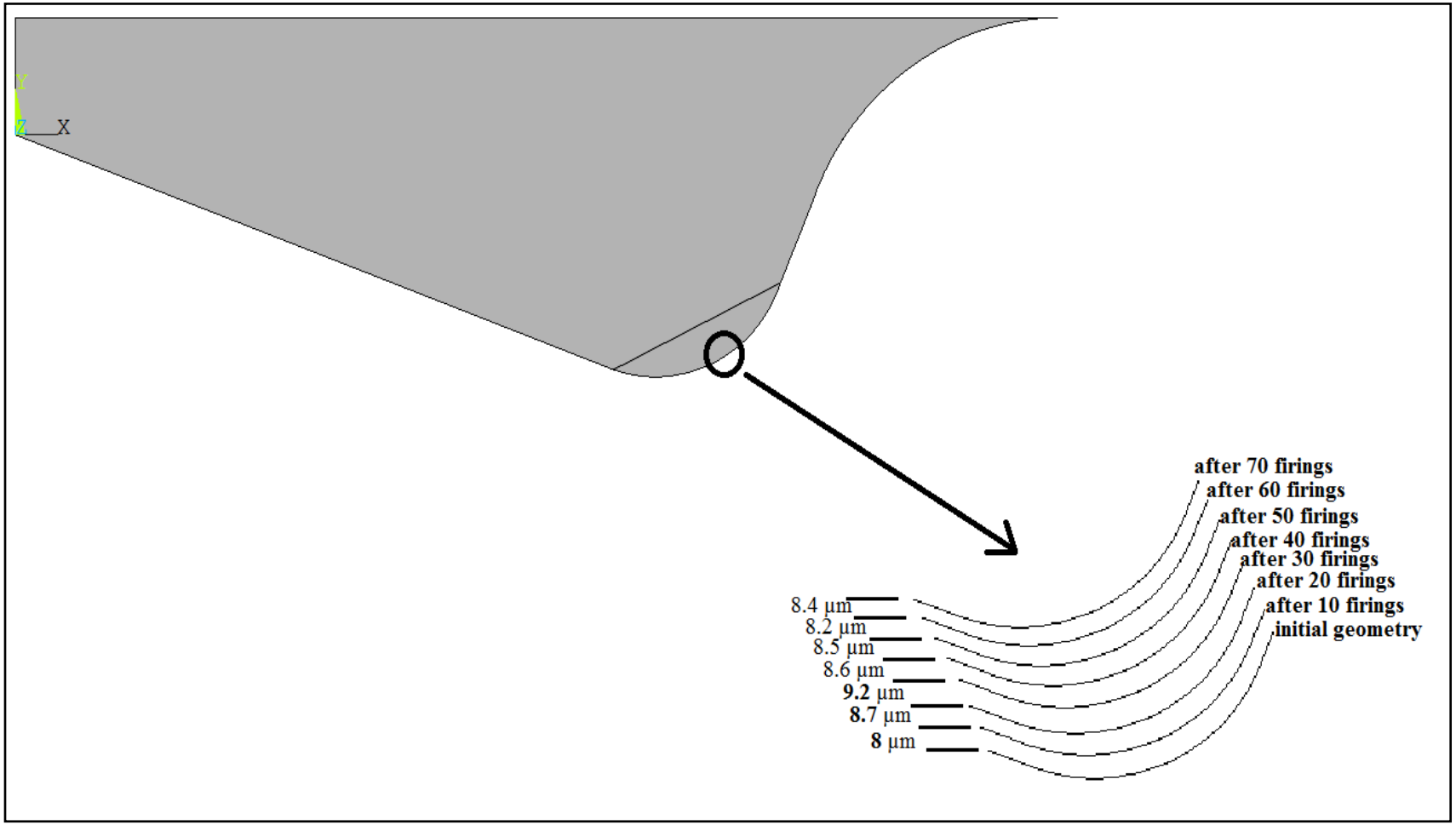

Figure 4-33 Sequential geometry changes in the release latch after each analysis

CHAPTER 5

DISCUSSION AND CONCLUSIONS

Wear in mechanical systems does not result in catastrophic failure of mechanical parts. However, wear results in crack initiation on the surface of materials and material failure is generally caused by propagation of these cracks in cycling loading. All of the studies made in this thesis work are based on establishing a procedure for predicting the amount of worn material in mechanical components of rail launchers that exists in the early stages of crack propagation. Experiments were made for measuring material loss due to wear. Contact pressure and temperature data were collected in firing tests in order to see whether they have effects or not on wear. Then, a numerical model of wear was constructed by the help of experimental results, in order to eliminate the need for additional firing tests.

5.1 DISCUSSION OF TEST RESULTS

Firing tests were made for this thesis study. There have been a total of ten firing tests. In three of them, temperature and pressure data of rocket motor jet were measured by the help of sensors located on the launcher. At the end of ten firing tests, the amount of worn material in investigated components of launcher was measured.

As mentioned before, the maximum temperature on rail was found as 65 ^{0}C and the maximum pressure was found to be 37 MPa. It was decided that these values of temperature and pressure have no significant effects on the mechanical properties of launcher parts.

At the end of ten firing tests, the contact surface measurements on the launcher rail and release latch were made. As shown in Appendix B, the results of surface measurements were used to calculate the amount of worn material. In Table 5-1, the calculated amount of worn materials is shown.

Table 5-1 The amount of worn material depth on the release latch

	The amount of worn material, μm
Launcher rail	1.266
Release latch	7.854

As it is given in the Table 5-1, the release latch of the launcher is faced with more severe wear than the rail. Therefore, it is decided that release latches are more critical than the rails and the modeling study is made on release latches.

The reason for less amount of worn material on the launcher rail should be the coating on the surface of the rail. The launcher rail is coated with hard-anodizing. For aluminum materials, hard-anodizing generates alumina (Al_2O_3) on the surface of the material. According to MIL-A-8625 anodic coatings for aluminum and aluminum alloys standard, "Type III hard-anodic coatings are intended to provide **wear and abrasion resistant** surfaces with improved corrosion protection due to greater thickness and weight than the conventional anodic coatings." Military standard also specifies, the thickness of the alumina surface on the materials is approximately 50 ± 10μm. As it is shown in

Table 5-2, very high hardness value of alumina compared to steel and aluminum makes it more wear resistant with respect to metallic materials.

Table 5-2 Mechanical properties of Alumina (Al_2O_3) [28]

Density (gr/cm^3)	3.96
Hardness (Rockwell C)	56
Ultimate tensile strength (MPa)	300
Modulus of elasticity (GPa)	370
Poisons ratio	0.22
Melting temperature (^{0}C)	2054

5.2 DISCUSSION OF THE SIMULATION RESULTS

In this thesis study, Archard wear law was used to evaluate wear depth on contacting surfaces because it is the most frequently used method in practical engineering applications. As mentioned previously, the wear constant used in Archard wear law is the connection between the experimental work and simulation. It is unique for different contacts of different components. Once the wear constant is obtained, the amount of wear can be simulated for every cycle of contact. Thus, the first aim in the simulation studies was to calculate the wear constant. Wear measurement results of the launcher release latch were used to calculate the wear constant and it was found as 0.02 for the contact between release latch and missile shoe. According to value of wear constant, the wear type is abrasive wear which is more severe than adhesive wear. As mentioned previously, the wear coefficient changes between 10^{-4} and 10^{-1} in abrasive wear. The wear type is an expected result because the contact area between the release latch and the missile shoe is small and large contact forces generated with the firing of the missile.

After calculating the wear coefficient, sequential analyses were made in order to find the wear depth of contact surface in release latch. At the end of seventh analysis, approximately 60 μm average wear depth was reached. This value was decided as wear depth limit at the beginning of thesis study because experiences show that when surface wear depth of release latch reaches to 60-80 μm, the surface cracks arise on the contact surfaces.

When wear depths evaluated at the end of each analysis is considered, it is realized that there is a linear growth in the values. This is the result of using constant wear coefficient which covers ten firings of missiles in the analysis. The wear coefficient between materials changes for repeated contacts [12]. As mentioned in Figure 5-1, the wear rate is initially high to steady in metallic materials. By using constant wear coefficient, initially high wear rate is covered for the rest of the contact. Thus, in the simulation for the same number of contacts N, deeper wear values were calculated and safer results were reached.

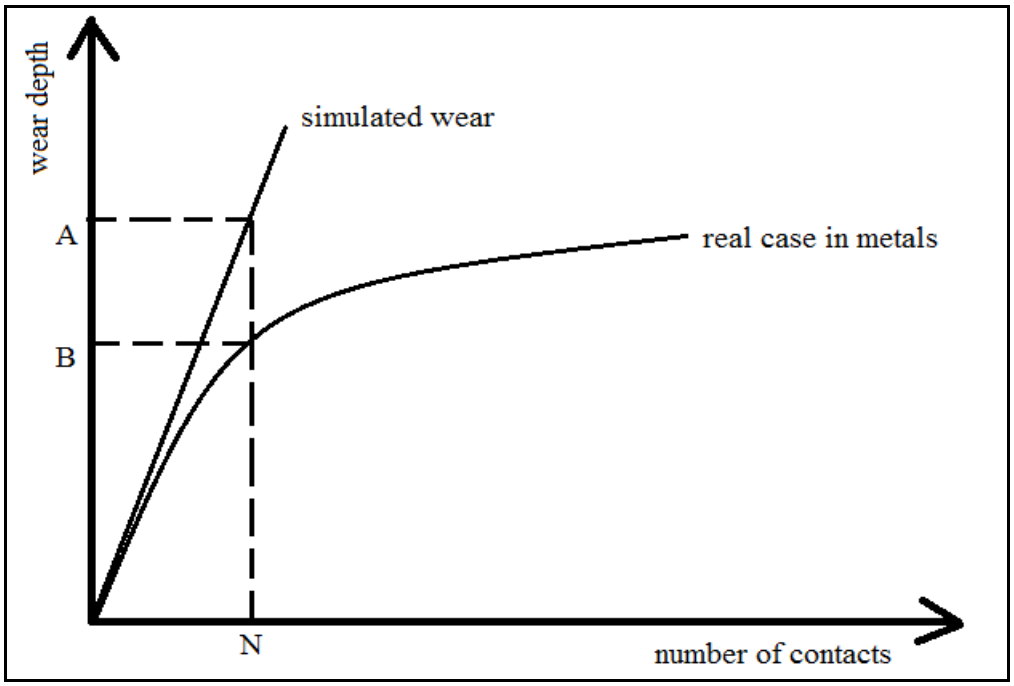

Figure 5-1 The graph of comparison between simulated wear and real case in metals

5.3 CONCLUSION

In order to eliminate the demand for firing tests, it was shown that a typical rail launcher was inspected in terms of its wear performance and a wear simulation procedure was established by using a commercial FE program and Archard wear law.

- The critical components of launcher were defined as launcher rail (AL-2024-T851) and release latch (AISI-4140).

- Wear measurements were made on the components which had been used in ten firing tests. The measurements showed that the average surface wear depth of the launcher rail and the release latch are 1.266 μm and 7.854 μm, respectively. Since wear on the release latch of the launcher was more severe, the wear simulation procedure was set for the release latch.

- In order to simulate wear by using Archard wear law, dimensionless wear coefficient must be known. Thus, wear coefficient was computed by using wear measurements on the release latch and it was determined as 0.02. This high value of wear coefficient shows that abrasive wear arises on the release latch.

- Once, the wear coefficient was calculated, sequential wear simulations were done. Linear increment was obtained in sequential wear simulation results. This linear behavior is the result of constant wear coefficient. However, considering constant wear coefficient is safer approach because it results in more severe wear, as mentioned in previous section. At the end of seventy missile firings, the contact surface of the release latch was worn approximately 60 μm which was defined as the wear depth limit at the beginning of the thesis study.

- Consequently, thesis study shows that dry wear between metallic materials can be modeled and be used to predict amount of worn material on launcher components up to surface crack initiation. Once the simulation procedure is fixed, it would be a powerful tool for predicting the life-time of the part due to wear.

5.4 RECOMMENDATIONS FOR FUTURE WORKS

This study was made in order to simulate wear performance of launcher components up to crack initiation. However, when surface cracks arise, crack propagation must be investigated in metals. A big portion of materials life-time is defined by its crack propagation simulations. Thus, as a future work, crack propagation caused by wear can be inspected in launcher components and the life-time of materials before failure can be predicted.

Moreover, as it is specified in modeling section, after each analysis run, the geometry of the model is updated manually with respect to calculated amount of worn material. A group of script codes can be written into FE program in order to make geometry update automatically. With automatic geometry update, faster wear analysis can be made, so analyses can be completed in a more time-efficient manner.

REFERENCES

[1] Lockheed Martin Corporation, “http://www.lockheedmartin..com” , Last Access Date: 18.05.2011

[2] Wikipedia, “http://en.wikipedia.org”, Last Access Date: 06.03.2011

[3] Deviantart, “http://scott2753.deviantart.com” , Last Access Date: 18.05.2011

[4] B.Lawton. “Thermo-chemical erosion in gun barrels”, 13th International Conference on Wear of Materials, vol. 251, issues 1-12, pp. 827-838, received October 2001

[5] Veritay Technology Inc., “http://www.veritay.com/”, Last Access Date: 12.06.2011

[6] F. Stefani, J.V. Parker, “Experiments to Measure Wear in Aluminum Armatures”, Magnetics, IEEE Transactions on, Vol. 35, Issue 1, pg. 100-106, January 1999

[7] S.Sopok, C. Rickard, S. Dunn, “Thermal-Chemical-Mechanical Gun Bore Erosio of an Advanced Artillery System Part two: Modelling and Predictions”, Wear 258, pg. 671-683, December 2003

[8] Gwidon W. Stachowiak, Andrew W. Batchelor, “Engineering Tribology”, Butterworth-Heinemann

[9] Harold A. Rothbert,” Mechanical Design Handbook”, McGraw-Hill Professional Publishing; Rev Sub edition, November 1, 1995

[10] Standard G40: Standard terminology relating to wear and erosion American Society for Testing and Materials (ASTM International, West Conshohocken 2005)

[11] Archard, J.F. (1953), “Contact and Rubbing of Flat Surfaces”, J. Appl. Phys. 24, 981-988

[12] Bharat Bhushan (2001), “Modern Tribology Handbook, Volume I Principles of Tribology”

[13] Bayer, R.G. (1994), “Mechanical Wear Prediction and Prevention”, Marcel Dekker, New York, 280.V.L. Popov,” Contact Mechanics and Friction”, Springer-Verlag Berlin Heidelberg 2010
[14] Poeton Industries Limited, “http://www.poeton.co.uk”, Last Access Date: 28.03.2011

[15] D.H. Buckley, Surface Effects in Adhesion, Friction, “Wear and Lubrication”, Elsevier, 1981

[16] Substances and Technologies, “http://www.substech.com” , Last Access Date: 28.03.2011

[17] Whitehouse, D.J. (1994), “Handbook of Surface Metrology”, Institute of Physics Publishing, Bristol, U.K.

[18] I.V. KRAGELSKY, V.V. ALISIN, “Friciton Wear Lubrication”, Tribology Handbook, Volume 1, Oxford; New York: Pergamon Press, 1981.

[19] Anonymous (1985), “Surface Texture (Surface Roughness, Waviness and Lay)”, ANSI/ASME B46.1, ASME, New York.

[20] Horst Czichos, Tetsuya Saito, Leslie Smith, “Springer Handbook of Materials Measurement Methods”, Springer 2006

[21] R.S. Sayles and T.R. Thomas “A Stochastic Explanation of Some Structural Properties of a Ground Surface” International Journal of Production Research, Vol. 14, 1976, pp. 641-655

[22] T.R. Thomas (editor) “Rough Surfaces” Longman Group Limited, 1982

[23] Mike Stewart, “A New Approach to the Use Of Bearing Area Curve”, International Honing Technologies and Applications, May 1-3, 1990, Novi\Michigan

[24] ISO 13565-2:1996(E), “Geometrical Product Specification (GPS) - Surface Texture: Profile Method; Surfaces having stratified functional properties- Part2: Height characterization using the linear material ratio curve”

[25] Staffan Johansson, Per H. Nilsson, Robert Ohlsson, Cecilia Anderberg, Bent-Göran Rosen "New Cylinder Liner Surfaces for Low Oil Consumption", Tribology Internatonal, vol. 41, pp. 854-859, recived February 2007.

[26] J.A. Greenwood and J.B.P. Williamson, “Contact of Nominally Flat Surfaces”, Proc. Roy. Soc., London, Series A,Vol. 295, 1966, pp. 300-319.

[27] C. E. Shannon, "Communication in the presence of noise", Proc. Institute of Radio Engineers, vol. 37, no.1, pp. 10–21, Jan. 1949. (Reprint as classic paper in: Proc. IEEE, Vol. 86, No. 2, Feb 1998)

[28] Material Property Data, “http://www.matweb.com” , Last Access Date: 05.06.2011

[29] Gwidon W. Stachowiak, Andrew W. Batchelor, Grazyna B. Stachowiak, “Experimental Methods in Tribology” , Tribology Series 44, Editor : D. Dowson, Elsevıer, June 2004

[30] Miguel A. Pando, Carl D. Ealy, George M. Filz, J.J. Lesko, and E.J. Hoppe, “A Laboratory and Field Study of Composite Piles for Bridge Substructures”, United States Department of Transportation-Federal Highway Administration, report no: FHWA-HRT-04-043, March 2006

[31] A.S. Birring and H. Kwun, “Ultrasonic Measurement of Wear”, Tribology International, Vol. 22, 1989, pp. 33-37

[32] Mona Öqvist, “Numerical simulations of mild wear using updated geometry with different step size approaches”, WEAR, vol. 249, pp. 6-11, received October 2000

[33] V Hegadekatte, N Huber, O Kraft “Finite element based simulation of dry sliding wear”, Modelling and Simulation in Materials Science and Engineering, vol. 13, pp. 57-75, received July 2004

[34] Molinari J F, Ortiz M, Radovitzky R and Repetto E A “Finite-element modeling of dry sliding wear in metals”, Eng. Comput. 18, pp. 592–609, 2001

[35] YanW, O’Dowd N P and Busso E P “Numerical study of sliding wear caused by a loaded pin on a rotating disc”, J. Mech. Phys. Solids 50, pp. 449–70, 2002

[36] Priit Podra, Sören Andersson “Simulating Sliding Wear with Finite Element Method”, Tribology International, 32, pp. 71-81, 1999

[37] ANSYS 13 HELP LIBRARY, 2011

[38] R. W. Smith, F. Ditrói, E. Corniani, Th. Wopelka, M. Jech, ”Measurement of Surface Wear Using Thin Layer Activation (TLA) technique”, International Topical Meeting on Nuclear Research Applications and Utilization of Accelerators

[39] Rajesh Kumar, Salil Kumar, Braham Prakash, A. Sethuramiah “Assessment of Engine Liner Wear from Bearing Area Curves”, WEAR, vol. 239, pp. 282-286, received May 1999

APPENDIX A

TECHNICAL SPECIFICATIONS

A.1 AMBIOS TECHNOLOGY XP-2 STYLUS PROFILER SPECIFICATIONS

Sample Stage Diameter: 200mm Microprocessor: Pentium
Scan Length Range: 50mm Operating System: Windows XP
X-Y Stage Translation: 150mm x 178mm Interface Method: Mouse/Keyboard
Sample Thickness: 1.25 inches Monitor: 17" SVGA
Stage Positioning: Motorized Power Requirements: 115V, 60 cycles or
Vacuum Chuck -250mm Hg 230V, 50 cycles
Vertical Resolution: 1 Å at 10μm, 10 Å at 100μm Shipping Weight: 158 lbs
Lateral Resolution: 100nm (w/computer) 223 lbs
Vertical Range: 100um max.
Step Height Repeatability: 10Å on 1um step, 1 sigma SD Dimensions: Depth Width Ht.
Max. Data Points per Scan: 50,000 (w/o computer) 24" 15" 11"
Sample Viewing: Color Camera
Standard Magnification: 40-160X motorized zoom
Field of View: 1-4mm
Stylus Tip Radius: 2.5 microns
Stylus Force Range: .05-10mg (programmable)
Software Leveling: Yes, cursor-controlled
Scan Filtering: Low-pass and high-pass adjustable filter
Stress Measurement S/W: Yes

Multi Points Measurement: 1024 Points Programming and Auto Measurement
3-D Image Profile: Yes (Option)
Roughness Parameters: Ra, Rq, Rp, Rv, Rt, Rz
Waviness Parameters: Wa, Wq, Wp, Wv, Wt, Wz
Step Height Parameters: Avg. Step Ht., Avg. Ht., Max. Peak, Max. Valley, Peak to Valley
Geometry Parameters: Area, Slope, Radius, Perimeter
Other Parameters: Stress analysis, height histogram, skewness, profile subtraction
Stylus: Submicron radius .2 micron (+/- .1 micron)
Stylus: Submicron radius .5 micron (+/- .4 micron)
Stylus: 2.5 micron radius
Stylus: 5.0 micron radius
Vibration Isolation System
Ambios Technology Reference Standard: 1µm Nominal Avg. Step Ht.
Step Height Stds: 20nm, 50nm, 100nm, 200nm, 0.5µm, 1.0µm, 5µm, 10µm
Extended Warranty for 12 additional months, including parts & labor (domestic only)
HP DeskJet 932C Color Inkjet Printer
• Semiconductors: step height, etched depths & stress
• Magnetic Disks: micro roughness and dub-off
• Hybrid Circuits: thick films and substrate roughness
• Industrial: chemical etching, coating and polishing

A.2 TECHNICAL SPECIFICATIONS FOR DATA ACQUSITION SYSTEM

ESA Messtechnik GmbH
Schlossstr. 119 - D-82140 Olching / Munich
Telefon: +49 (0)8142 444 130 - Fax: +49 (0)8142 444 131
Internet: www.esa-messtechnik.de
E-Mail: info@esa-messtechnik.de

Signal Conditioner Amplifier System *Traveller* CF

NEW

Description:

Traveller CF is a Signal Conditioner Amplifier System with Card-Flash data storage. Flexible channel numbers and simple, straight forward operational procedures make the system meet the latest requirements of digital measurement technology and digital data processing. A built-in PCM-encoder enables telemetric operation with fast data transfer rates and high data security. System *Traveller* CF excellently satisfies all the sophisticated demands of stationary and mobile measurements of mechanical and electrical quantities..

Figure A-1 The technical specitifition for data acqusition system used in firing tests

- Low power, low voltage, fully digitalised system
- Arbitrarily selectable and changeable channel identification
- Continuous real time data transfer with up to 8 MB/sec via USB 2.0 Port
- Multiple Synchronisation of four CF-units resulting in 128 channels system capacity
- Complete Off-Line system setup through frontplate keyboard
- Real time data acquisition under hostile environmental conditions directly on Card-Flash-Memory without computer connection
- Built-in PCM-Encoder (IRIG 106) for data transfer as serial data stream (with bit rate of up to 10.0 MBits/sec) for telemetric or cable operation

Technical Specifications (Basic Unit):

Housing:	For 32 and 64 channels systems with LCD-display and frontplate keyboard
Number of Channels:	8 analog channels per analog board (up to 4 or 8 boards per system)
Data Acquisition:	Simultaneous data acquisition sampling process of all channels in system
A/D-Converter:	16 bit A/D-converter for each analog channel; range ±2,500 VDC; Programmable sampling rate of up to 100.000 samples per second per channel
Filter:	Digital hardware filter for each channel (noise reduction)
Interface:	USB2.0 interface (compatible with USB1.1) for data transfer and setup commands to or from PC (USB-Modus)
Additional Interface:	RS232C interface for connection event markers like AT-MARK-2 or AT-MARK-3 (or modem)
Data Storage and Data Readout:	Data stream can be stored on CF card memory, inserted in system slot. Sampling rate with continuous writing of data to CF card: 600kS/s max. Data at CF card memory can also be transferred to PC through special PCMCIA or USB-Adapter. CF card will be identified by PC as standard hard disk drive. WINDOWS® compatible file system implemented on the system's CF cards. CF card storage space up to 2 GB. Optionally, CF cards can be replaced by standard hard-disk-drive device (Opt. HDD).
Trigger:	Analog signal – rising edge (programmable level and duration); analog signal – falling edge (programmable level and duration); analog signal - level (programmable level and duration).
Power Supply:	10 to 36 VDC
Size and Weight:	205 x 305 x 115 mm, 3 kg - for 32 channels system housing 205 x 305 x 230 mm, 5 kg – for 64 channels system housing

Plug-in Board Features:

- Analog signal bandwidth up to 50 kHz per channel
- Separate, programmable 16 bit A/D-converter for each channel
- Integrated, programmable 0 to 8 VDC excitation voltage supply for connected sensors
- Permissable current of excitation power supply max. 320 mA with overload protection
- Built-in bridge completion resistors for strain gauge applications
- Integrated, programmable low-pass filter up to 10 000 Hz
- ± 5 V analog output for each channel (short circuit proof)

Figure A-1 continued

Technical Specifications Strain Gauge Input Board Mod. SGA-0D:

Number of Channels:	8 complete signal conditioner amplifier channels per board
Input:	120 Ω, 350 Ω strain gauge quarter bridge circuits, 50 Ω to 5000 Ω strain gauge half and full bridge circuits and strain gauge based transducers.
Input Voltage:	± 2,5 V
Input Overload Voltage Protection:	± 30 V
Input Impedance:	10 MΩ
Signal Bandwidth:	0 to 10 kHz @ gain 100x
Bridge Excitation:	Software-programmable common DC-excitation for all 8 channels, **Range:** 0 to 7,0 VDC max. in steps of 2,5 mV **Current:** 320 mA max. per board with overload protection
Measurement Range:	Strain gauges (gauge factor K=2): at U_B= 1,0 to 5,0 VDC and gain = 10: ± 500.000 to ± 100.000 µm/m, at U_B= 1,0 to 5,0 VDC and gain = 100: ± 50.000 to ± 10.000 µm/m, at U_B= 1,0 to 5,0 VDC and gain = 1000: ± 5.000 to ± 1.000 µm/m, Potentiometers: at U_B= 5,000 VDC and gain = 1: ± 2,500 V (F.S.R.)
Balance Range:	±100% of measurement range, resolution 16 bits
Balance Time:	3 s, independent of number of channels
Calibration:	+1000 µm/m for 120 Ω and 350 Ω quarter bridges (shunt resistor across internal bridge completion); -500 µm/m for half bridges (shunt resistor across internal half bridge arm); -1000 µm/m for quarter bridges with temp. compensation gauge (shunt resistor across internal half bridge arm)
Filter (for each analog channel):	4-Pol Butterworth: Cut-off frequency 4000 Hz (-3dB) Digitally averaging noise reduction filter
Analog Output:	± 5 V for each channel

Technical Specifications Strain Gauge Input Board Mod. MBA-0 – SGA-0:

	Number of Channels:	8 complete signal conditioner amplifier channels per board
Analog Inputs:	**Input Impedance:**	20 MΩ shunted by 600pF
	Configuration:	Quarter, half, or full-bridge strain gage and transducer or source voltage. Internal half bridge, 350 Ω and 120 Ω dummy, internal calibration shunts.
	Differential Voltage:	± 2,5 V
	Common Mode Voltage:	± 2,5 V
	Input Protection Voltage:	protected from damage up to +/-30V VDC
Bridge Constant Voltage Excitation:	**Range:**	0.0V to 8V (software programmable), increments of 2.5mV, max. current 40mA
	Accuracy:	0,1 % ± 5 mV
	Temperature Stability :	0,01% /°C
Balance:	**Type:**	automatic electronic balance circuitry
	Range:	±10 000 µm/m for Vexc.=5V and gain: 50, 100, 200, 400 V/V ±100 000 µm/m for Vexc.=5V and gain: 1, 2, 4, 8 V/V
	Balance Time:	3 s, independent of number of channels
Calibration:	**Internal shunt calibration resistors:**	RC1 = 174,65 kΩ, ± 0,1 %; 1000 µm/m (0,50 mV/V) for 350 Ω and Gage-Factor 2,00 RC2 = 59,86 kΩ, ± 0,1 %; 1000 µm/m (0,50 mV/V) for 120 Ω and Gage-Factor 2,00
	Calibration procedure:	Internally controlled electronic switches for internal and external, unipolar or bipolar calibration

Figure A-1 continued

Amplifier:	**Gain:**	1; 2; 4; 8; 50; 100; 200; 400 (If You replace a gain step a gain of 800 is possible)
	DC Gain Accuracy:	± 0,2 %
	DC Gain Stability:	30 ppm/°C
	Linearity:	0.02% of Full Scale Range
	Frequency Response:	DC to 50 kHz: -3dB at all gain settings and full output
	Slew Rate:	0,5 V/µs
	Noise:	(with 350 Ω source impedance), Referred to Input (RTI) : <1.5mV RMS at input frequency in range 0.1 Hz - 10 kHz
	Temperature Co. of Zero:	Max. ± 1µV/°C
	Common-Mode Rejection:	CMR=80dB typical for Gain = 1, 2, 4, 8 CMR=100dB typical for Gain = 50, 100, 200, 400
Analog-Output:	**Output:**	± 5 V for each channel
	Output-Filter:	Five-pole Butterworth low-pass filter with software selectable 3dB bandwidths of 10Hz to 10kHz

Figure A-1 continued

APPENDIX B

WEAR MEASUREMENT AND SIMULATION RESULTS

B.1 MEASUREMENT RESULTS OF THE RAIL PARTS

The measured regions were numbered as shown in Figure B-1.

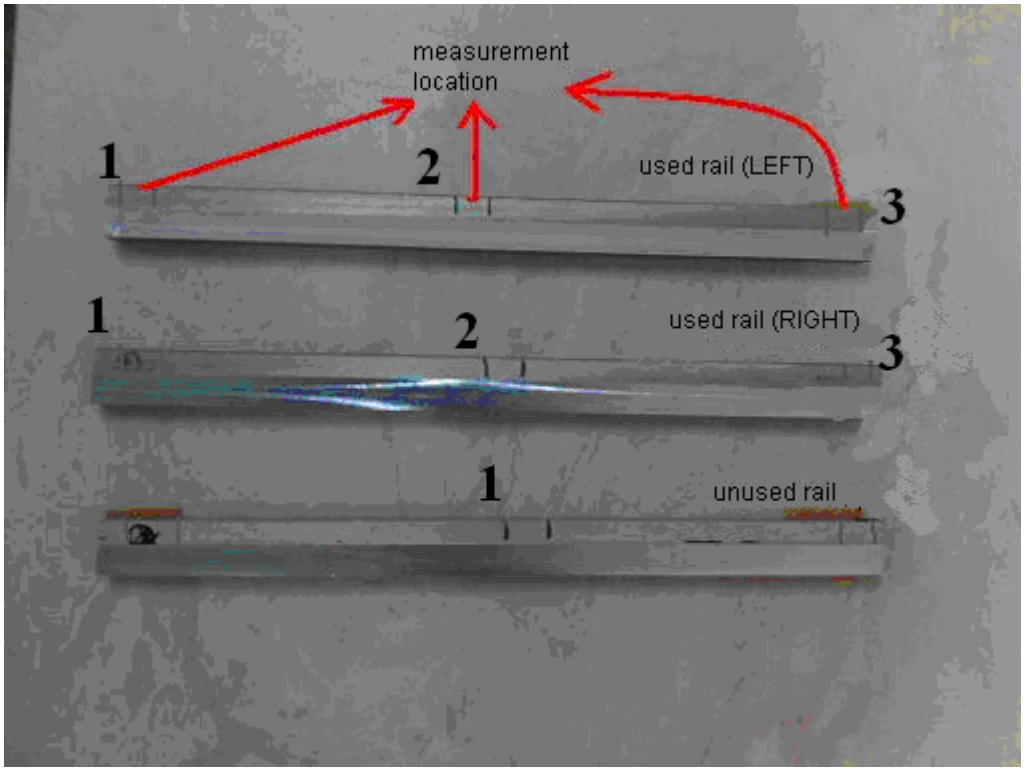

Figure B-1 Numbered regions of measured parts

According to the given numbers, surface profiles, BAC's and calculated BAC parameters were shown in below figures and tables.

Measurement results for the left side of used rail are given below (regions are given in respective order):

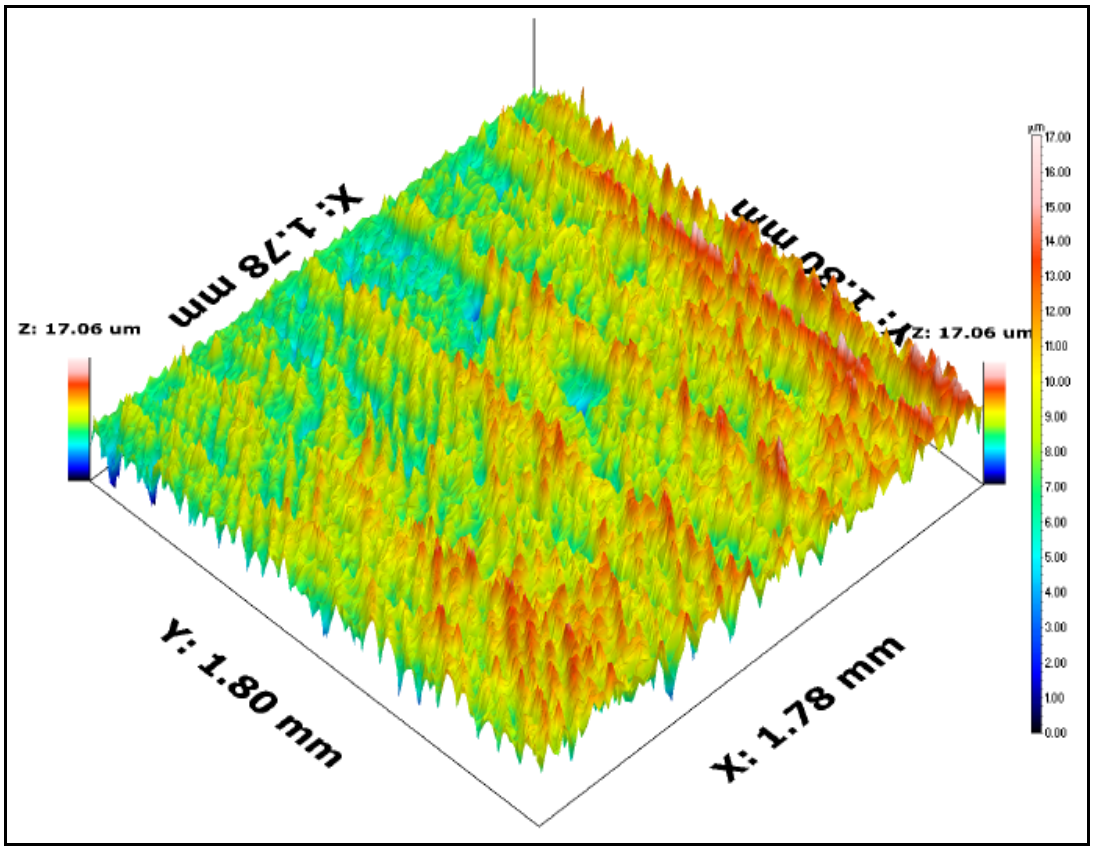

Figure B-2 3D surface profile of the left side and region 1

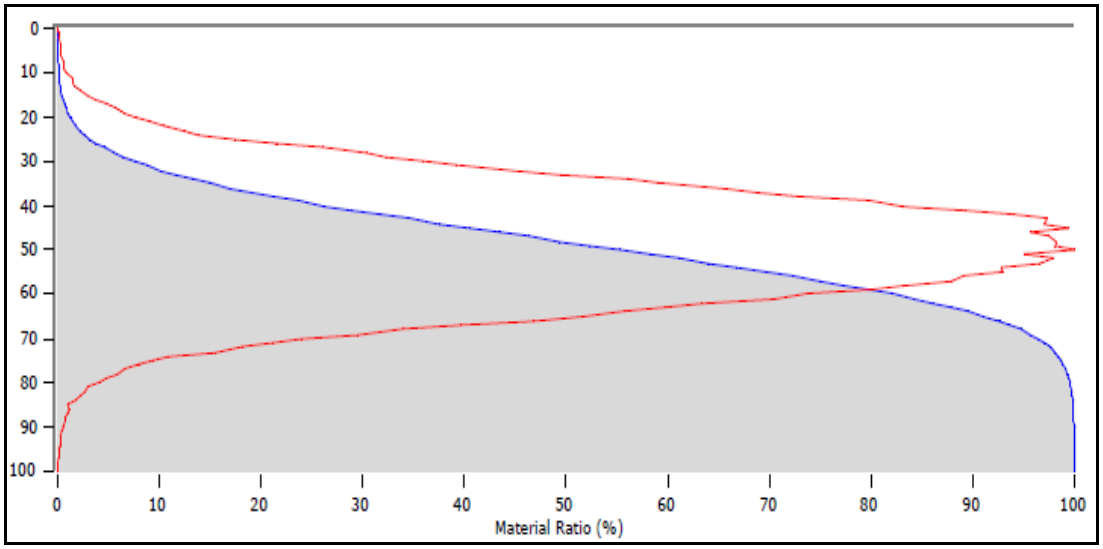

Figure B-3 BAC of the left side and region 1

Table B-1 BAC parameters of the left side and region 1

PARAMETERS	VALUES	DESCRIPTION
R_k (µm)	5.87	Core roughness depth
R_{vk} (µm)	1.76	Reduced valley depth
R_{pk} (µm)	1.97	Reduced peak height
Mr1 (%)	8.852	Material ratio 1
Mr2 (%)	91.725	Material ratio 2

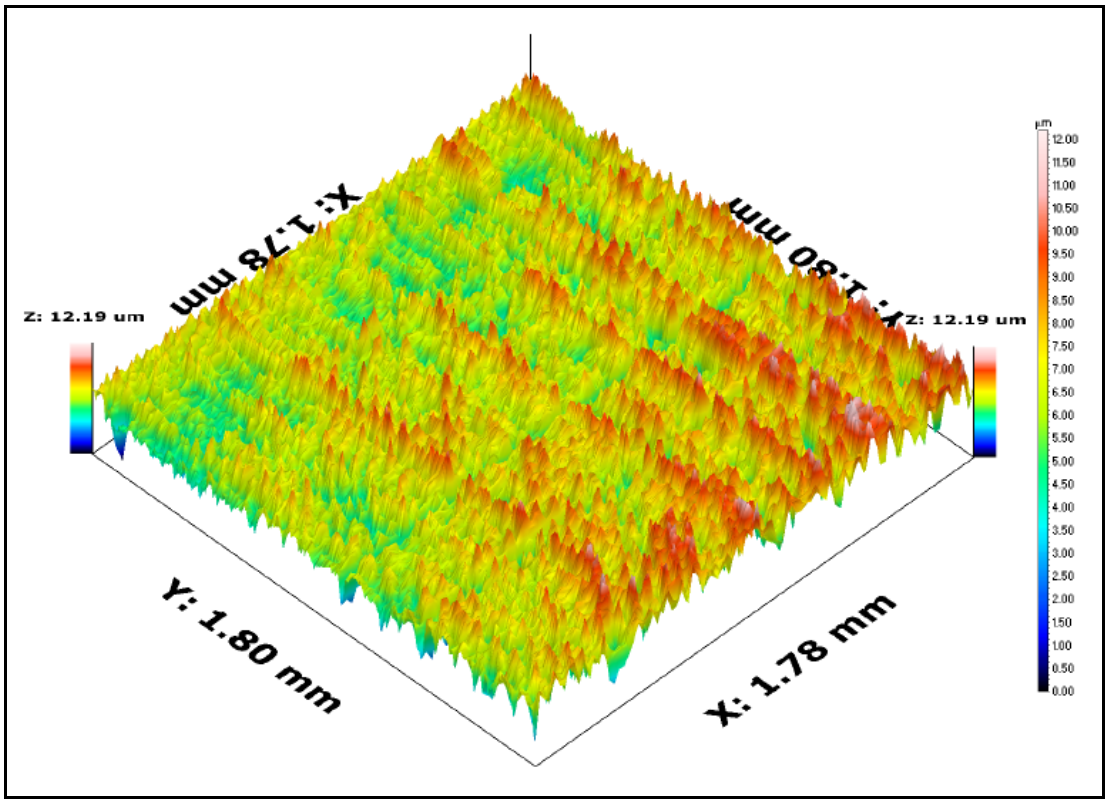

Figure B-4 3D surface profile of the left side and region 2

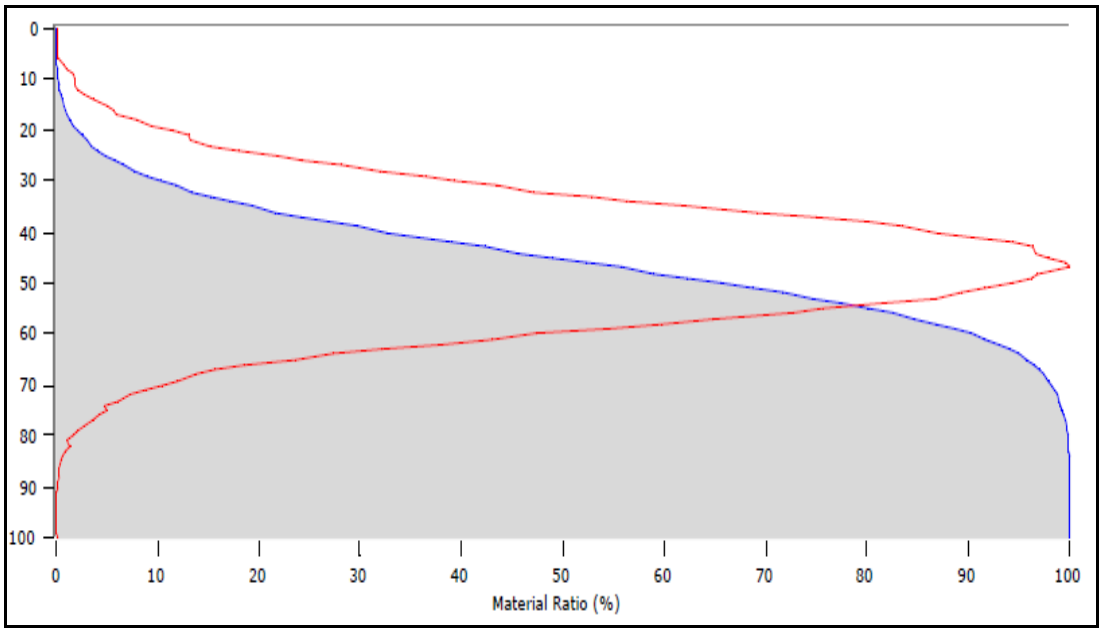

Figure B-5 BAC of the left side and region 2

Table B-2 BAC parameters of the left side and region 2

PARAMETERS	VALUES	DESCRIPTION
R_k (µm)	3.76	Core roughness depth
R_{vk} (µm)	1.31	Reduced valley depth
R_{pk} (µm)	1.48	Reduced peak height
Mr1 (%)	10.185	Material ratio 1
Mr2 (%)	91.302	Material ratio 2

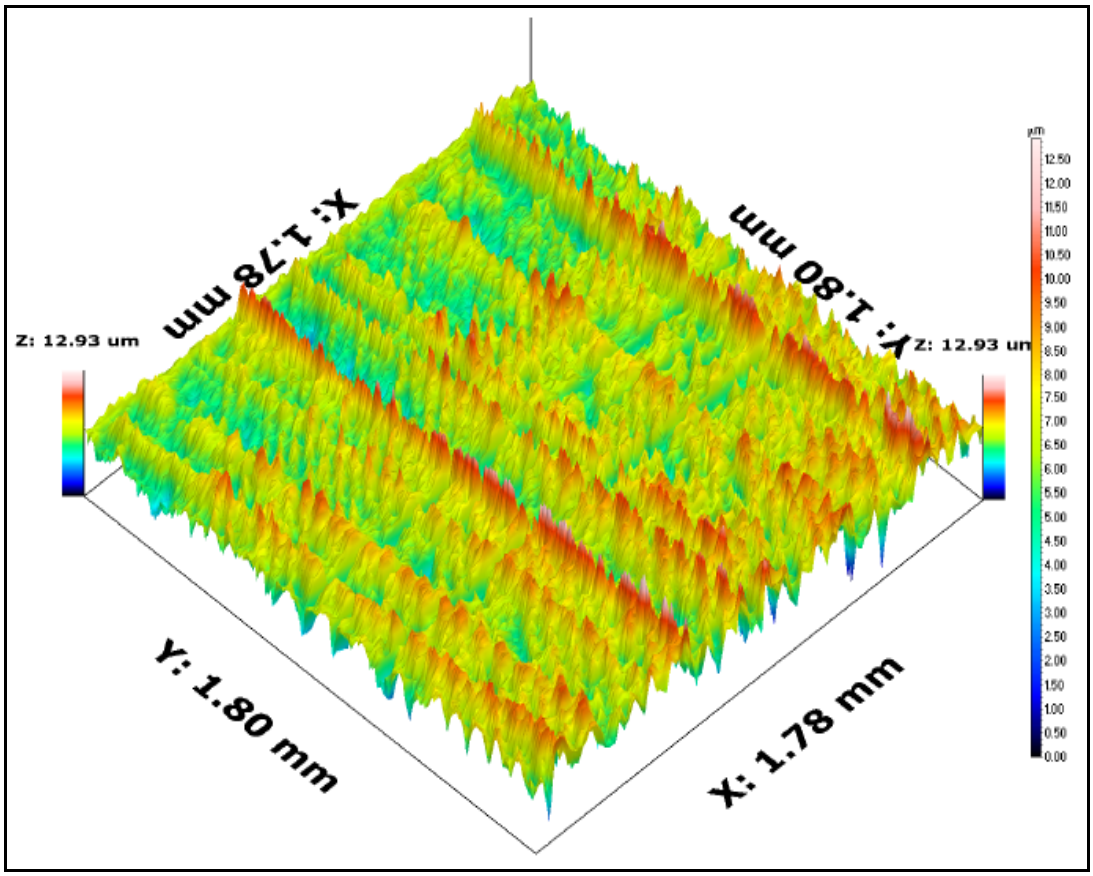

Figure B-6 3D surface profile of the left side and region 3

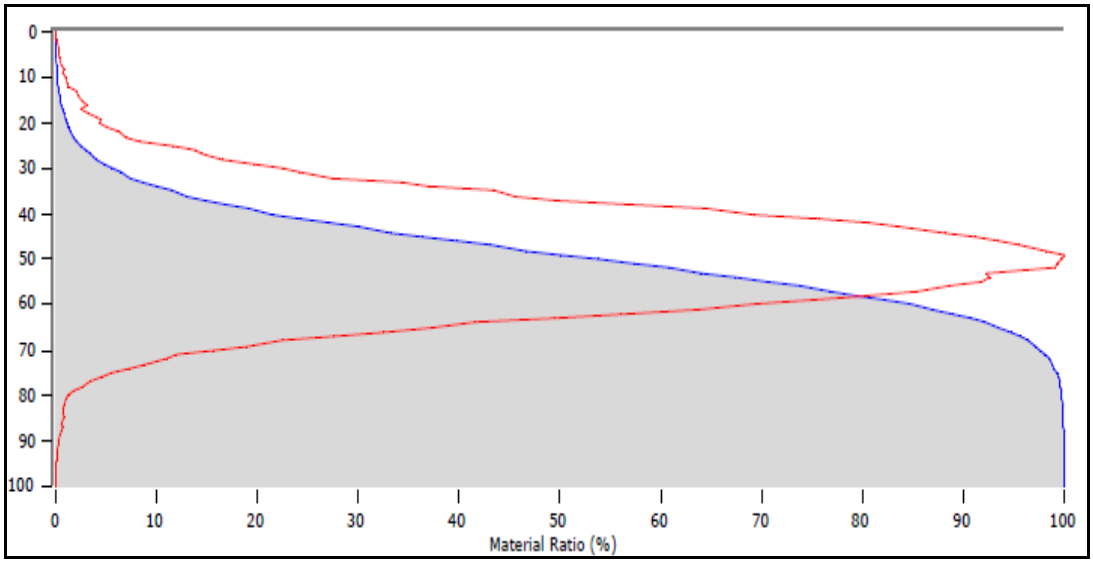

Figure B-7 BAC of the left side and region 3

Table B-3 BAC parameters of the left side and region 3

PARAMETERS	VALUES	DESCRIPTION
R_k (µm)	3.83	Core roughness depth
R_{vk} (µm)	1.24	Reduced valley depth
R_{pk} (µm)	1.69	Reduced peak height
Mr1 (%)	10.190	Material ratio 1
Mr2 (%)	91.836	Material ratio 2

Measurement results for the right side of used rail are given below (regions are given in respective order):

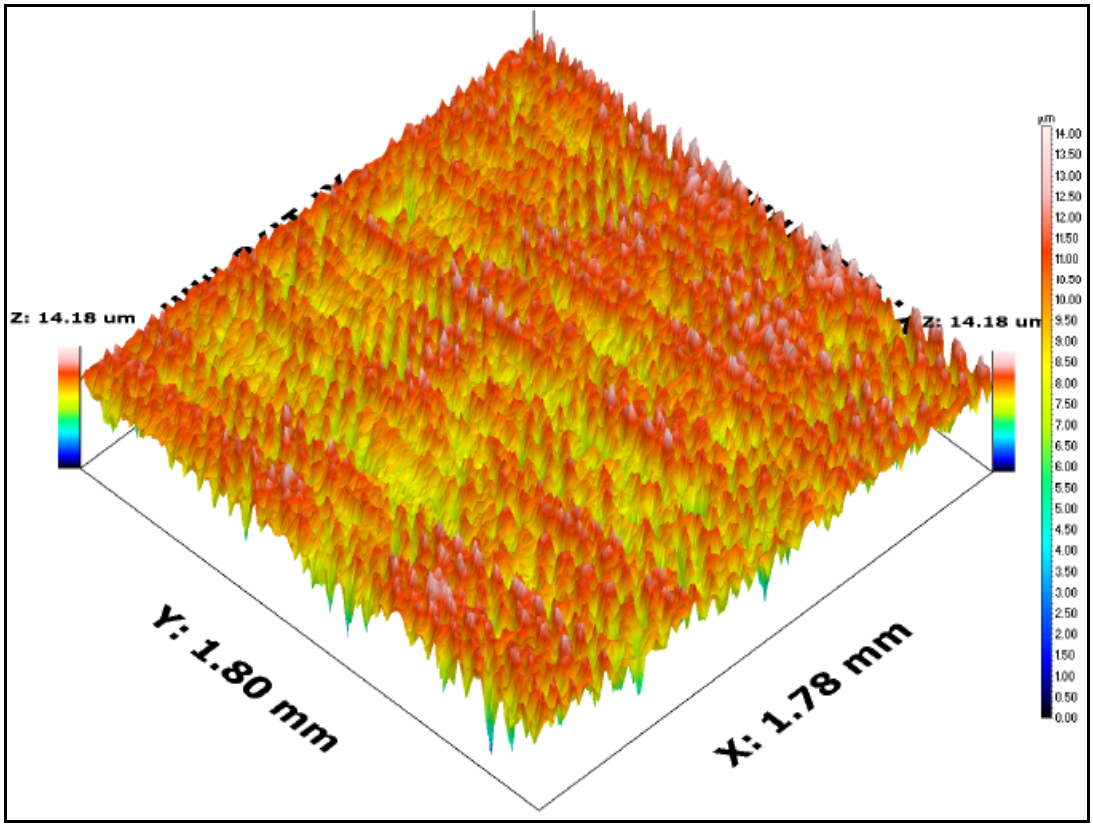

Figure B-8 3D surface profile of the right side and region 1

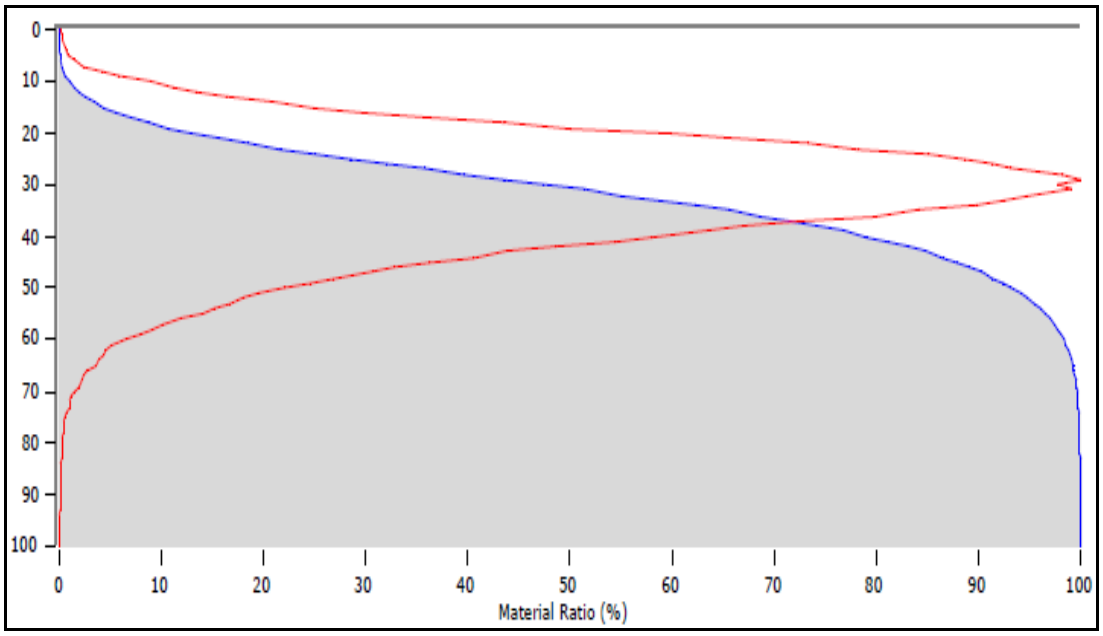

Figure B-9 BAC of the right side and region 1

Table B-4 BAC parameters of the right side and region 1

PARAMETERS	VALUES	DESCRIPTION
R_k (µm)	3.84	Core roughness depth
R_{vk} (µm)	2.15	Reduced valley depth
R_{pk} (µm)	1.06	Reduced peak height
Mr1 (%)	7.312	Material ratio 1
Mr2 (%)	86.703	Material ratio 2

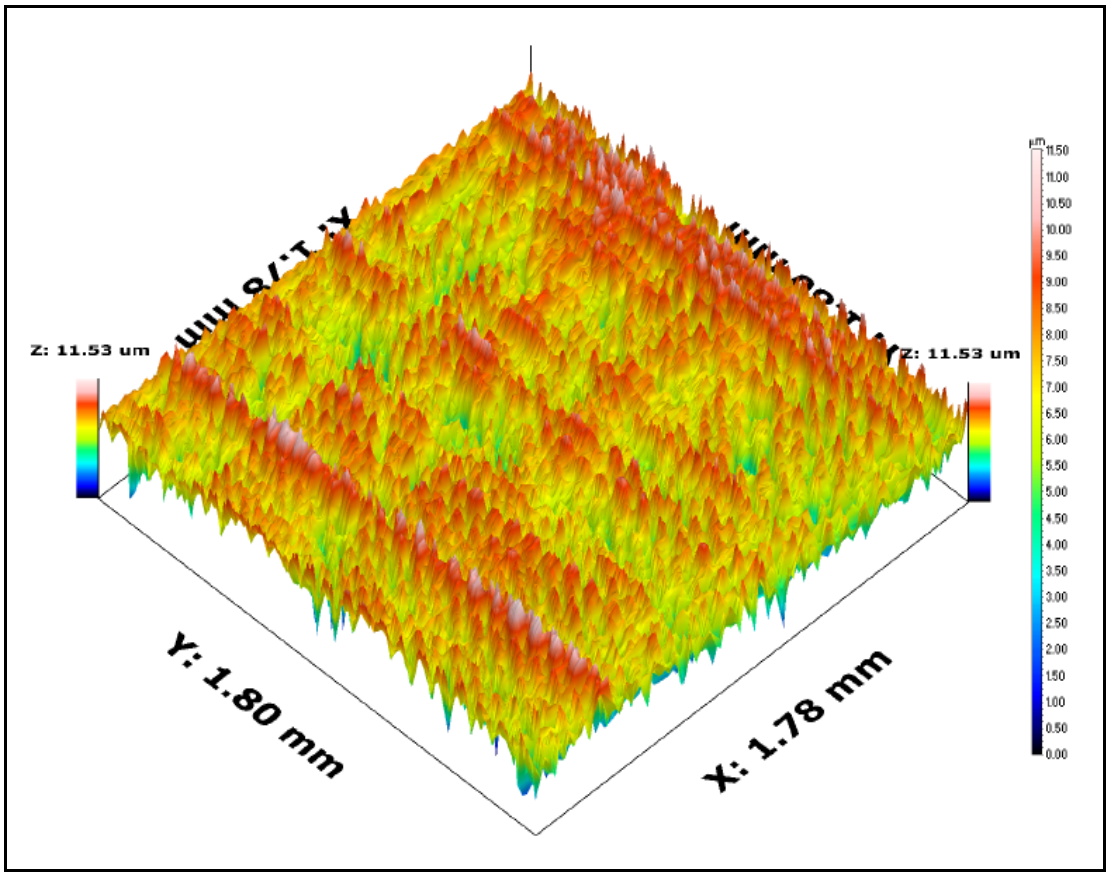

Figure B-10 3D surface profile of the right side and region 2

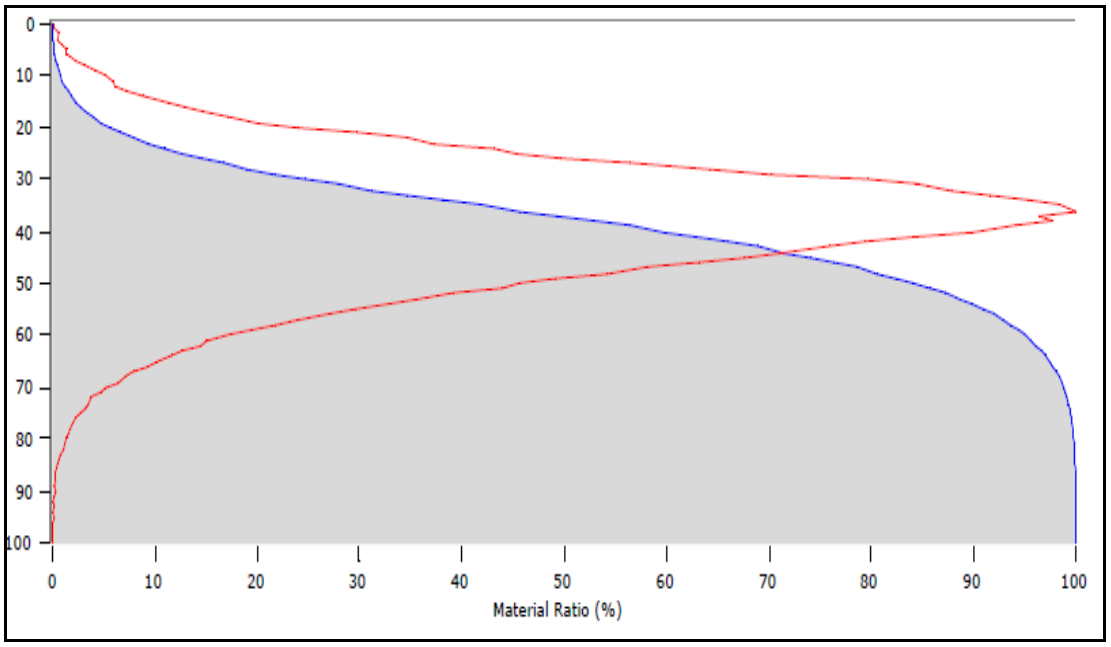

Figure B-11 BAC of the right side and region 2

Table B-5 BAC parameters of the right side and region 2

PARAMETERS	VALUES	DESCRIPTION
R_k (µm)	3.34	Core roughness depth
R_{vk} (µm)	1.80	Reduced valley depth
R_{pk} (µm)	1.21	Reduced peak height
Mr1 (%)	9.045	Material ratio 1
Mr2 (%)	86.834	Material ratio 2

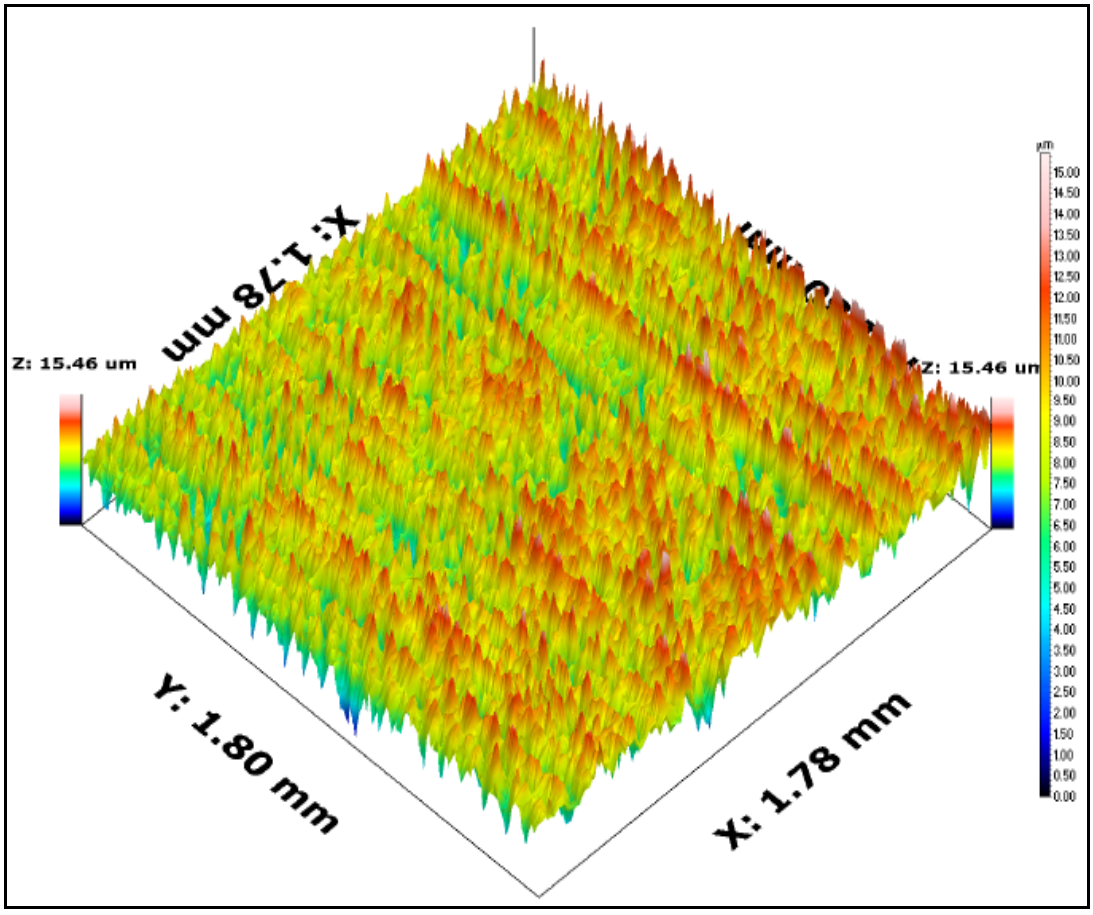

Figure B-12 3D surface profile of the right side and region 3

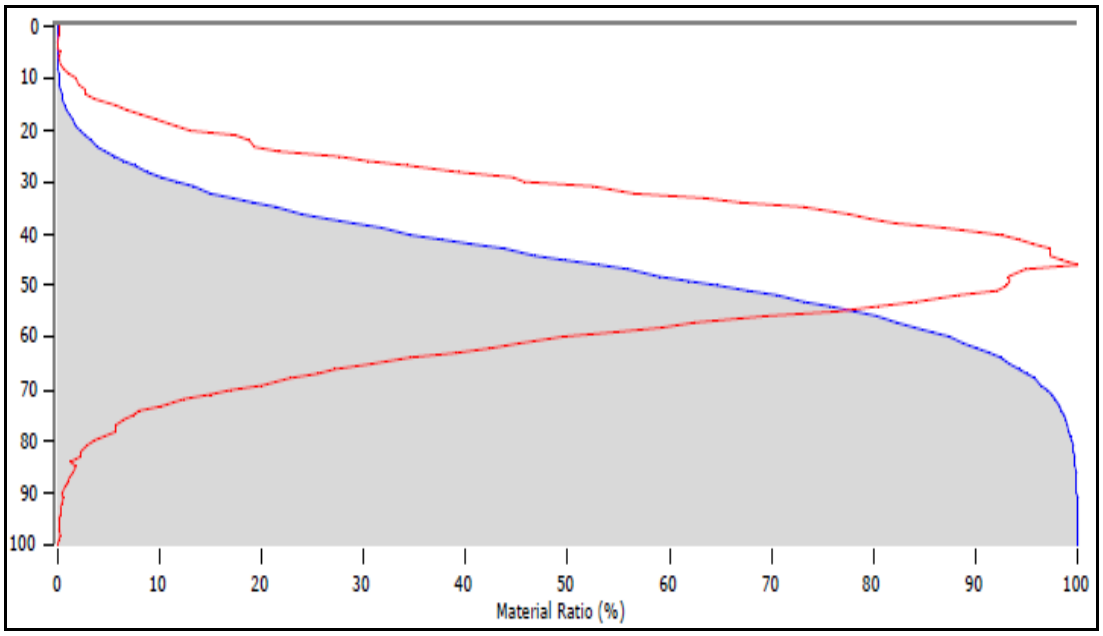

Figure B-13 BAC of the right side and region 3

Table B-6 BAC parameters of the right side and region 3

PARAMETERS	VALUES	DESCRIPTION
R_k (µm)	5.21	Core roughness depth
R_{vk} (µm)	2.01	Reduced valley depth
R_{pk} (µm)	1.74	Reduced peak height
Mr1 (%)	9.193	Material ratio 1
Mr2 (%)	90.034	Material ratio 2

Measurement results for the right side of used rail are given below (regions are given in respective order):

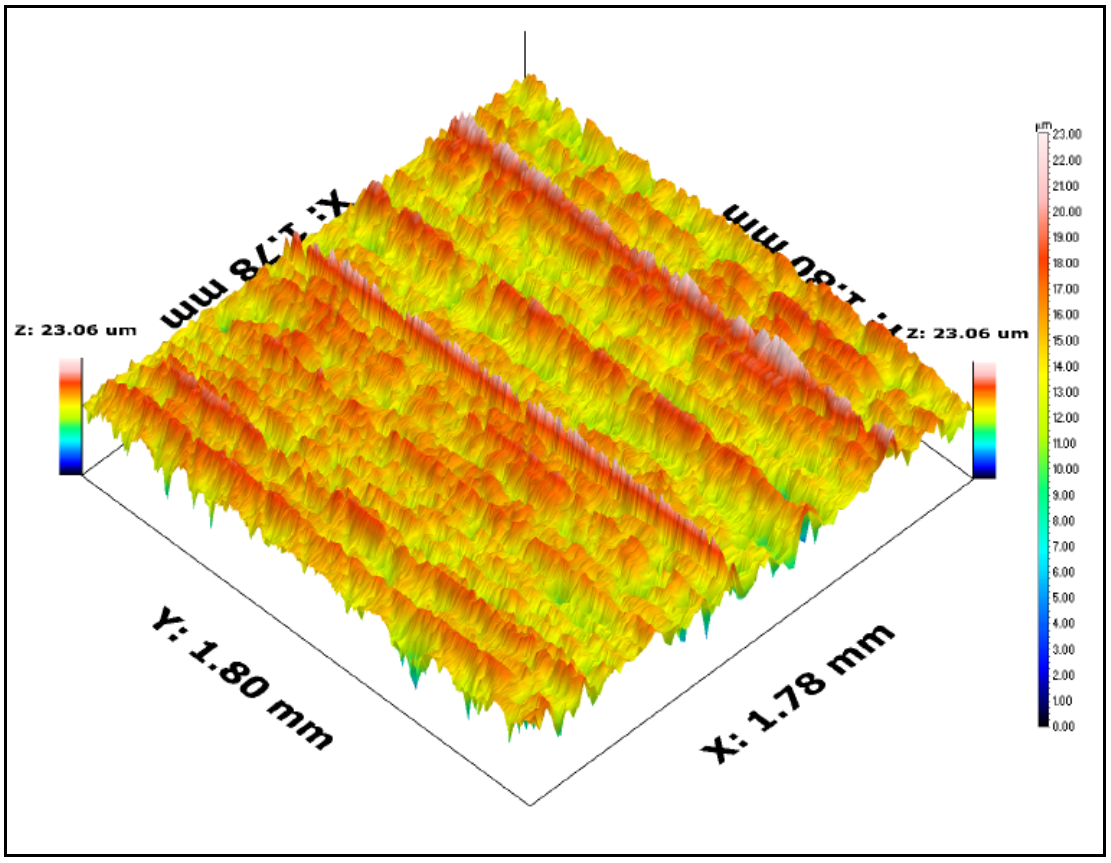

Figure B-14 3D surface profile of the unused part

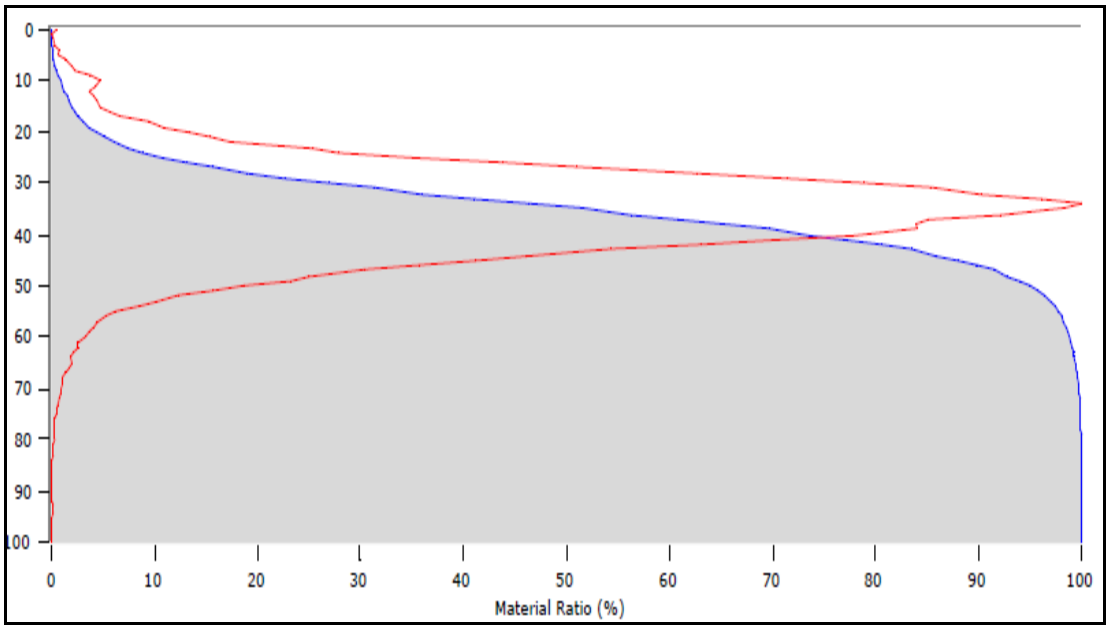

Figure B-15 BAC of the unused part

Table B-7 Table 0 6 BAC parameters of the unused part

PARAMETERS	VALUES	DESCRIPTION
R_k (μm)	4.84	Core roughness depth
R_{vk} (μm)	2.75	Reduced valley depth
R_{pk} (μm)	2.55	Reduced peak height
Mr1 (%)	9.572	Material ratio 1
Mr2 (%)	88.626	Material ratio 2

B.2 REACTION FORCES ON THE SHOES OF MISSILE

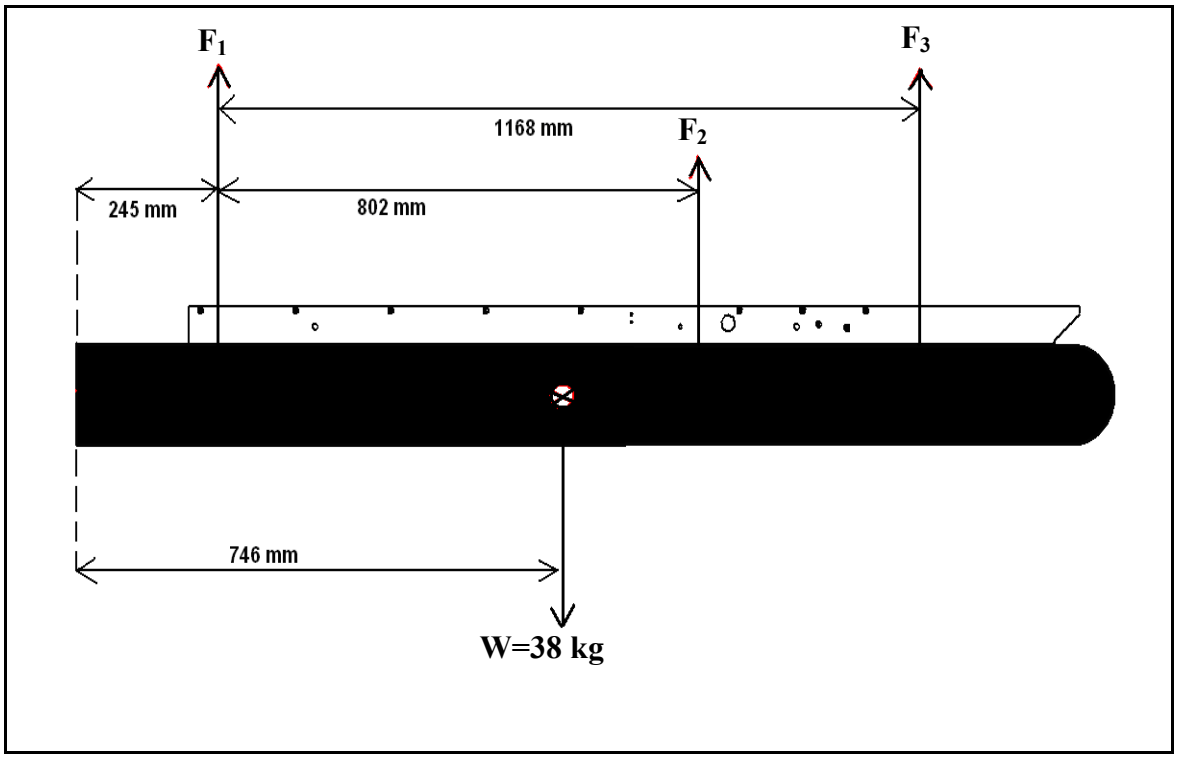

Figure B-16 The free body diagram of launcher rail

If $F_3 = 0$:

$$F_1 + F_2 = 38$$

and

$$(746 - 245)F_1 = (802 + 245 - 746)F_2$$

Then:

$$F_2 = 23.7 \cdot kg$$

$$F_1 = 14.3 \cdot kg$$

B.3 MATHCAD CALCULATIONS OF AMOUNT OF WORN MATERIAL

UNUSED RAIL

$R_k := 4.84$

$M_{r1} := 0.09572$

$R_{vk} := 2.75$

$M_{r2} := 0.88626$

$R_{pk} := 2.55$

$$R_{ktot} := M_{r1}\cdot\left(R_{vk} + R_k + \frac{R_{pk}}{2}\right) + \left(M_{r2} - M_{r1}\right)\cdot\left(R_{vk} + \frac{R_k}{2}\right) + \left(1 - M_{r2}\right)\cdot\frac{R_{vk}}{2}$$

$R_{ktot} = 5.092$

LEFT SIDE OF USED RAIL (REGION 1)

$R_k := 5.87$

$M_{r1} := 0.08852$

$R_{vk} := 1.76$

$M_{r2} := 0.91725$

$R_{pk} := 1.97$

$$R_{ktotleft} := M_{r1}\cdot\left(R_{vk} + R_k + \frac{R_{pk}}{2}\right) + \left(M_{r2} - M_{r1}\right)\cdot\left(R_{vk} + \frac{R_k}{2}\right) + \left(1 - M_{r2}\right)\cdot\frac{R_{vk}}{2}$$

$R_{ktotleft} = 4.726$

RIGHT SIDE OF USED RAIL (REGION 1)

$R_k := 3.84$

$M_{r1} := 0.07312$

$R_{vk} := 2.15$

$M_{r2} := 0.86703$

$R_{pk} := 1.06$

$$R_{ktotright} := M_{r1}\cdot\left(R_{vk} + R_k + \frac{R_{pk}}{2}\right) + \left(M_{r2} - M_{r1}\right)\cdot\left(R_{vk} + \frac{R_k}{2}\right) + \left(1 - M_{r2}\right)\cdot\frac{R_{vk}}{2}$$

$R_{ktotright} = 3.851$

WORN MATERIAL

$Wear_{left1} := R_{ktot} - R_{ktotleft}$

$Wear_{left1} = 0.366$ (in micrometers)

$Wear_{right1} := R_{ktot} - R_{ktotright}$

$Wear_{right1} = 1.241$ (in micrometers)

LEFT SIDE OF USED RAIL (REGION 2)

$R_k := 3.76$

$M_{r1} := 0.10185$

$R_{vk} := 1.31$

$M_{r2} := 0.91302$

$R_{pk} := 1.48$

$$R_{ktotleft} := M_{r1} \cdot \left(R_{vk} + R_k + \frac{R_{pk}}{2} \right) + \left(M_{r2} - M_{r1} \right) \cdot \left(R_{vk} + \frac{R_k}{2} \right) + \left(1 - M_{r2} \right) \cdot \frac{R_{vk}}{2}$$

$R_{ktotleft} = 3.236$

RIGHT SIDE OF USED RAIL (REGION 2)

$R_k := 3.34$

$M_{r1} := 0.09045$

$R_{vk} := 1.80$

$M_{r2} := 0.86834$

$R_{pk} := 1.21$

$$R_{ktotright} := M_{r1} \cdot \left(R_{vk} + R_k + \frac{R_{pk}}{2} \right) + \left(M_{r2} - M_{r1} \right) \cdot \left(R_{vk} + \frac{R_k}{2} \right) + \left(1 - M_{r2} \right) \cdot \frac{R_{vk}}{2}$$

$R_{ktotright} = 3.337$

WORN MATERIAL

$Wear_{left2} := R_{ktot} - R_{ktotleft}$

$Wear_{left2} = 1.856$ (in micrometers)

$Wear_{right2} := R_{ktot} - R_{ktotright}$

$Wear_{right2} = 1.755$ (in micrometers)

LEFT SIDE OF USED RAIL (REGION 3)

$R_k := 3.83$

$M_{r1} := 0.10190$

$R_{vk} := 1.24$

$M_{r2} := 0.91836$

$R_{pk} := 1.69$

$$R_{ktotleft} := M_{r1}\cdot\left(R_{vk} + R_k + \frac{R_{pk}}{2}\right) + \left(M_{r2} - M_{r1}\right)\cdot\left(R_{vk} + \frac{R_k}{2}\right) + \left(1 - M_{r2}\right)\cdot\frac{R_{vk}}{2}$$

$R_{ktotleft} = 3.229$

RIGHT SIDE OF USED RAIL (REGION 3)

$R_k := 5.21$

$M_{r1} := 0.09193$

$R_{vk} := 2.01$

$M_{r2} := 0.90034$

$R_{pk} := 1.74$

$$R_{ktotright} := M_{r1}\cdot\left(R_{vk} + R_k + \frac{R_{pk}}{2}\right) + \left(M_{r2} - M_{r1}\right)\cdot\left(R_{vk} + \frac{R_k}{2}\right) + \left(1 - M_{r2}\right)\cdot\frac{R_{vk}}{2}$$

$R_{ktotright} = 4.575$

WORN MATERIAL

$Wear_{left3} := R_{ktot} - R_{ktotleft}$

$Wear_{left3} = 1.863$ (in micrometers)

$Wear_{right3} := R_{ktot} - R_{ktotright}$

$Wear_{right3} = 0.517$ (in micrometers)

AVERAGE AMOUNT OF WORN MATERIAL

$$Wear := \frac{Wear_{left1} + Wear_{left2} + Wear_{left3} + Wear_{right1} + Wear_{right2} + Wear_{right3}}{6}$$

$Wear = 1.266$ (in micrometers)

UNUSED RELEASE LATCH

$R_k := 4.972$

$M_{r1} := 0.1162$

$R_{vk} := 7.281$

$M_{r2} := 0.8298$

$R_{pk} := 6.227$

$$R_{ktotunused} := M_{r1} \cdot \left(R_{vk} + R_k + \frac{R_{pk}}{2} \right) + \left(M_{r2} - M_{r1} \right) \cdot \left(R_{vk} + \frac{R_k}{2} \right) + \left(1 - M_{r2} \right) \cdot \frac{R_{vk}}{2}$$

$R_{ktotunused} = 9.375$

USED RELEASE LATCH

$R_k := 0.784$

$M_{r1} := 0.0898$

$R_{vk} := 1.207$

$M_{r2} := 0.8428$

$R_{pk} := 0.963$

$$R_{ktotused} := M_{r1} \cdot \left(R_{vk} + R_k + \frac{R_{pk}}{2} \right) + \left(M_{r2} - M_{r1} \right) \cdot \left(R_{vk} + \frac{R_k}{2} \right) + \left(1 - M_{r2} \right) \cdot \frac{R_{vk}}{2}$$

$R_{ktotused} = 1.521$

THE AMOUNT OF WORN MATERIAL IN RELEASE LATCH

$Wear := R_{ktotunused} - R_{ktotused}$

$Wear = 7.854$ (in micrometers)

B.4 SEQUANTIAL ANALYSIS AND WEAR RESULTS

Table B-8 Nodal pressure and sliding distance values at the end of 20 firing

NODE #	PRESSURE (max) (MPa)	SLIDING DISTANCE (mm)
NODE	J	J
264131	3618,64	0,296
264219	1555,51	0,354
264237	1490,80	0,366
264221	1486,09	0,368
264223	1562,44	0,349
264225	1471,59	0,342
264227	1704,37	0,368
264229	1539,77	0,350
264231	1606,83	0,365
264233	1495,52	0,360
264235	1700,86	0,365
264239	1706,35	0,360
264241	1511,58	0,365
264243	1683,01	0,362
264245	1445,80	0,348
264247	1701,17	0,355
264249	1510,65	0,352
264251	1522,96	0,330
264217	1451,40	0,309
264255	1554,27	0,317
264257	1680,01	0,307
264259	1538,93	0,287
264261	1609,62	0,278
264263	1511,44	0,287
264265	1500,84	0,297
264267	1186,34	0,251
264269	1374,97	0,242
264271	1240,04	0,244
264273	1181,58	0,227
264275	1299,19	0,219
264277	1220,60	0,163
264279	1253,83	0,136
264281	952,26	0,129
264283	208,07	0,110
264285	157,11	0,071

Table B-9 The amount of worn material depth at each node at the end of 20 firing

NODE #	AMOUNT OF WEAR (mm)
264131	0,021
264219	0,011
264237	0,011
264221	0,011
264223	0,011
264225	0,010
264227	0,013
264229	0,011
264231	0,012
264233	0,011
264235	0,012
264239	0,012
264241	0,011
264243	0,012
264245	0,010
264247	0,012
264249	0,011
264251	0,010
264217	0,009
264255	0,010
264257	0,010
264259	0,009
264261	0,009
264263	0,009
264265	0,009
264267	0,006
264269	0,007
264271	0,006
264273	0,005
264275	0,006
264277	0,004
264279	0,003
264281	0,002
264283	0,000
264285	0,000

Table B-10 Nodal pressure and sliding distance values at the end of 30 firing

NODE #	PRESSURE (max) (MPa)	SLIDING DISTANCE (mm)
NODE	J	J
9020096	3881,05	0,214
9020099	2094,58	0,361
9020101	1584,43	0,369
9020103	1679,55	0,369
9020105	1684,38	0,347
9020107	1623,69	0,330
9020109	1557,88	0,367
9020111	1673,87	0,351
9020113	1617,47	0,365
9020115	1747,33	0,361
9020117	1625,79	0,364
9020119	1668,22	0,361
9020121	1573,92	0,365
9020123	1656,97	0,352
9020097	1614,24	0,367
9020129	1669,68	0,346
9020127	1486,79	0,333
9020125	1580,08	0,350
9020153	1502,69	0,338
9020151	1512,25	0,317
9020149	1609,71	0,298
9020147	1557,66	0,296
9020145	1611,14	0,278
9020143	1475,76	0,268
9020141	1518,29	0,278
9020139	1266,71	0,279
9020137	1223,68	0,242
9020135	1233,61	0,244
9020133	1242,07	0,236
9020131	1134,25	0,190
9020161	1173,97	0,182
9020159	1136,22	0,173
9020157	313,40	0,058
9020155	883,38	0,149
9020165	458,17	0,122

Table B-11 The amount of worn material depth at each node at the end of 30 firing

NODE #	AMOUNT OF WEAR (mm)
9020096	0,017
9020099	0,015
9020101	0,012
9020103	0,012
9020105	0,012
9020107	0,011
9020109	0,011
9020111	0,012
9020113	0,012
9020115	0,013
9020117	0,012
9020119	0,012
9020121	0,011
9020123	0,012
9020097	0,012
9020129	0,012
9020127	0,010
9020125	0,011
9020153	0,010
9020151	0,010
9020149	0,010
9020147	0,009
9020145	0,009
9020143	0,008
9020141	0,008
9020139	0,007
9020137	0,006
9020135	0,006
9020133	0,006
9020131	0,004
9020161	0,004
9020159	0,004
9020157	0,000
9020155	0,003
9020165	0,001

Table B-12 Nodal pressure and sliding distance values at the end of 40 firing

	PRESSURE (max) (MPa)	SLIDING DISTANCE (mm)
NODE #	J	J
990	3735,37	0,160
995	1685,76	0,409
999	1550,11	0,348
1003	1535,57	0,378
1007	1439,72	0,365
1011	1463,59	0,355
1015	1497,15	0,366
1019	1421,24	0,329
1023	1546,37	0,343
1027	1542,45	0,328
1031	1526,32	0,288
1035	1407,34	0,296
1039	1367,80	0,278
1043	1339,49	0,270
1047	1170,59	0,226
991	1273,98	0,181
1055	1127,91	0,136
1059	326,92	0,071

Table B-13 The amount of worn material depth at each node at the end of 40 firing

NODE #	AMOUNT OF WEAR (mm)
990	0,012
995	0,014
999	0,011
1003	0,012
1007	0,011
1011	0,010
1015	0,011
1019	0,009
1023	0,011
1027	0,010
1031	0,009
1035	0,008
1039	0,008
1043	0,007
1047	0,005
991	0,005
1055	0,003
1059	0,000

Table B-14 Nodal pressure and sliding distance values at the end of 50 firing

	PRESSURE (max) (MPa)	SLIDING DISTANCE (mm)
NODE #	J	J
990	3664,61	0,187
995	1627,71	0,399
999	1530,73	0,361
1003	1438,27	0,367
1007	1438,55	0,366
1011	1524,33	0,365
1015	1437,58	0,346
1019	1500,90	0,358
1023	1396,37	0,314
1027	1431,12	0,329
1031	1408,66	0,298
1035	1427,82	0,296
1039	1395,38	0,278
1043	1405,86	0,261
1047	1154,99	0,235
991	1203,85	0,162
1055	1285,58	0,154
1059	346,81	0,081

Table B-15 The amount of worn material depth at each node at the end of 50 firing

NODE #	AMOUNT OF WEAR (mm)
990	0,014
995	0,013
999	0,011
1003	0,011
1007	0,011
1011	0,011
1015	0,010
1019	0,011
1023	0,009
1027	0,009
1031	0,008
1035	0,008
1039	0,008
1043	0,007
1047	0,005
991	0,004
1055	0,004
1059	0,001

Table B-16 Nodal pressure and sliding distance values at the end of 60 firing

NODE #	PRESSURE (max) (MPa)	SLIDING DISTANCE (mm)
NODE	J	J
1010	3672,77	0,176
1038	1689,25	0,365
1034	1481,66	0,373
1030	1429,60	0,356
1026	1403,88	0,355
1022	1481,73	0,355
1018	1471,28	0,356
1014	1477,15	0,320
1009	1509,19	0,314
1185	1391,58	0,310
1181	1329,88	0,307
1177	1395,42	0,296
1173	1314,79	0,259
1169	1265,53	0,260
1165	1170,50	0,244
1161	1032,46	0,181
1126	901,66	0,124
1130	347,07	0,081

Table B-17 The amount of worn material depth at each node at the end of 60 firing

NODE #	AMOUNT OF WEAR (mm)
1010	0,013
1038	0,012
1034	0,011
1030	0,010
1026	0,010
1022	0,011
1018	0,010
1014	0,009
1009	0,009
1185	0,009
1181	0,008
1177	0,008
1173	0,007
1169	0,007
1165	0,006
1161	0,004
1126	0,002
1130	0,001

Table B-18 The amount of worn material depth at each node at the end of 70 firing

	PRESSURE (max) (MPa)	SLIDING DISTANCE (mm)
NODE	J	J
990	3698,82	0,163
993	2374,10	0,268
995	1699,95	0,354
997	1736,80	0,387
999	1599,83	0,363
1001	1674,24	0,354
1003	1493,44	0,368
1005	1538,19	0,340
1007	1426,43	0,355
1009	1659,91	0,339
1011	1490,04	0,355
1013	1760,15	0,351
1015	1503,26	0,347
1017	1771,04	0,343
991	1509,69	0,320
1021	1717,03	0,336
1023	1437,67	0,324
1025	1591,33	0,331
1027	1391,64	0,310
1029	1575,55	0,318
1031	1401,94	0,307
1033	1529,58	0,297
1035	1445,07	0,296
1037	1451,24	0,259
1039	1339,48	0,269
1041	1403,71	0,241
1043	1248,47	0,251
1045	1306,90	0,233
1047	1199,24	0,235
1049	1172,87	0,218
1051	1219,47	0,209
1053	993,61	0,114
1019	25,09	0,009
1057	1148,07	0,197
1059	274,11	0,030

Table B-19 The amount of worn material depth at each node at the end of 70 firing

	AMOUNT OF WEAR (mm)
990	0,012
993	0,013
995	0,012
997	0,013
999	0,012
1001	0,012
1003	0,011
1005	0,010
1007	0,010
1009	0,011
1011	0,011
1013	0,012
1015	0,010
1017	0,012
991	0,010
1021	0,012
1023	0,009
1025	0,011
1027	0,009
1029	0,010
1031	0,009
1033	0,009
1035	0,009
1037	0,008
1039	0,007
1041	0,007
1043	0,006
1045	0,006
1047	0,006
1049	0,005
1051	0,005
1053	0,002
1019	0,000
1057	0,005
1059	0,000